Sustainable energy comes in colors:

Yellow - solar

Cyan - wind

Blue - hydro

Red - thermal

University of Alberta

Energy Management for Automatic Monitoring Stations in Arctic Regions

by

Demian Pimentel

A thesis submitted to the Faculty of Graduate Studies and Research
in partial fulfillment of the requirements for the degree of

Doctor of Philosophy
in
Energy Systems

Electrical and Computer Engineering

Spring 2012
Edmonton, Alberta

To Max and Bruno.

Abstract

Automatic weather monitoring stations deployed in arctic regions are usually installed in hard to reach locations. Most of the time they run unsupervised and they face severe environmental conditions: very low temperatures, ice riming, etc. It is usual practice to use a local energy source to power the equipment. There are three main ways to achieve this: (1) a generator whose fuel has to be transported to the location at regular intervals (2) a battery and (3) an energy harvesting generator that exploits a local energy source. Hybrid systems are very common.

Polar nights and long winters are typical of arctic regions. Solar radiation reaching the ground during this season is very low or non-existent, depending on the geographical location. Therefore, solar power generation is not very effective. One straightforward, but expensive and inefficient solution is the use of a large bank of batteries that is recharged during sunny months and discharged during the winter.

The main purpose of the monitoring stations is to collect meteorological data at regular intervals; interruptions due to a lack of electrical energy can be prevented with the use of an energy management subsystem. Keeping a

balance between incoming and outgoing energy flows, while assuring the continuous operation of the station, is the delicate task of energy management strategies.

This doctoral thesis explores alternate power generation solutions and intelligent energy management techniques for equipment deployed in the arctic. For instance, harvesting energy from the wind to complement solar generation is studied. Nevertheless, harvested energy is a scarce resource and needs to be used efficiently. Genetic algorithms, fuzzy logic, and common sense are used to efficiently manage energy flows within a simulated arctic weather station.

Acknowledgements

The research presented in this thesis was supported by the Natural Sciences and Engineering Research Council of Canada (NSERC), the Fonds Québécois de la Recherche sur la Nature et les Technologies (FQRNT), the Informatics Circle of Research Excellence (iCORE), and the Faculty of Graduate Studies and Research (FGSR) of the University of Alberta.

I appreciate the support of my supervisors, Dr. Petr Musilek and Dr. Andrew Knight. They provided the tools and guidance I required to attain the goals of my doctoral research project.

I thank Dr. Martin Sharp and Dr. Alex Gardner for sharing their expertise in automatic weather stations, along with technical information, data sets, and pictures related to the Arctic & Alpine Research Group projects.

I also acknowledge the help of Dr. Brian Fleck and Graeme Comyn, who provided training and facilitated the use of the recirculating wind tunnel that was used to experiment with the wind flutter generator.

I recognise Dr. Kodjo Agbossou, who forged the path that allowed me to pursue my doctoral studies.

I am grateful to Dr. Ahmed Chériti, Dr. Daniel Massicotte, Dr. Adam Skorek, and Dr. Witold Pedrycz, from whom I learned valuable lessons and who in different ways positively influenced my career.

To Liliana, thank you for sharing this experience with me.

Table of Contents

List of Tables

List of Figures

List of Symbols and Acronyms

δ – declination

ϵ – sky brightness coefficient

η – efficiency

ω – hour angle

φ – latitude

λ – longitude

η – roundtrip efficiency of a storage device

γ – surface azimuth

µW – microwatt

ρ – constant power/air density

σ – energy storage capacity

θ – angle of incidence

θ_Z – solar zenith angle

β – surface inclination

Ω – ohm

% – percentage

© – copyright

® – registered

° – degree

°C – degree Celsius

°N – degrees North

°W – degrees West

A – ampere

A/D – analog to digital

AARG – Arctic & Alpine Research Group

AC – alternating current

Ah – ampere-hour

a_S – solar altitude angle

AWS – automatic weather station

B – capacity of a storage device

B_0 – initial stored energy of a storage device

BAPM – battery aware power management

C – power consumption

C100 – 100 hours discharge rate

C20 – 20 hours discharge rate

cf. – confer (compare)

CI – computational intelligence

cm – centimetre

cm^2 – square centimetre

cm^3 – cubic centimetre

CPU – central processing unit

CWEC – Canadian Weather for Energy Calculations

CWEEDS – Canadian Weather Energy and Engineering Datasets

d – duty cycle

dB – decibel

DC – direct current

DFS – dynamic frequency scaling

DHI – diffuse horizontal irradiation

DHI – direct horizontal insolation

DNI – direct normal insolation

DPM – dynamic energy management

DVFS – dynamic voltage and frequency scaling

DVS – dynamic voltage scaling

e.g. – *exampli gratia* (for example)

EC – Environment Canada

EHS – energy harvesting system

ETR – extraterrestrial irradiation

GA – genetic algorithm

GHI – global horizontal insolation

GHI – global horizontal irradiation

GOES – geostationary operational environmental satellite

HAPM – harvesting aware power management

Hz – Hertz

I – irradiation

i.e. – *id est* (this is)

kg – kilogram

kJ – kilojoule

km – kilometre

kW – kilowatt

kWh – kilowatt-hour

l – litre

Li-ion – lithium-ion

m – air mass

m – meter

m/s – meter per second

m^2 – square meter

mA – milliampere

MPPT – maximum energy point tracking

mV – millivolt

mW – milliwatt

N – newton

NASA – National Aeronautics and Space Administration

Ni-Cd – nickel-cadmium

Ni-Mh – nickel-metal hydride

NSRDB – National Solar Radiation Database

nW – nanowatt

p – panel (solar)

P – power

$P(\ )$ – continuous and bounded function

PV – photovoltaic

Q – battery capacity

R – resistance

R_b – beam radiation ratio

RF – radio frequency

RMS – root mean square

s – second

S – sun

S_α – solar altitude

SI – international system

SOC – state of charge

T – temperature

TMY3 – typical meteorological year

V – volt

v – voltage

VDC – volts direct current

W – watt

W – wind

Wh – watt-hour

X – any finite real number

x – any parameter

Chapter 1 - Introduction

Batteries are ubiquitous power sources that are used in most low power systems. Although the energy and energy density of chemical batteries is low, they have many advantages: they are reliable, cheap, and can be transported easily and safely. As of this date (2011), they are the only commercial choice for low power mobile applications. Also, they offer a handy solution for equipment located in remote or hard to reach areas, where the energy grid is inaccessible and the use of engine-generators cannot be justified.

The use of batteries to power equipment installed in places of difficult access is challenging. Primary and secondary batteries need to be replaced at the end of their lifetime, and the isolated equipment will need regular maintenance, sometimes for the sole purpose of battery replacement. The use of rechargeable batteries requires an additional source of electric energy. Two different approaches can be used to supply energy to the system: (1) electrical energy is generated from an indigenous source of energy, or (2) a fuel generator is used to locally produce electricity.

For low power systems, there are few commercial harvesting or fueled solutions available, while many are still undergoing research and development. Hence, low power electrical energy generation is an emerging field, and the lack of widespread solutions reflects the need for sustained research efforts in this area. This opens the door to a rich set of research opportunities in the field of standalone electrical energy generation for low power applications.

The paradigm changes with the use of low power harvesting or fueled devices. The energy harvester or the fueled generator becomes the main source of electrical energy, while the battery is relegated to the role of energy buffer (it stores excess electrical energy from the source and delivers it to the load when needed). Currently, the list of viable low power generators is short, and they fall into the following categories: fuel cells, radioisotope energy generators, microengines, and *energy harvesting devices*. Some of the technologies derived from the latter categories are in early commercialization stages, but most of them are still under research and development.

Energy harvesting devices (or energy scavenging devices) collect energy from the environment. Power sources based on this approach are a promising alternative to batteries since they can be designed to power systems for an unlimited time without user intervention and can function autonomously as long as their physical components last. For devices that are meant to work in hard to reach areas, energy harvesting appears to be the most effective solution. The problems associated with resource-consuming refueling, or battery replacements, simply vanish.

Numerous midpower and high power commercial energy harvesting systems (EHS) are available; for low power applications, the list is limited to solar panels, some small wind turbines, piezoelectric devices, and thermoelectric generators. However, there are still technological issues to be solved before the full potential of these devices can be exploited. Some problems encountered are the low efficiency of the energy harvesters, the need for intermediate energy converters, relatively energy hungry loads (electronic circuits, actuators that are powered by the energy source) and energy management issues.

The most popular energy harvester for low power applications is probably the solar panel. Apart from its low efficiency, the main problems with this

generator are that the availability of solar energy is subject to daily and seasonal cycles, and that certain weather conditions obstruct solar radiation. Astronomical patterns can be predicted with the use of simple models, e.g., duration of day-night cycles and sun position, but weather covers a broad range of stochastic phenomena that are hard to model. Hence, solar energy systems are generally used in conjunction with secondary batteries which serve as an energy buffer.

In arctic areas, winters are long and the polar night can last for months, depending on the latitude. Solar radiation is very low or non existent during this season, and a solar energy system is useless. However, this problem can be overcome with the use of oversized batteries. They store harvested solar energy during the sunny seasons, and provide electricity to the system during the months when darkness prevails. This solution seems straightforward, but the transportation of large batteries to remote arctic locations is difficult. In addition, batteries exhibit poor performance at low temperatures, require periodic maintenance, and require replacement after a few years of use. Even for properly sized systems, there is a high risk of exhausting the battery long before the winter ends (worst case scenario). It is worth studying additional solutions such as adaptive or *intelligent energy management* techniques, and/or the addition of an electric generator of a different nature.

Extracting energy from the wind is a viable approach. Unfortunately, wind turbine generators do not scale-down well and their moving parts suffer from icing and ice riming (rime forms when water vapour condenses and freezes on contact with a surface whose temperature is below the freezing point). Wind flutter generators are based on a newer technique that extracts energy from the wind in a different way than turbines do. They are cheap, simple, and relatively efficient devices that are well suited for low power applications. Wind flutter generators have fewer moving parts than wind turbines, and this can be advantageous in cold regions. Nevertheless, there

are very few scientific studies related to this technology, and its performance under winter conditions is unknown.

The use of energy harvesting power sources in remote or hard to reach locations is an attractive choice, especially when the equipment is left unsupervised for long periods. Unfortunately, the performance of these devices depends on climatological conditions and they can fail to provide electricity due to variations of the energy source. Once more, proper energy management schemes are imperative. Low power fueled energy generators should not be disregarded. In general, fuels and innovative fuel generators have much higher energy and energy densities than chemical batteries, making them easier to transport. With the use of fueled generators, the stochastic climatic variable of energy harvesting devices is eliminated. The main problems are the lack of commercial solutions for low power applications, the transportation of fuel to the site at regular intervals, and the unknown performance of these devices in arctic climates.

In arctic areas, automatic weather stations (AWS) are used to monitor and record data related to climatological and weather phenomena. These unmanned systems are typically scattered across uninhabited locations, and their year-long, uninterrupted operation depends heavily on the power source they use. All power sources used in automatic weather stations are subject to special operating conditions, as listed below:

- Access to remote arctic locations is seasonal, expensive, and time consuming; it is required to retrieve data (unless there is satellite telemetry), and to install and maintain equipment.
- Equipment is unsupervised and exposed to the forces of nature: adverse weather conditions and the presence of wild life.
- The performance of power sources is affected by temperature.

- Additional energy consuming functionalities like satellite communications modules for real-time data transmission and deicing systems add an overhead to the power source.

1.1 Research Project Description

The doctoral research project presented in this thesis is on the crossroads of three different fields of study: energy systems, intelligent systems, and arctic systems. The main goal of this thesis was to study unconventional solutions to efficiently energize unsupervised low power systems deployed in arctic regions. To accomplish this task, a multidisciplinary approach was employed. First, an adequate understanding of climatic and astronomical phenomena affecting the arctic was required. Energy requirements of automatic monitoring stations were estimated and possible power sources were identified. Second, it was realised that a balance between incoming and outgoing energy fluxes guarantees the continuous operation of the system. This is where the area of energy systems plays an important role.

Automatic weather stations in the arctic and their power supplies are subject to extreme and sometimes unpredictable operational conditions. An efficient use of the scarce energy resources in isolated arctic areas is necessary. Computational intelligence techniques can assist in the design of efficient energy management strategies for automatic weather stations in the arctic. To date, there is limited information on this topic.

The first task consisted of the study of automatic weather stations in the arctic and the identification of problems affecting the operation and reliability of their power supplies. With this information, a list of candidate power sources for low power applications in the arctic was elaborated. This included new and “old” technologies such as fuel cells, radioactive batteries, solar panels, wind generators, and other energy harvesting devices. Solar panels and wind generators appear to be a good option, but their use requires efficient management of the harvested energy.

Another undertaking was the study of energy management issues for energy harvesting devices. Energy harvesting theory was obtained from recent publications, and energy management strategies for energy harvesting devices were identified. Although most of the literature covers energy management for embedded or mobile devices, the same principles can be applied or extended to other systems, e.g., weather stations.

One additional difficulty is that solar and wind energy generators used in the arctic face particular operational conditions and stochastic weather. Monitoring stations usually have a data logger, which acts as a central processing unit of limited capabilities. Although the implementation of a power management algorithm within the system is necessary, this should not become an overhead for the data logger or the energy budget—i.e., the algorithm needs to be powerful, yet simple. Proper energy management techniques based on computational intelligence should be able to comply with both requirements.

A simulator for automatic monitoring stations was programmed using the MATLAB®/Simulink® platform. The simulator focuses on the energy and energy aspects of the station, and covers solar and wind power generation, energy conversion, energy routing, battery, load, and energy management modules. This simulator is useful for different purposes, which range from energy availability assessments to the design and testing of energy management algorithms. The input to the simulator is climatological data that can be real or synthetic. Energy studies were made for solar and wind energy at select locations in the arctic, and intelligent harvesting aware power management algorithms based on fuzzy logic were designed and tested with the simulator.

The next task was to apply computational intelligence techniques to develop ad hoc energy management algorithms for arctic monitoring stations. Stations with different energy requirements were studied, ranging from basic

monitoring stations to stations equipped with satellite communication capabilities. Real meteorological data were used to evaluate the energy production capabilities of different energy harvesters and to run simulations. Four climatic databases that offered suitable time series for energy calculations were identified. They covered several locations across the Canadian Arctic and Alaska.

Performance of the energy management algorithms was measured using normal and worst case scenarios. For typical or average years, two specialized databases provided data series of typical weather conditions spanning over one year. Worst case scenarios were assessed using climatological data sets covering several years of data.

An iterative design process occurred—i.e., during the phase of algorithm testing, the simulator was improved to meet new requirements. This process stopped when both the simulator and the algorithms were considered to be free of defects. Finally, the simulation system was used to test the performance of the algorithms and to gather appropriate data. The simulator can also be used in future research projects. Although manuals were not prepared, this thesis provides a good reference.

Additionally, a newer wind generator based on the aeroelastic flutter phenomenon was found to offer an interesting alternative to wind turbines. This simple device consists of a tensioned mylar ribbon coupled to an electromagnetic transducer; it generates electricity when an air flow makes the ribbon flutter. A lack of technical information about this device led to the creation of a set of experiments: a wind tunnel was used in an effort to obtain data for the characterization of the generator. Some parameters of interest used during the experimentation were ribbon tension, wind speed, wind direction, load, and power output. A simple mathematical energy generation model was created based on observations made and data collected.

Part of the research effort focused on a study of the interactions between two harvesting generators: a typical solar panel and a wind flutter generator. Solar panels are frequently used to power equipment in the arctic, and wind generation can be a very good complement; especially, wind flutter generators were found to perform satisfactorily at low wind speeds. To the author's knowledge, this is the first research attempt to pair both energy harvesting generators and assess them in cold climates by means of numerical simulations.

The last part of the project consisted of gathering data generated by different simulations and analyzing the results. Metrics were developed to measure the performance of the algorithms.

To complement the research activities, three papers were published and were presented at national and international conferences, and one more was recently submitted. Presentations at two University of Alberta symposia were also made during 2010. At least two additional peer-reviewed journal papers based on this thesis will be submitted.

1.2 Project Goals

A literature review was conducted to study power generation alternatives for low power equipment deployed in cold climates. Automatic monitoring stations are the hub of this research and establishing their energy requirements was an important step. Energy harvesting theory was studied in order to understand its implications for automatic monitoring stations.

One goal of the research was to create models of the various parts that form the automatic weather station and power source. Experimentation with a wind flutter generator prototype and mathematical model development were employed to study a dual source (solar/wind) energy harvesting system.

Another goal was to program a multisource simulator with the obtained mathematical models and use it to develop and test energy management

algorithms for energy harvesting systems in cold climates. The simulator was used to determine solar and wind energy production profiles for arctic locations as well.

Appropriate metrics to assess the reliability of different energy management algorithms were developed and computational intelligence was used to formulate energy management algorithms for automatic weather stations in the arctic.

1.3 Methodology

Scientific publications, manufacturers' and developers' Web pages, and books were consulted to obtain the necessary practical and theoretical information to establish the research framework. Determination of the monitoring stations architecture and energy requirements was essential. Alternatives to low power systems in arctic regions were identified with an emphasis on power generation from solar and wind sources. Real climatological data were used to establish credible energy production profiles of energy harvesters and to provide a basis for the energy management simulations.

A literature review of automatic weather station subsystems, power source components, and mathematical models was performed. It was realised that the models could be complemented from several sources as long as the effects of very low temperatures were emphasized. Some models needed to be developed. For instance, testing of the wind flutter generator using a wind tunnel and gathering pertinent data allowed the creation of a mathematical model for simulation purposes.

A platform to develop the automatic weather station simulator was chosen. Several options were available, and MATLAB®/Simulink® was a good candidate due to its widespread availability and flexibility. The simulator required programming and testing.

Adequate metrics to test the energy management algorithms for automatic weather stations were determined and used to assess the performance of the algorithms under different scenarios. These algorithms were simple (data logger requirement) and were developed with the aid of computational intelligence. Testing was done with real meteorological data for different arctic locations.

1.4 Thesis Structure

Chapter 1 includes a general introduction and presents the framework of the doctoral research project described in this thesis.

Chapter 2 defines the structure, energy requirements, and problems associated with automatic weather stations deployed in the arctic. A section about climatological databases identifies sources of information that can be used for solar and wind energy calculations in the arctic.

Chapter 3 is an introduction to energy harvesting, and covers a study of energy sources, energy harvesters, fueled generators, and energy harvesting systems. An energy harvesting theory is presented and energy management issues and strategies are discussed.

Chapter 4 describes models of energy harvesting systems. It covers energy sources, energy transducers, energy storage, energy converters, and loads. A special emphasis is placed on the study of a wind flutter generator, for which original data are provided.

Chapter 5 introduces an energy simulator for automatic weather stations in cold regions. The simulator framework, architecture, input datasets, and parameters are discussed.

Chapter 6 covers intelligent energy management. A technique to determine the dimensions of a power source's components based on genetic algorithms is developed, a fuzzy energy management strategy is described, and a

satellite communications energy-wise approach is introduced. Data from the experiments are provided.

Chapter 7 presents the conclusions of the thesis, provides a list of contributions to the field made by this research, and suggests future research opportunities.

Following the bibliography, Appendices 1–3 include the programming scripts and Simulink® block schemes used by the simulator.

Chapter 2 - Energy Requirements of Automatic Weather Stations in the Arctic

2.1 Special Considerations

Automatic weather stations (AWS) in arctic regions usually operate on solar panels and lead-acid batteries. During sunny seasons the solar panels provide electricity to the station and keep the batteries charged. The energy stored in the batteries is used when the amount of incident solar radiation is too low to fully energize the system (dawn, dusk, overcast sky, shadows, low angles of incidence), and when the solar resource is absent (night, polar night, bad weather, negative angles of incidence).

A power source consisting of a solar panel and a small secondary battery can cope very well with short periods of low or no irradiance (night, some cloudy days). Arctic regions receive very low or no solar radiation during the winter (polar night). Continuous operation of the monitoring station during this season requires a considerable amount of energy—i.e., a bulky and heavy bank of batteries. If the energy contained in the batteries is entirely consumed before the end of the polar night, the station becomes nonoperational. For equipment deployed in the arctic, this poses a serious problem—access to the site is seasonal and expensive.

When a long period of darkness is expected, the solar panel and chemical battery approach can still be used, but it is no longer convenient. Other sources of energy, along with the respective hardware, have to be considered. There are several alternatives; unfortunately, they are relatively new and immature technologies—especially where low or midenergy applications are

considered. In arctic environments, the severity of the weather poses an additional challenge. Hence, the design, testing, and installation of reliable power sources are difficult and expensive procedures.

Power sources for the arctic fall into three main categories: (1) chemical batteries, (2) fuel generators, and (3) *energy harvesting* generators, e.g., solar panels. Energy harvesting devices are a primary choice, since they extract energy from the local environment and do not depend on refueling. Generally, the conversion efficiency from the local source of energy (solar, wind, thermal gradient) to electric energy is low, harvesting devices usually deliver very low power and often need power conditioning. Despite this, fuel generators and energy harvesters (other than solar panels) can be integrated into the arctic energy system in order to alleviate the solar panel-secondary battery-polar night problem.

Choosing an adequate power supply is only part of the answer to powering arctic weather stations. Transporting equipment to remote arctic locations requires special logistics, it is time consuming and expensive. To minimize weight, size, and cost, the power source should not be oversized, yet it should be able to energize the equipment at all times. Careful ad hoc sizing of the power source is required, since different locations have dissimilar weather, and energy requirements of monitoring stations depend on the equipment used and the purpose of the system.

Another key point is energy management. The energy efficiency of the AWS can be boosted with the use of special energy management strategies at a system or subsystem level. If energy harvesters are the main source of energy, the use of adequate energy management techniques can guarantee the continuous operation of the system with minimal energy loss.

Other power sources, such as fuel cells and radioactive batteries, can profit from similar energy management approaches. These sources can be coupled

to batteries or energy harvesting devices to ensure efficient energy delivery when it is needed.

When dealing with the power supply of equipment operating in arctic regions, the following circumstances should be taken into account.

- Equipment is subject to harsh weather conditions: very low temperatures, strong winds, icing, snow accretion, and ice riming.
- Due to weather conditions, power supplies might not run at peak performance and might need to be over-sized, increasing installation costs; however, the power supply has to be as small and light as possible.
- Access to remote arctic locations is seasonal, expensive, and time consuming. Access is required to install and maintain equipment and to retrieve data.
- Equipment is left unsupervised for several months. In case of failure, sending personnel to deal with the problem is costly and not always possible.
- Real-time data transmission eliminates trips whose sole purpose is to retrieve data, but requires a satellite transmitter that increases energy consumption considerably.
- Rime, ice, and snow accumulation affect equipment performance; deicing equipment is beneficial.

Automatic monitoring stations deployed in arctic locations can be entirely powered using local energy sources. Primary batteries can be a poor choice as they need to be replaced when their energy is depleted; secondary batteries can be recharged with the use of an external power source. Solar radiation can be used for this purpose, but other energy sources such as wind and thermal gradients should be used to energize the system during winter.

The main problem with fuel powered generators is that fuel (the energy carrier) has to be transported to onsite locations on a regular basis. However, one great advantage is that the power supply is guaranteed to work as long as there is fuel. Under this scenario, equipment failure is the main reason for a system shutdown. Similar reasoning applies to energy harvesting generators. A properly sized and designed generator should be able to power the load even when the energy source is absent for long periods of time. Unfortunately, an energy harvesting power source depends on local weather and can fail to provide energy under unforeseen worst-case scenarios [1] or due to mechanical malfunction.

In arctic applications, robust power sources that supply year-long uninterrupted energy are crucial. In this chapter, automatic arctic monitoring stations and their energy requirements are introduced. Figure 2.1 depicts the energy flow of a simplified monitoring station.

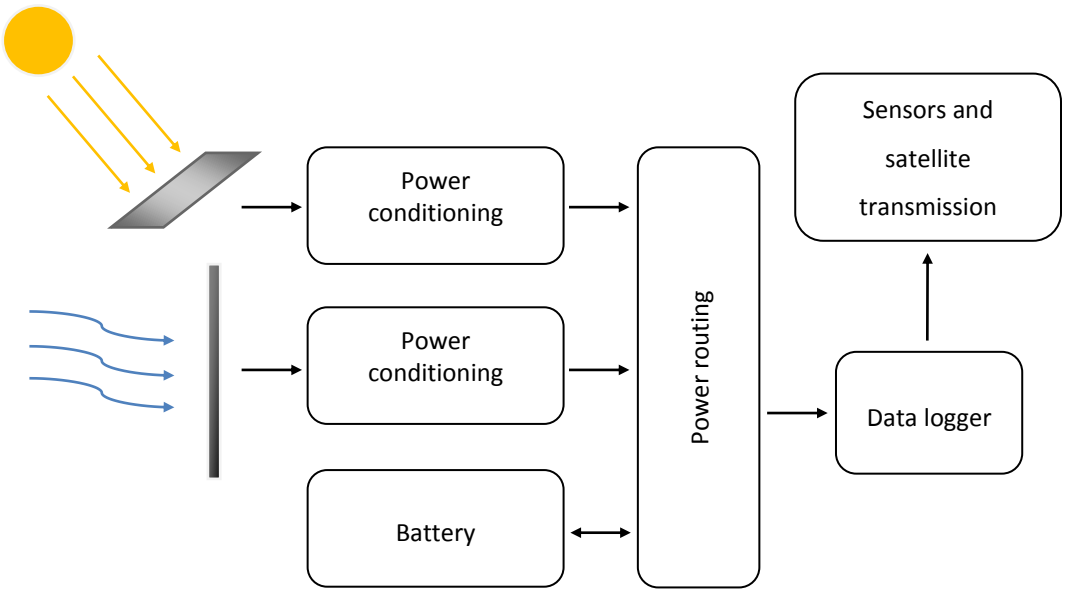

Figure 2.1 Energy flow in an automatic monitoring station.

The power source extracts and converts solar and wind energy into electrical energy. A rechargeable battery is used to deal with short and long term fluctuations of energy sources (solar, wind). Finally, power routing is used to

transmit energy to the load, which typically consists of a data logger, sensors, and, in some cases, a satellite transmission module.

2.2 Description of a Generic Arctic Monitoring Station

A basic AWG is composed of a power source, a data logger, and sensors. Usually, a mast is used to support the equipment. A picture of a monitoring station installed in the arctic is presented in Figure 2.2. A solar panel (facing away from camera) and a rechargeable battery supply the system with electrical energy. The data logger is a programmable device that samples the sensors and records the associated sampled data at specified time intervals. The sensors are devices used to measure physical quantities, e.g., wind speed and direction (anemometer), relative humidity (hygrometer), ambient temperature (thermometer), solar radiation (pyranometer), and snow depth (sonar), among others. The output of the sensors is an electric signal—a voltage, a current, or both, depending on the instrument.

Figure 2.2 shows an antenna used for satellite communication. A geostationary operational environmental satellite (GOES) transmitter is used to communicate via satellite with a receiving station. This device allows real time monitoring from a remote location, provides a way to prevent the logger's buffer from overloading, and minimizes the risk of data loss. Unfortunately, the GOES transmitter takes a high toll on the energy budget of the station.

As a reference, the power requirements of a typical remote monitoring station from Environment Canada (EC) are shown in Table 2.1. It was previously discussed that one common approach to energize a monitoring station is with a power supply consisting of a solar panel and a lead-acid battery. If the station is located in the arctic, the solar panel can energize the monitoring station and charge the battery during the summer. When winter arrives, the battery has to be fully charged and able to energize the station for several months. For the energy requirements shown in Table 2.1, it can be

easily demonstrated that although the average power consumption is low (1.6 W), 90 days of operation require a 12 V, 1000 Ah lead-acid bank of batteries with a weight of at least 300 kg (assuming 70% discharge) [2]. However, this is an ideal case. The need for a larger bank of batteries can be assumed since self-discharge and the effects of cold on the battery's performance were not considered, and 90 days of autonomy can be insufficient for many locations across the arctic.

The need for additional energy sources becomes evident: the use of an additional energy harvesting device that is relatively compact and lightweight can have a huge impact on the size of the bank of batteries. In this case, the rechargeable batteries are needed only for short term back-ups—i.e., to provide energy when none of the local energy sources are available. Following the simplified example in the last paragraph, a single 12 V, 100 Ah, 30 kg back-up battery is enough to power the system for up to nine days.

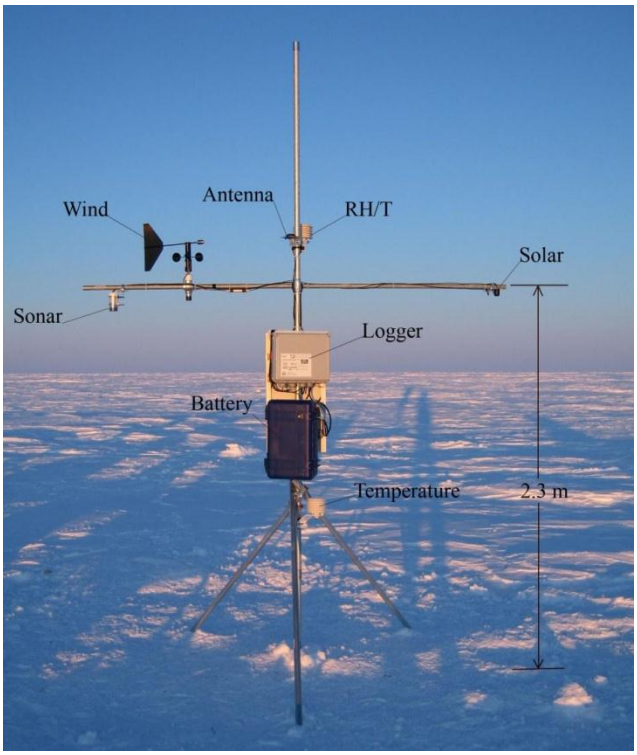

Figure 2.2 An automatic arctic monitoring station (with permission of Alex Gardner).

Table 2.1 Environment Canada energy usage data.

Equipment	90 Day Energy (Ah @ 12 V)
Data Logger	84
Snow Depth Sensor	60
Pressure Sensor	9
Wind Sensor	43
GOES Transmission	80
Other	10
Total	**286**

2.3 Environment Canada Monitoring Stations

EC operates weather stations across Canada, which are used to measure, record, and transmit meteorological data. Temperature, snow and rain precipitation, barometric pressure, and wind speed and direction are the commonly measured phenomena. The stations can be unsupervised (automatic) or supervised [3].

Figure 2.3 is a map that plots the location of weather and climatological stations across Canada. Stations located in high arctic regions have long polar nights and face more severe climatological conditions than stations located in southern areas. But stations in subarctic, arctic, and high arctic regions share the same common problems: low or null solar radiation during winter, extremely low temperatures, etc. For this reason, stations located north of parallel 60 are referred to as “arctic” [4]. This includes Yukon, the Northwest Territories, and Nunavut. Although the boundaries of the Labrador Peninsula extend beyond parallel 60, there is only one station (C. Hopes Advance) located in this area. Similarly, almost all of Alaska is located north of parallel 60, and climatological data coming from Alaskan sources will be used as an additional reference. Note: Nunavut is a relatively new Canadian Territory and on the map of Figure 2.3 it is still shown as a part of the Northwest Territories.

Although not all of EC's weather monitoring stations located in arctic regions are automated, some manned stations are a relevant source of data for energy harvesting studies. This is discussed in section 2.5.

2.3.1 Energy Requirements

Table 2.2 lists the components used in EC *Reference Climate Station*. This station is used as a framework throughout this thesis. The purpose of Table 2.1 is to demonstrate the use of each component, along with the current consumption characteristics specified by Environment Canada [5].

Notes: 1) EC provided three modes of operation for the data logger—i.e., quiescent, processing, and measurement. The results presented in Table 2.1 were simplified; processing and measurement modes were merged to provide a single active current consumption mode. 2) For the sensor SR50 – sonic ranger, the modes of operation provided by EC were "off," "quiescent," and "measurement." The quiescent and measurement modes were merged to obtain the active current consumption. 3) Similar reasoning was used for the GOES transmitter, where the modes of operation were "quiescent," "GPS fix," and "transmit." The active current consumption was obtained using an average of the GPS fix and transmit modes. To present a standardized set of current consumption characteristics for all the devices, a single duty cycle along with its equivalent "inactive" and "active" current consumption was computed. 4) The sensor TBRG (rain gauge) consumes current only when it is raining. During measurement, 0.05 mA will be consumed momentarily, and the frequency of the measurements depends on the rain rate. Since the overall consumption of this device is very low and it is weather dependant, the TBRG sensor was not considered on Table 2.1. 5) EC provided a list of several sonic wind sensors that can be used in the system (from manufacturers Vaisala, Thies, RM Young, Gill, and Climatronics). On average, these sensors are considered to be running continuously, with a consumption of 20 mA.

The equipment is powered using a 12 VDC signal. The average consumption of each component is computed using the current consumption (in mA) during inactive and active modes. The duty cycle specifies the percentage of time the device is active. For any device, the average current consumption is computed according to equation (2.1).

$$I_{average} = N_{devices} \times \int \left[D_{cycle} \times I_{active} + \left(1 - D_{cycle}\right) \times I_{inactive} \right], \quad (2.1)$$

where $I_{average}$ is the average current, $N_{devices}$ is the number of devices, D_{cycle} is the duty cycle, I_{active} is the device's active mode current and $I_{inactive}$ is the device's sleep mode current.

From Table 2.2, it is clear that the consumption of some sensors is several orders of magnitude lower than the consumption of the data logger, the sonic ranger, the sonic wind sensor, and the GOES transmission module. Figure 2.4 shows the current consumption distribution for EC Climate Reference Station. The data logger and the GOES transmitter each consume almost one third of the total energy budget, followed by the snow depth sensor (21%) and the sonic wind sensor (15%). The rest of the equipment consumes the relatively low amount of 7%.

The consumption distribution in Figure 2.4 can assist in the development of energy management strategies. Four strategies are listed below.

1) The simplest way to save energy is by duty cycling the entire weather station. For example, one hour of normal activity and one hour of complete inactivity should reduce energy consumption by half. The second and third strategies require more planning.
2) Individual sensors can be entirely shut down, leading to some energy savings. Turning off the snow depth sonic sensor will spare 20% of the energy consumption. Only selected categories of measured data are lost, and they can be reprogrammed to be sampled at a lower rate.

3) The actual duty cycles in Table 2.2 can be lowered to achieve some energy savings. The problems with this strategy are that the data logger and GOES transmitter duty cycles depend on the duty cycles of the sensors (cannot be modified at will), and that the quality of the data might be affected (one measurement is actually made with the average of several samples). This strategy is probably the most complex, and the one that could yield fewer benefits.
4) It is clear that the satellite communication module consumes a large amount of energy. When real time data transmission is not a priority and the system is at risk of exhausting its energy resources, the energy management strategy should force the in-buffer storage of measured data. Transmission is held until energy production is resumed, e.g., when the solar energy production is at its peak. If this strategy is applied properly, it should allow an efficient method to manage the energy flows without any performance (or data) loss.

The main problem with strategies 1, 2, and 3 is that data sampling rates are affected, but these methods can provide a way of keeping the station active and making measurements at a reduced rate in cases where energy production is low.

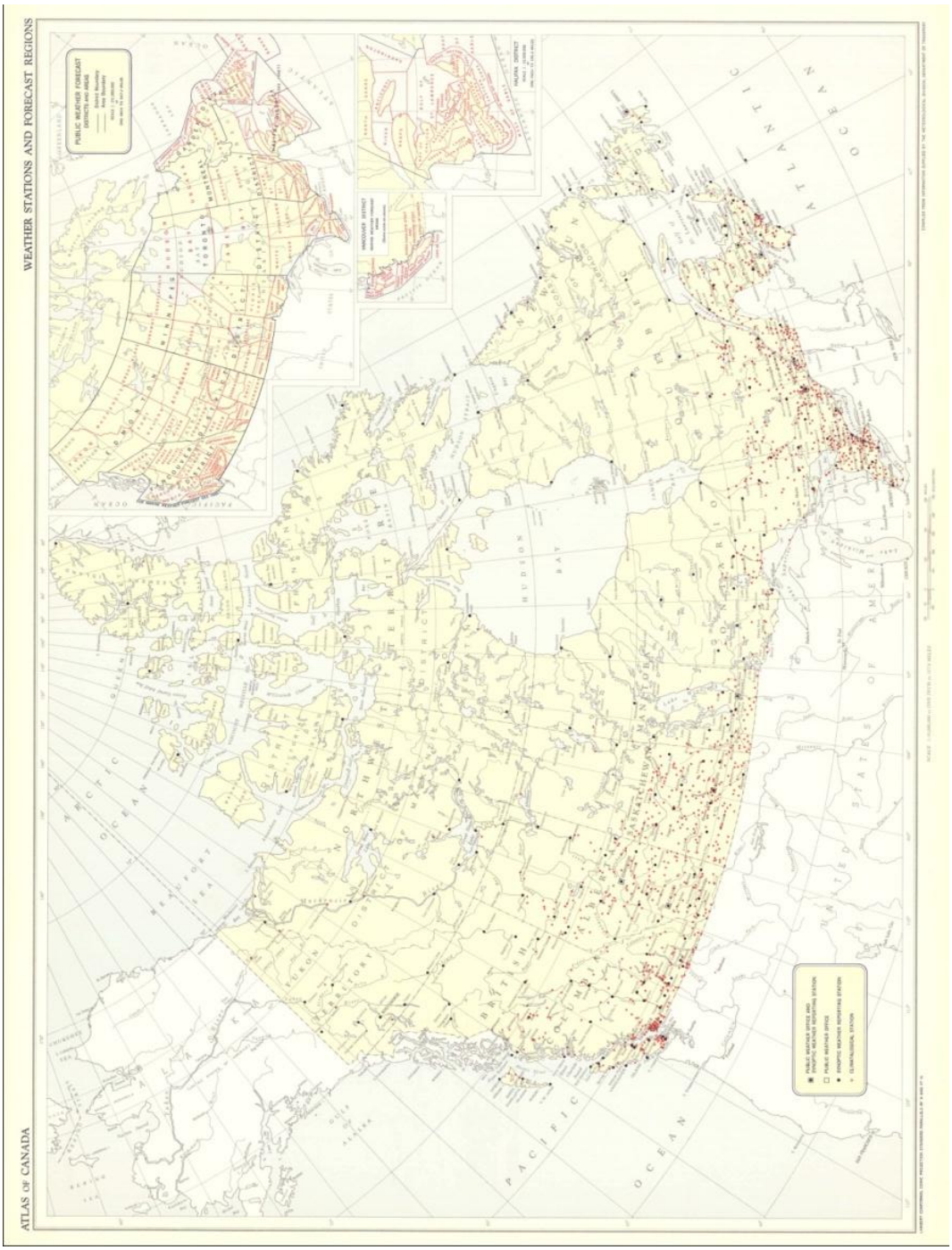

Figure 2.3 Canadian weather stations and forecast regions [6].

Table 2.2 Environment Canada's Reference Climate Station components and average consumption (@12 V).

Component	Use	Number of devices	Duty cycle	Consumption (mA)		
				Inactive	Active	Average
23x Logger	Data logger	1	0.56	2	68	39
SR50 sonic ranger	Snow depth	2	0.33	0	42	28
Setra 270	Barometric pressure	1	0.27	0	16	4.3
Geonor Interface	Data logger signal interface	1	0.33	0	13	4.3
Vaisala HMP45	Temperature and Relative Humidity	1	0.04	0	4	0.2
RMY 5103	Wind direction	2	0.008	0	0.1	0.002
RMY 5103	Wind speed	1	0.008	0	0	0
YSI 44212	Temperature probes	1	0.008	0	0.023	0.0002
	Soil Temperatures	7	0.008	0	0.063	0.004
Various models	Sonic wind sensor	1	100	0	20	20
Campbell Sci COM200 COM210	Modem	1	0.00047	0.12	140	0.2
GOES Tx	Communication with GOES	1	0.034	1	1041	37
					Total	**133**

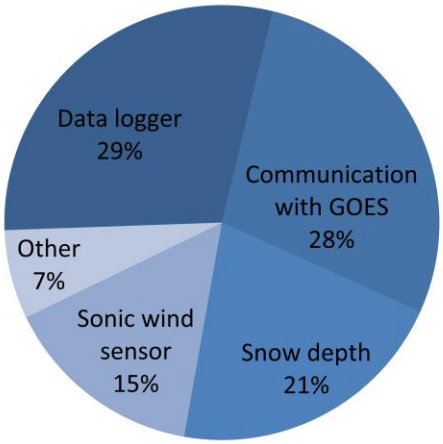

Figure 2.4 Percentage distribution of current consumption for Environment Canada's Reference Climate Station.

2.4 University of Alberta Arctic & Alpine Research Group

The Arctic & Alpine Research Group (AARC) at the University of Alberta operates four AWS on Devon Island, see Figure 2.5 and Table 2.3 [7]. The main purpose of these stations is to measure climatological phenomena to monitor and study glaciers and ice sheets.

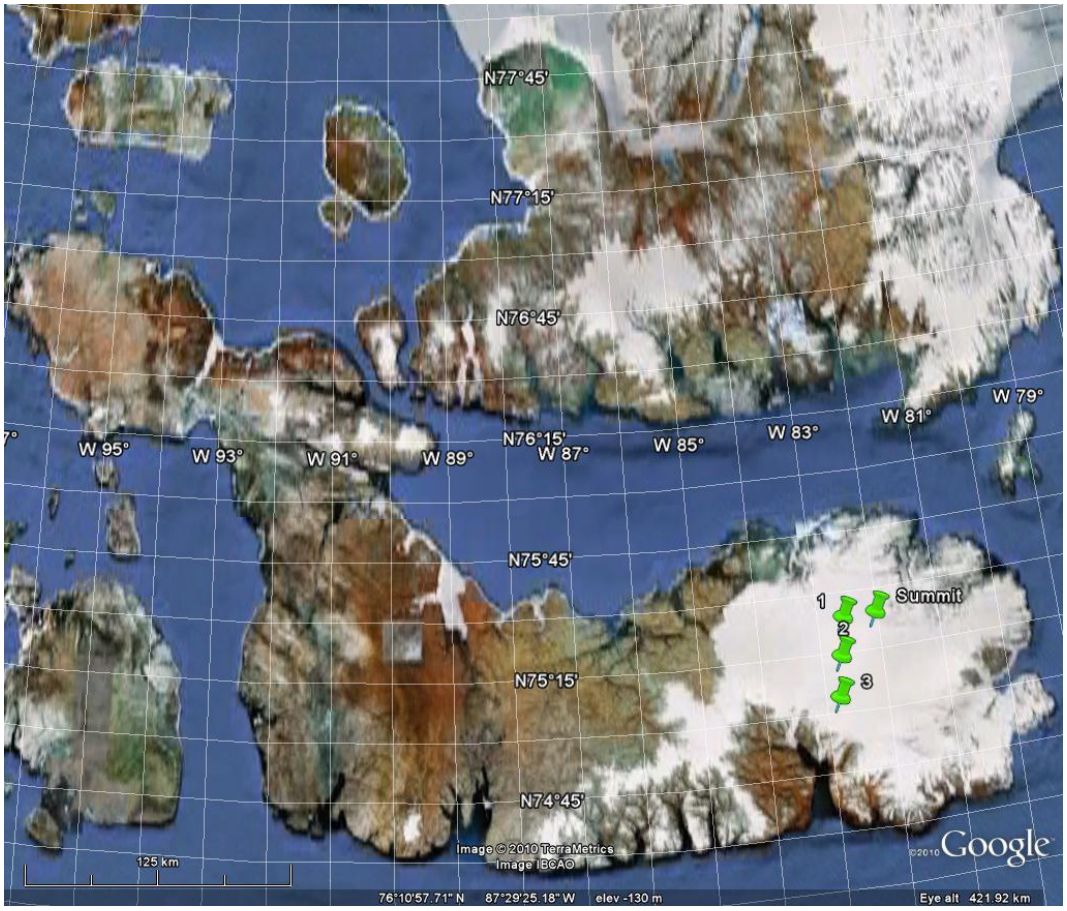

Figure 2.5 Locations of the University of Alberta's Arctic & Alpine Research Group monitoring stations on Devon Island.

Table 2.3 AARG monitoring stations.

Station	Latitude (°N)	Longitude (°W)	Elevation (m above the sea level)
1	75.34	82.68	1802
2	75.18	82.78	1415
3	75.01	82.88	994
Summit	75.34	82.14	1933

Although the purpose of the Arctic & Alpine Research Group stations is not the same as EC's stations, both platforms share the same structure and problems—i.e., a station has a data logger, a solar panel and battery power supply, and sensors. Most of the sensors used in both platforms serve the same purpose, e.g., to measure temperatures, relative humidity, snow depth, radiation components and wind speed. One AARG station is also equipped with a GOES transmitter. A list of the equipment used in a typical AARG station is provided in Table 2.4 [8]. The largest energy consumers are the data logger, the snow depth sonic sensor, and the satellite communication transceiver. In contrast, the rest of the equipment consumes a negligible amount of energy. Thus, the energy budget of this reference station is analogous to EC's Reference Climate Station energy distribution. The power source for the AARG station consists of a 12 V, 26 Ah lead-acid battery, and a 18 W solar panel.

EC and AARG systems operate under similar arctic climate conditions and are intended to collect data without interruption. Creating an energy budget for AARG stations can be done by following the approach presented in section 2.3.1. Due to the similarities between the platforms, further exploration of the current consumption of an AARG station would provide comparable results. In fact, Environment Canada's Reference Climate Station is used as a framework throughout this work, and the same techniques, principles, and findings can be applied to other EC and AARG stations.

Numerous agencies deploy AWS in the North American arctic for different research projects and purposes. Examples are: the Geological Station of Canada operates stations on the Devon Island Ice Cap, the Agassiz Ice Cap, and the Meighen Ice Cap; and the Greenland Climate Network has 18 automatic weather stations monitoring Greenland's ice sheet [9].

Table 2.4 Arctic & Alpine Research Group typical monitoring station components.

Component	Use	Voltage (V)	Consumption (mA)		Other
			Inactive	Active	
Campbell CR-10	Data logger	9.6 to 16	0.7	13	Analog measurement: 35 mA
Li-Cor LI200s	Pyranometer	No energy required	0	0	0 – 12 mV (output) 100 Ω shunt
Kipp & Zonen	Pyranometer	No energy required	0	0	0 – 125 mV (output)
Vaisala MP35CF	Relative humidity and temperature	7 to 28	0	< 2	
RM Young	Wind Monitor	Switched excitation voltage provided by data logger	0	< 0.01	
Vaisala PTB101	Barometric pressure		< 0.001	< 4	
REBS Q7	Net radiometer	No energy required	0	0	
Campbell Scientific SR50-L	Snow depth	9 to 16	2	250	Measurement takes 0.6 s on average
Iridium Satellite transceiver	Satellite communication	12	0	< 330	

2.5 Climatological Databases

In section 2.3.1, the energy requirements for Environment Canada's Reference Station were presented. If an energy harvesting power supply is used, then the average energy production must match or exceed the station's

energy requirements. Estimation of the harvested energy from wind and solar radiation can be done using models of the energy transducers (solar panels, wind generators), models of the energy sources, or real climatological data.

The location of the AWS plays an important role in the choice between a model of the energy source or real climatological data for the estimation of energy production. Unless proper climatological data have previously been collected for several years at the station's location, the only solution is the use of a model of the energy source. The model will be able to predict average energy production but its accuracy will be limited. Since weather patterns change with time and from location to location, even sites at similar coordinates can have different energy production potentials, e.g., collected wind energy by a generator located at the Devon Ice Cap summit will not be the same as the energy produced by a device located lower down on the ice cap.

An energy production model for a location for which no climatological data are available can be created using data interpolation and weather modeling methods. Usually, several years of data collected from neighbouring locations are required. For wind and solar energy, energy production maps and tools created using these techniques are accessible on the Internet. The Canadian Wind Energy Atlas [10] and the Photovoltaic Potential and Solar Resource Maps of Canada [11] are two convenient sources of information.

Wind and solar energy maps provide good insight into the energy production potential for a particular area; refer to Figure 2.6 and Figure 2.7. However, the use of these maps for an accurate estimation at a specific location is not recommended, since the resolution of the maps is low, e.g., 5 km in the case of the Canadian Wind Energy Atlas. When higher resolution is required, custom simulations for the location of interest must be performed.

When a satisfactory source of climatological data is available for the location of the automatic monitoring station, the estimation of energy production becomes easier. The studies, results, and analyses presented in chapters 4 and 5 are based on the assumption that the automatic monitoring stations are located at sites for which there is an appropriate source of meteorological data.

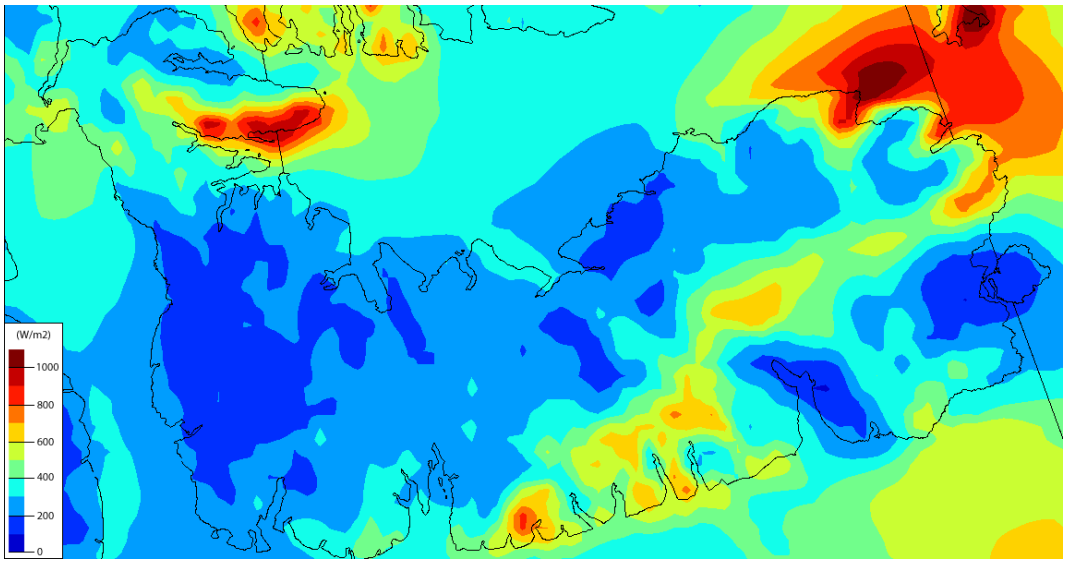

Figure 2.6 Mean wind energy map of Devon Island for the winter season (December, January, February), 30 m altitude. © Copyright 2003 Environment Canada [10].

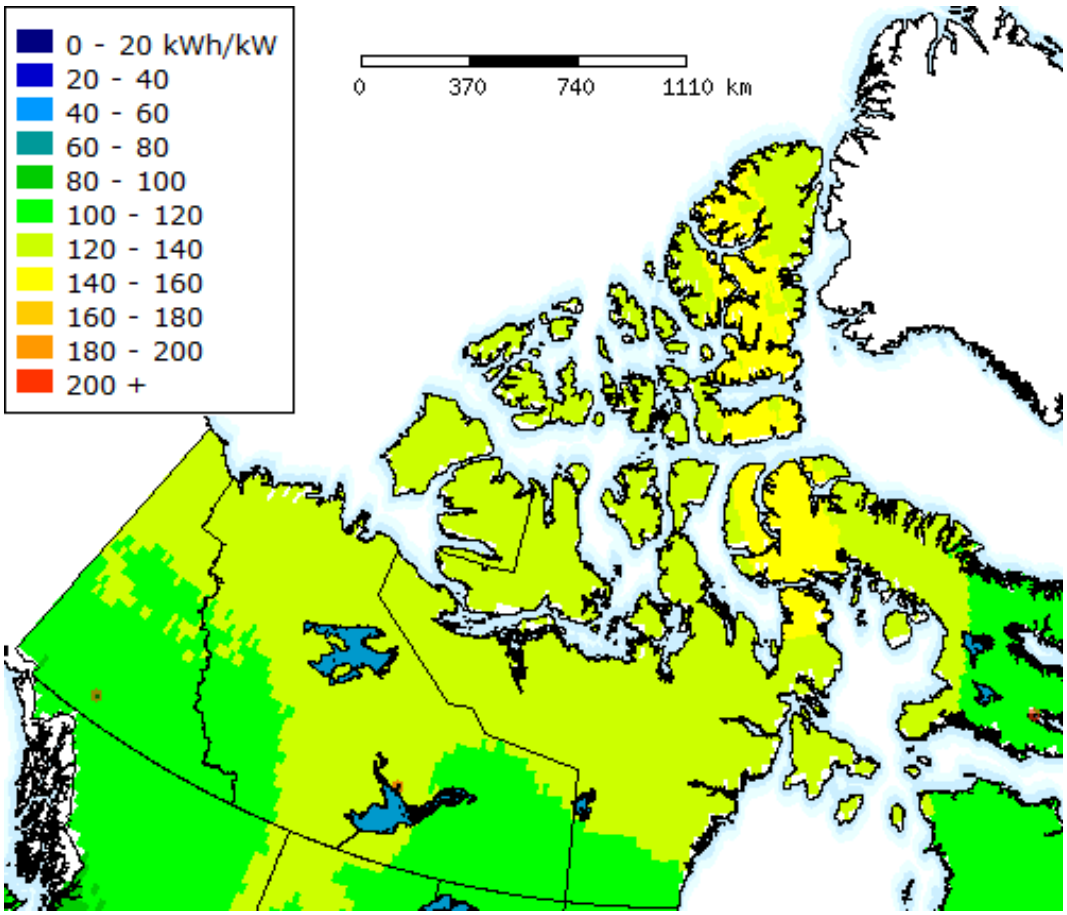

Figure 2.7 Canadian arctic photovoltaic potential, south facing, tilt equals latitude, June. This reproduction is a copy of an official work that is published by the Government of Canada and it has not been produced in affiliation with, or with the endorsement of, the Government of Canada [11].

Unfortunately, not every climatic database is suitable for engineering and energy calculation. Some essential elements are the quality of the data (ratio of estimated vs. measured), the accuracy of the measurements or estimations, the length of the series (number of years), the completeness of the series (missing points), the sampling rates (days, hours), and the availability of key parameters (wind speed and direction for wind energy estimation purposes).

Four databases that can be used for renewable energy studies in arctic locations are presented in Table 2.5. The Canadian Weather Energy and Engineering Data Sets (CWEEDS) is a digital database that contains hourly

weather records for 145 locations in Canada, including several spots in the arctic. The length of the series is up to 48 years, depending on the location. The CWEEDS includes several fields that are required to estimate the output power of solar panels and wind generators; see Table 2.6. Hence, the CWEEDS is useful in the design of wind and solar energy harvesting systems [12].

Table 2.5 Databases used for renewable energy studies.

Name	Origin	Cost	Comments
CWEEDS[a]	Canada [13]	Free	• Hourly data • Several years (decades) • Stations classified by data quality • Main uses: estimate energy production, test worst-case scenarios
NSRDB[b]	USA [14]	Free[e]	
CWEC[c]	Canada [13]	Free	• CWEEDS and NSRDB subsets • One typical meteorological year • Main uses: sizing, comparison between different systems, configurations and locations
TMY3[d]	USA [14]	Free	

a. Canadian Weather Energy and Engineering Data Sets.
b. National Solar Radiation Database.
c. Canadian Weather for Energy Calculations.
d. Typical Meteorological Year.
e. When downloaded from .mil, .gov, .edu, and .k12 domains.

Table 2.6 CWEEDS fields used for solar and wind energy estimations.

Field	Data element	Units
101	Extraterrestrial irradiance	kJ/m^2
102	Global horizontal irradiance	kJ/m^2
103	Direct normal irradiance	kJ/m^2
104	Diffuse horizontal irradiance	kJ/m^2
206	Dry bulb temperature	0.1°C
208	Wind direction	0°-359°
209	Wind speed	0.1 m/s

The Canadian Weather for Energy Calculations (CWEC) database is a subset of the CWEEDS. Each CWEC file represents one year of the most typical

meteorological conditions occurring at the site of interest. An algorithm determines typical months from the CWEEDS, and concatenates them to form a fictional year (from January 1 to December 31). If a leap year's February is selected as a typical month, then it is truncated to 28 days. This produces uniform sets that consist of 8760 fixed format records. In the case of the CWEEDS, one year of data has 8760 records, or 8784 records whenever a leap year occurs.

The CWEEDS and CWEC databases have counterparts in the United States. The National Solar Radiation Database (NSRDB) was developed for similar purposes and is analogous to CWEEDS. Similarly, the Typical Meteorological Year (TMY3) database is equivalent to CWEC. Although the study of energy harvesting power sources for automatic weather stations in the Canadian arctic is the main purpose of this research, the NSRDB and the TMY3 database can provide information about weather for energy calculations in Alaska, and are a good complement to the Canadian databases.

In chapters 4 and 5, datasets from CWEEDS, NSRDB, CWEC, and TMY3 are used as input for an energy harvesting generation simulation module that estimates solar and wind energy production at specified time intervals. Since the work developed in this thesis focuses on wind and solar power generation, not all variables included in the databases are of interest. The formatting of the Canadian and U.S. databases is different, so parsing is necessary to create uniform sets of data for input to the simulator presented in chapter 5. For this purpose, two Python scripts that automatically parse the original datasets into custom datasets were programmed.

2.5.1 Locations of Interest

Only 18 locations in the Canadian arctic region were included in the CWEC database. These locations are plotted on the map in Figure 2.8. A complete energy generation study for a particular location requires the CWEC dataset and the CWEEDS, since their uses differ – see Table 2.5. Furthermore, files

that provide high quality data (a low percentage of derived or estimated entries) are considered to be more relevant. The CWEC database has only three entries for Canadian arctic sites that met the requirement of a maximum of 25% of derived data: Inuvik, Resolute, and Whitehorse. For this reason, these three locations are used as a reference throughout this thesis. Additionally, one location in Alaska that complies with similar requirements was selected: Barrow (TMY3). The reference locations—Inuvik, Resolute, Whitehorse, and Barrow—are plotted in dark blue (dark grey) in Figure 2.8.

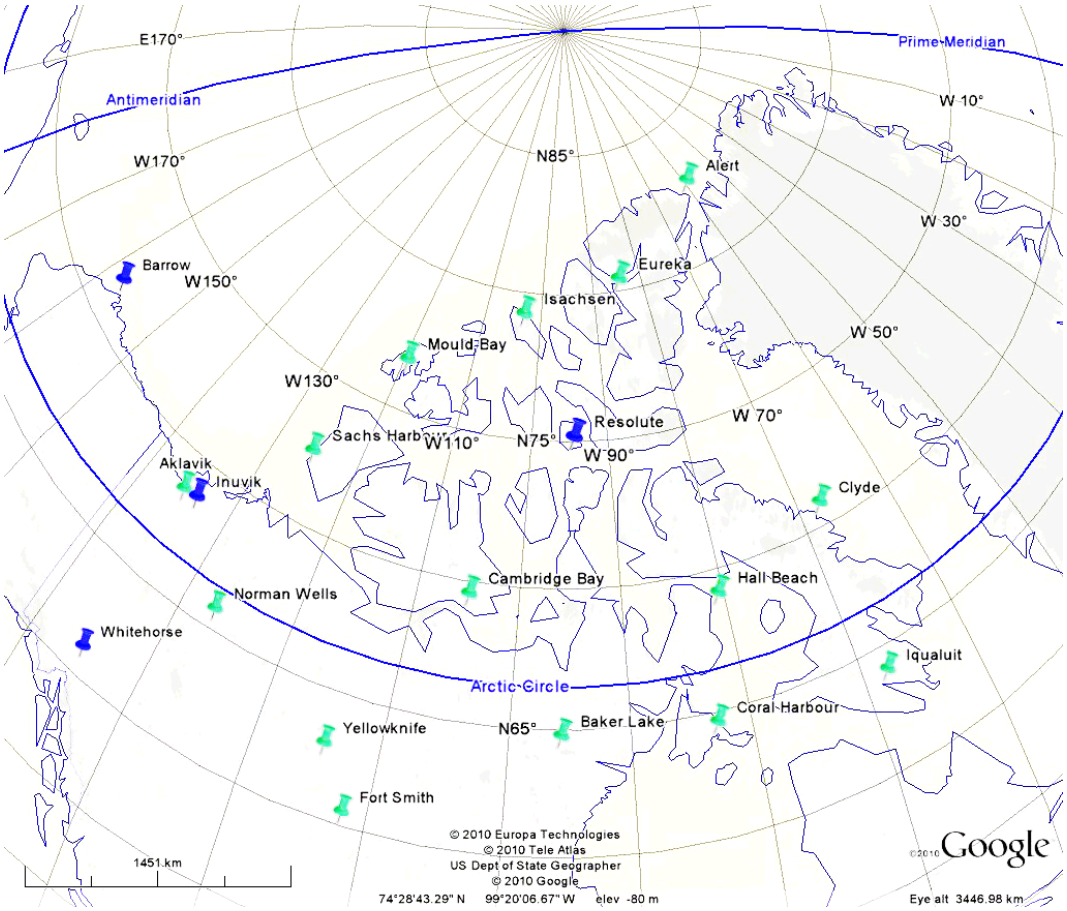

Figure 2.8 Distribution of locations that are included in the CWEC database. One location from the TMY3 database is also shown – Barrow, Alaska.

2.6 Conclusion

Automatic weather or climate monitoring stations deployed in arctic regions work under harsh weather conditions and face major operational challenges. Although the average power consumption of these systems is relatively low,

the use of power supplies based on solar panels and lead-acid batteries is not effective during the winter. The batteries lose efficiency at low temperatures and they are required to supply energy to the system for several weeks or months, depending on the location. Other sources of energy can be exploited year-long (wind, thermal gradients), and the integration of these sources with the power supply subsystem can be advantageous.

Various agencies deploy and operate automatic monitoring stations in the arctic. Stations from distinct groups are used to collect data for different projects and purposes. Despite this, the weather stations share a common structure and are subject to similar operational conditions. The power consumption profile of a reference station from EC is used as a reference throughout this thesis.

Finally, estimation of energy production for local energy sources is a first step in the design of energy harvesting generators. Special attention is given to wind and solar energy, but thermal energy should be studied as well. Specialized databases can supply the climatological data necessary to calculate power generation potentials at nominated arctic sites. Chapter 3 provides a richer view of energy harvesting generators and other possible fuel generators for arctic applications.

Chapter 3 - Energy Harvesting

3.1 Power Sources for Arctic Applications

In Chapter 2 the use of large batteries to power standalone equipment in arctic locations was discussed. It is a "simple" but inefficient approach, and the alternatives such as fuel generators and energy harvesting systems are better options. Secondary batteries can then be used in conjunction with those generators and serve as energy buffers. The main purpose of this chapter is to introduce several technologies that are viable to power equipment in cold climates. A focus on low power systems is kept throughout the chapter.

In Chapter 2, a list of challenges that are faced by equipment installed in remote arctic locations was provided. When choosing a power source, the following factors should be considered:

- Harsh weather conditions affect performance;
- Small and lightweight power sources are preferable;
- Unsupervised equipment must be reliable;
- Additional modules create additional overhead on the power source.

Harvesting energy from the environment is a viable choice. One frequent approach is the use of solar panels, but they produce little energy during the long winter months and require a large storage battery. For reference, the energy requirements of an EC weather station were shown in Table 2.1. Let's suppose that the power sources for this station are a solar panel and a lead-acid battery. A simple mode of operation is described: the solar panel

energizes the monitoring station and charges the battery during sunny seasons. When winter arrives, the battery is fully charged and stores enough energy to power the station for several weeks or months, until solar energy production is resumed. In Chapter 2 it was shown that the average energy requirements of the station are very low (1.6 W), and that for 90 days of autonomous operation, a 300 kg bank of lead-acid batteries is required. Transportation of such load to a remote arctic location is difficult and expensive, and the complete replacement of the full bank of batteries will be required after a few years. Removal and disposal of batteries further increase operation costs.

The identification of power sources that offer advantages over chemical batteries is the starting point of this chapter. Batteries, fuel generators, and energy harvesters are presented in the following pages, with an emphasis on energy harvesting systems.

3.1.1 Primary and Secondary Batteries

The first chemical battery was developed by Alessandro Volta two centuries ago. Since then, batteries have been used for multiple applications. Nowadays, they are the most common power source for stand-alone systems. Linden states that "electronic devices require low-cost and readily available lightweight batteries that have both high specific energy and power and high energy and power densities" [15]. Unfortunately, batteries are far from reaching these requirements: they are heavy, bulky, and they contain limited energy [16]. This can be partly attributed to the century-dated principles of batteries versus the state-of-the-art electronics they usually feed: in comparison, battery development has been too slow [17]. Not surprisingly, one of the principal problems of batteries is their "relatively low energy densities" [16].

Recently, new cell chemistries have allowed the development of high drain applications. One example is lithium-ion secondary batteries that have more

efficient chemistry than other battery types. These rechargeable batteries show long life cycles and possess high energy densities. However, they are costly, have a low power output, and can catch fire or explode under certain circumstances [18, 19]. Despite recent improvements in the performance of several cell chemistries, the energy requirements of electronic equipment are continuously increasing [17, 19]. For reference, Table 3.1 lists basic properties of commonly used battery chemistries [20]. Although lead-acid batteries present lower energy densities than other battery types, they are inexpensive and reliable. They are a good choice for stand-alone applications and they are widely used for energy storage in solar and wind energy systems.

Table 3.1 Properties of batteries.

Battery type	Vol. Energy density	Grav. Energy density	Self-discharge	Cycle life
Alkaline	300	125	4	1
Ni-Cadmium	100	30-35	15-20	300
Ni-Metal hydride	175	50	20	300
Li-ion	200	90	5-10	500
Lead-acid	85	45	40	250

Chemical batteries are far from being ideal energy storage devices. Despite this, they are omnipresent and it is not hard to imagine that they will have a place in future developments. Batteries are versatile and can be employed in a broad range of applications. Particularly, chemical batteries can be used in hybrid energy systems, where they play the role of energy buffer. For instance, they can be used to improve the efficiency of fuel generators and to deal with variations of the energy source in harvesting systems.

Current research on lithium batteries targets an improvement in performance so they can be used in the newest applications [19]. Some examples for ultralow power applications include microbatteries [19] and ultrathin flexible batteries [18]. The list is long, and other nonexplored

chemistries that can lead to higher energy and higher energy density are possible [19].

Finally, it is worth mentioning that secondary batteries are not the only storage devices that can be used in low power systems. Capacitors can be used for very short term storage and can help in dealing with transients. These electrical energy storage devices are able to receive and deliver considerable amounts of energy over short periods of time. Chemical batteries fall short in this property. However, capacitors cannot be used for midterm or long term energy storage, which is required in wind and solar energy harvesting applications. A newer technology, the ultracapacitor, sits between batteries and capacitors. Ultracapacitors are electrochemical devices that are suitable for short term and midterm storage. They are preferred for high drain applications. Since monitoring stations do not require high power bursts for operation, and their storage needs are in the range of days, weeks, and months, capacitors and ultracapacitors are not further discussed.

3.1.2 Fuel Energy Generators

3.1.2.1 Fuel Cells

The principle of the fuel cell was established almost 200 years ago by William Grove. Fuel cells produce electrical energy by the means of "reverse" electrolysis where an oxidant and a reductant passing *through* their respective electrodes will yield an electrical current. This mechanism is not much different from the mechanism in a chemical battery. The main advantage of fuel cells is that they can produce electricity as long as there is fuel and a source of oxygen. The most commonly used oxidizing and reducing agents are oxygen and hydrogen, respectively. Methanol is also a popular reductant.

Although the principle of a fuel cell is very simple, a functional fuel cell is not easy to develop. Fuel cell technology is being actively researched. Prototype

microfuel cells already exist and could shortly compete with rechargeable batteries for low power applications [21]. Hybrid fuel cell/battery systems are also possible.

Compared with batteries of similar volume and weight, a fuel cell system can provide up to 10 times more energy on a single charge; recharging takes a few seconds [22], the time to replace or refill a fuel tank, and fuel cell systems require low maintenance. The main disadvantages of the fuel cell are the production of waste heat and water, the high cost, the need for an external source of energy (fuel), and the risk of freezing at low temperatures.

Although no commercial low power fuel cells are known at this writing, some midenergy systems are already on the market. Ballard Power Systems in Burnaby, British Columbia, scheduled their "FCgen-1020ACS" polymer electrolyte membrane fuel cell to be available in 2010 [23]. This system is intended to be a power backup unit and the smallest unit is rated at 300 W. This fuel cell can operate at temperatures ranging from -20 to 52 °C, with start-up as low as -10 °C. With proper insulation, this fuel cell can be used in very cold climates.

3.1.2.2 Microengines

Microheat engines are another possible power source for stand-alone systems [24, 25]. According to a recent literature survey made by Flipsen, currently available miniengines have lower specific costs than energy harvesters and fuel cells. In addition, their specific energy and energy density are competitive with those of the highest performing energy harvesters and fuel cells [24].

Microengines seem to be good candidates to power standalone equipment. The main problems with these generators are noise, exhaust fumes, need for refueling, and unstable electrical energy generation [24]. Current issues for embedded microengine generators are the fuel tank, on-system controllers, power conditioning, electricity storage (microengines operate at low duty

cycles), thermal management, and packaging [25]. Currently, no commercial microengines are available.

3.1.2.3 Radioisotope Energy Generators

Radioisotope energy generators convert the radiated kinetic energy of unstable isotopes into electrical energy. This energy can feed low power autonomous electronic systems for up to hundreds of years. Radioisotope energy generators have very high energy densities and have power densities up to six times higher than energy harvesting devices and batteries [26]. Furthermore, radioisotope performance is not affected at extremely low or near fusion temperatures, relegating temperature issues to other materials of the system [27].

There are two energy conversion techniques: direct and indirect. One example of direct conversion is the radioisotope batteries modeled in [26]. These batteries use photovoltaic technology to "capture" decaying particles. An indirect conversion technique using radioactive thin films is presented in [27]. It uses a piezoelectric material, a silicon beam, an air-gap capacitor and a radioisotope emitter to convert the radiated kinetic energy into electrical energy.

Radioisotope energy generators have some disadvantages. First of all, there are safety hazards due to the damage radiant energy can inflict on humans and animals [25], although some authors claim that they can be used safely [27] and that radiation shielding is possible [28]. Another concern is the collection and disposal of *scattered* radioactive waste. Energy management issues need to be considered as well. Radioactive materials decay continuously at known rates. These devices are current sources that produce a constant, but time-decreasing stream of electrons. As a consequence, electrical energy is used, stored, or lost, and the power output will decrease over time.

The BetaBatt is a direct energy conversion radioactive battery that appears to be at a commercialization stage [29]. It can use tritium as fuel, with a lifetime of 12 years. Other radioactive isotopes with longer or shorter lifetimes can be used as well. BetaBatts promise a working temperature range from -100 to 150°C, which far exceeds requirements for arctic applications.

3.1.3 Energy Harvesting Sources and Generators

Energy sources for harvesting devices can be found everywhere. Choosing one or the other depends on the application's requirements and on the environmental conditions. For example, a photovoltaic transducer is not viable in a shaded location and a piezoelectric harvester cannot power a large system. In the arctic, energy can be scavenged from sunlight, wind flows, and temperature gradients. Table 3.2 provides a comparison of energy densities of different energy harvesting systems; the systems are classified according to the source of energy [25]. Energy sources for energy harvesting applications are discussed in this section and models of solar and wind energy harvesters are provided in chapter 4.

Table 3.2 Power densities of energy harvesting systems.

Energy Source	Power density
Solar (outside)	15 mW/cm^2
Solar (inside)	10 µW/cm^2
Temperature (5°C Gradient)	40 µW/cm^2
Human Energy	330 µW/cm^3
Airflow (5 m/s)	380 µW/cm^3
Vibrations	200 µW/cm^3
Acoustic Noise (100 dB) [30]	960 nW/cm^3

3.1.3.1 Electromagnetic Radiation

Electromagnetic energy can be obtained from light or from radio frequency radiation. One of the most available sources of energy is sunlight and photovoltaic panels can be used to harvest this energy. Their output is a

direct current that is a function of the light intensity, the temperature, and the load. In cold climates, the efficiency of solar panels increases, and this helps to balance the low average solar radiation reaching arctic areas.

Estimating the energy production of a solar panel is a nontrivial undertaking. Apart from global horizontal insolation (GHI) and diffuse horizontal insolation (DHI), other parameters need to be taken into account. These include the azimuth and inclination of the solar panel surface, and the terrestrial coordinates of the location where it is installed. Algorithms that are widely used for this purpose are described in [31-33].

Figure 3.1 shows a generic polarization curve of a solar panel. Different solar irradiation levels will produce unique polarization curves. Furthermore, the power output depends on the load connected to the solar panel. For a given set of operating conditions, there is an optimal load that maximizes the energy. In order to maximize energy transfer, a maximum power point tracking (MPPT) strategy can be used.

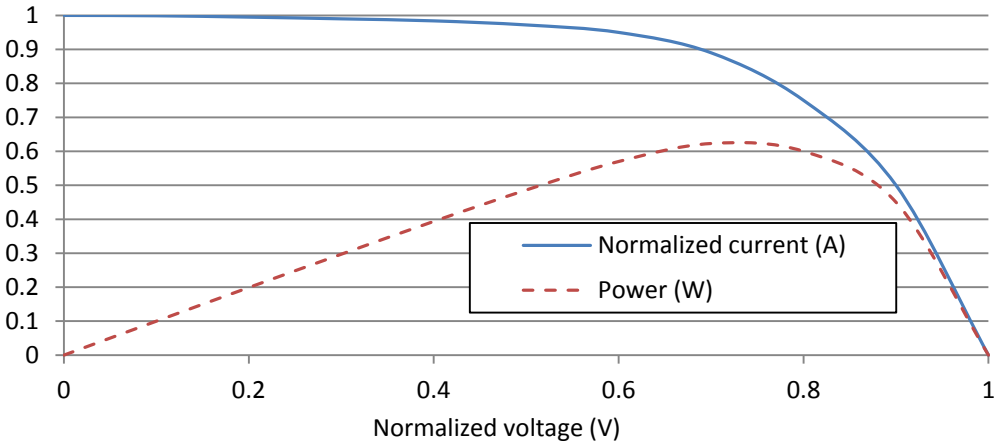

Figure 3.1 Example of a solar panel polarization curve.

MPPT is a technique that optimizes energy delivered to the load. This method requires monitoring of the incoming energy to determine the optimal operation point, and an adaptive load. Adapting the load is not easy. This can be done following different approaches, such as the use of a special energy

converter to “simulate” the required load, routing more or less energy to the battery, adjusting the duty cycle, or varying the workload.

An MPPT energy management system for solar energy harvesting devices was proposed in [34]. The energy converter is a charge pump that is adjusted in order to deliver maximum energy to the load (battery or electronic circuitry). A related work is presented in [35]. To operate at the maximum energy point, a power management unit determines the operation point and adjusts the load accordingly.

3.1.3.2 Mechanical

Kinetic energy can be harvested from the environment, and several methods can be used for this purpose. Some of them are piezoelectric properties, electrostatic energy, and magnetic induction [20]. The last two generate electricity when the movement of a proof mass creates an excitation on an electrostatic or electromagnetic transducer. The mechanical deformation of piezoelectric materials produces an electrical current. The output of these three kinetic energy harvesters is an alternating current signal.

An omnipresent source of kinetic energy is the wind [36]. Wind availability depends on location and on climatological conditions. Typically, wind turbines coupled to a rotary electrical generator are used to harvest energy from the wind. The output can be either a direct or alternating current, depending on the type of generator. Currently, the smallest low power commercial wind turbines are rated at 50 W, and their cost is around $600 [37].

A different wind flow harvesting approach, the aeroelastic flutter generator, was recently developed [38]. Unlike generators based on turbines, flutter generators are direct conversion technologies and have no rotor, bearings, or gears. While scaling down wind turbine generators is a nontrivial task, small aeroelastic flutter generators are very simple devices. According to the developer, who named this technology “windbelt,” these systems can be

manufactured for energies ranging from one milliwatt to a few megawatts, and the manufacturing cost of a low power device can be as low as a few dollars [38].

Wind flutter generators have fewer moving parts than turbine generators, and this can provide an advantage in cold climates. Although wind turbine generators are already being used for arctic applications [1], they tend to suffer from ice riming and ice accretion. Because the smallest energy generators available on the market are oversized for the energy requirements of weather monitoring stations, the use of wind flutter generators in cold environments should be studied.

3.1.3.3 Thermal

The energy in thermal gradients can be exploited in the arctic, especially when a natural source of thermal energy is present [20]. The efficiency of these systems is usually very low and grows as the thermal gradient becomes larger [25]. Theoretically, any temperature gradient can be used to generate electricity using the Seebeck effect [20]. Thermocouples are the most common thermal transducers and are based on the Seebeck principle. Their output is a direct current that is directly related to the difference in temperature between two electrodes. Another transducer, based on a different approach, is a piezoelectric material that is excited by means of thermal expansion cycles [25], delivering an alternating current signal. These generators can be used for low power applications, with the advantage that thermal gradients often occur naturally.

Energy chips are thermoelectric generators that can be candidates to power equipment in cold regions [39]. They are based on thermionics and thermotunneling principles and require a temperature gradient to operate. According to the developers, these devices have energy densities of up to 10 W/cm^2, but the power output actually depends on the temperature difference between the “cold” and “hot” sides. Energy chips have reached a

precommercialization stage, and other companies offer similar products as well [40, 41].

The use of thermoelectric generators in cold regions is currently theoretical. Temperatures below the earth's surface (soil or ice) are almost constant throughout the year, and a temperature gradient with ambient air or surface objects can be produced. Since the temperature of air depends on weather conditions, the production of electrical energy would be subject to the same rules as wind and solar generators. Unfortunately, there is a lack of information about the use of thermoelectric generators at low temperatures.

3.1.4 Comparison of Energy Systems

Potential power sources for stand-alone equipment used in cold environments were discussed in previous sections. They include chemical batteries, solar panels, wind fluttering generators, thermoelectric generators, fuel cells, microengines, and radioactive batteries.

Batteries can be used to store excess energy harvested from the environment or produced by a fuel generator. The stored energy is employed when the environmental source is not able to meet the system's requirements. For this reason, chemical batteries play an important role in power sources intended for arctic applications. Table 3.3 compares the performance of several battery chemistries at room and low temperatures [42]. Lithium-ion and nickel-metal hydride batteries have considerably higher energy densities than lead-acid batteries at room temperatures. This advantage greatly diminishes at low temperatures and the energy densities of all chemistries are very similar at -20 °C. Lead-acid batteries are widely used in cold climates because they have an acceptable performance at low temperatures and they are affordable.

Table 3.3 Parameters of chemical batteries used in cold environments.

Parameter	Lead-acid	Ni-MH	Li-ion
Specific energy @ -20°C (Wh/kg)	30	50	30
Volumetric energy density @ -20°C (Wh/l)	55	115	50
Specific energy 23°C (Wh/kg)	45	>55	70
Volumetric energy density @ 23°C (Wh/l)	85	>125	110
Operational @ -30°C	Yes	Yes	Yes
Charge acceptance @ 0°C	Medium	Medium	Good
Self-discharge 100-50% SOC @ 23°C (months)	15	12	20
Life span (years)	4	>5	>5
Cost	Low	High	High

Table 3.4 presents some characteristics of potential low power sources for cold climates. While some sources provide stable and predictable power, others behave stochastically. Energy harvesting sources can be classified in the following way [43]:

- *Uncontrollable and predictable*. These are sources that can be modeled but they cannot be forced to produce energy at will, e.g., solar energy.
- *Uncontrollable and unpredictable*. Such sources are hard to model for practical purposes. Similar to the previous group, they cannot be forced to generate energy at will, e.g., some sources of vibrational energy.
- *Fully controllable*. The energy can be produced at will, as in self-powered flashlights.
- *Partially controllable*. One example is radio frequency identification (RFID) systems where the RF source is well known but the final amount of energy that the tag receives depends on factors such as distance to the source.

Therefore, the nature of the energy harvesting source has a direct impact on the energy management strategy. For instance, some energy management strategies use a model of the energy source to predict the energy availability at any given time [44]. Other important features of the energy source to consider are periodicity, output signal (direct or alternating current), and voltage-current characteristic (for maximum energy point operation). Reviews of energy harvesting systems and energy management issues are presented in sections 3.2 to 3.5.

Table 3.4 Characteristics of potential energy sources for cold climates.

Energy Source	Generator	Periodicity	Output	Secondary Storage Required	Voltage Regulation [25]	Commercial Availability [25]
Solar	Photovoltaic cell	Daily & annual	DC	Yes	Maybe	Yes
Wind	Flutter generator / Wind turbine	Daily (weak) & annual (strong) [45]	AC	Yes	Yes	Near [38]
Temperature gradient	Thermoelectric	Depends on source	DC	Yes	Maybe	Yes [39-41, 46]
Hydrogen	Fuel Cells	N/A	DC	No*	Yes	Yes [23]
Tritium	Radioactive Battery	N/A	DC	No*	Yes	Near [29]

* The use of a storage device can provide some advantages.

3.2 Energy Harvesting Systems

Energy harvesting (or scavenging) systems and fuel generators that can be used in arctic applications were introduced in section 3.1. Energy harvesting is a practical approach that does not rely on fuels; hence, the focus of the thesis is on solar and wind energy production for stand-alone equipment deployed in cold regions.

Energy harvesting power sources can provide unlimited amounts of energy over the long run, but they usually fail to provide the instantaneous energy that electronic systems require. Therefore, a balance between the energy source and the load is essential, and the energy source should not be considered as a separate entity. A better approach is a global view of the harvesting source and the load: an energy harvesting system.

A viable energy harvesting system is efficient. The system efficiency involves all the components: the energy source, the energy transducer, the energy converter, the storage, and the load (typically, electronic circuitry, transducers and actuators). Power conversion, transfer, buffering, and consumption must be accounted for in the design of EHSs [47]. It is important to note that a system that operates with both highly efficient and nonefficient subsystems is simply nonefficient, e.g., a piece of hardware with low energy efficiency will drain energy from a highly efficient power source. Since trade-offs exist between the environmental energy source, the energy harvester, the power conversion, the energy storage subsystems, and the load, energy management is a difficult task [30].

Traditional energy management schemes might not be suitable for energy harvesting systems. Although some concepts of classical energy management can be applied to power harvesting systems, the dynamics of harvesting systems are very different (an energy harvester cannot produce electricity at will). This leads to a specialized research field of *harvesting aware power management* (HAPM). Section 3.5 introduces this topic.

Figure 3.2 shows a basic scheme of an EHS with two sources. Note that energy sources of different natures can be used to extend the power generation capabilities. However, this comes with a cost: synchronization of the energy sources with the rest of the system is required.

An energy harvesting power source has the potential to produce an unlimited amount of electrical energy. Thus, the lifetime of an EHS is limited only by an eventual component failure. But energy harvesters can supply energy only while the excitation is present, and there is a need to design energy-balanced systems (see section 1.4) [48]. Another issue is that the electric output signals of energy transducers often need power conditioning—i.e., electronic loads require a stable direct current signal. Accordingly, proper conversion (rectifiers, step-up or step-down converters) and storage devices (batteries,

capacitors, or ultracapacitors) have to be added to the system along with a consistent energy management strategy.

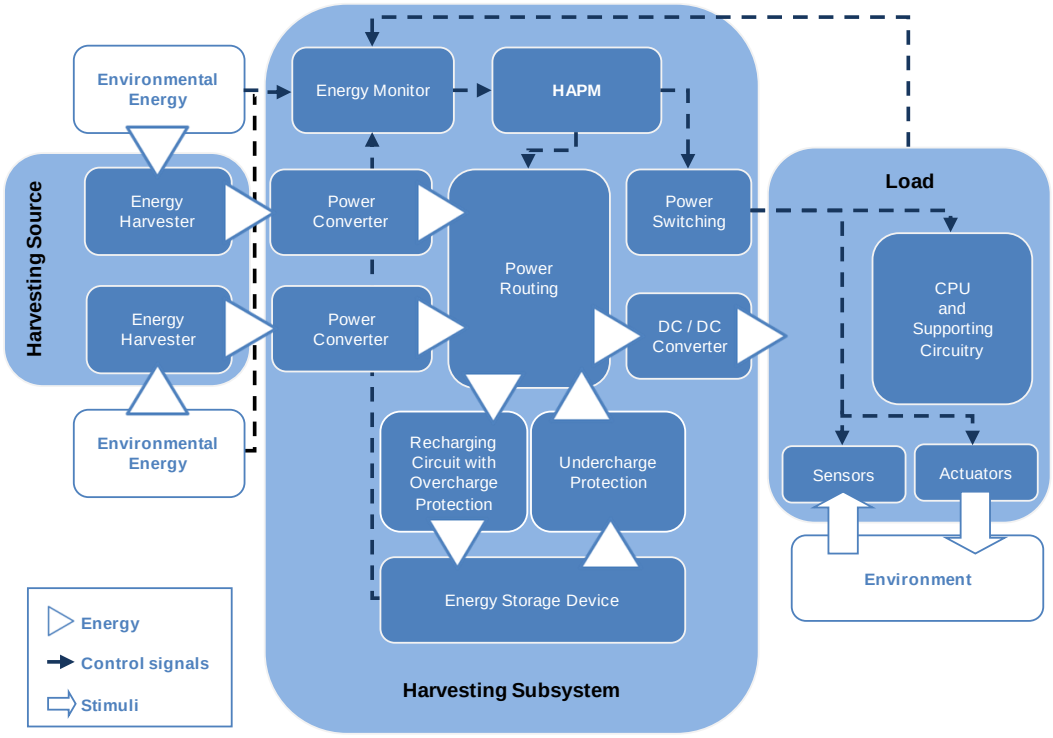

Figure 3.2 Diagram of an energy harvesting system.

Several strategies can be used to improve the efficiency of an EHS. They range from energy availability prediction for duty cycling tuning [44] to maximum energy point tracking subsystems to maximize energy transfer from the harvester to the load [35]. These techniques can be further optimized when combined with the proper hardware [49]. Although these methods address only some aspects of the HAPM problem, they can be combined and improved to boost the system's overall efficiency. Thus, a global vision of the system is necessary in the design of successful HAPM schemes.

This section provides insight into fundamental configurations of EHSs and introduces the main components of their subsystems: the *harvesting source*, the *harvesting subsystem*, and the load. "Understanding" the hardware is

essential in HAPM design since energy management issues are better dealt with when the characteristics of the hardware are considered.

3.2.1 Environment Powered versus Battery Powered

HAPM takes into account an extensive set of challenges compared to battery aware power management (BAPM). BAPM strategies are usually simpler and are normally based on the battery's state of charge [50]. In contrast, HAPM must be studied from a systems perspective: a device's HAPM strategy should account for all the components of the system and their modes of operation [30].

EHSs do not necessarily depend on batteries for functioning. Instead, batteries can be used as energy reservoirs that can be recharged using harvested energy [25, 51]; the stored energy will be useful when the excitation energy from the source is absent. Other options include ultracapacitors as energy reservoirs [30, 34, 47, 52, 53] and hybrid battery-ultracapacitor systems [30, 53]. Battery-less devices are possible for systems designed to operate when harvested energy is available [35]. Each configuration involves its own trade-offs and appropriate HAPM techniques should be integrated.

Compared to batteries, which can supply relatively high power (bursts), energy harvesters have a limited power output (*cf.* Table 3.2) and the instantaneous power that they can deliver is directly linked to the characteristics of the energy source. However, the amount of energy that can be delivered by an energy harvester in a "perpetual" mode of operation is "infinite." HAPM strategies need to deal with these facts, and their goals should be minimization of energy loss, implementation of an energy-neutral mode of operation (see section 1.4), and assurance that the system works at the desired utility level.

Despite the notable differences, BAPM can be seen as a subset of HAPM techniques. Many techniques already in use in battery systems can be

employed or adapted to HAPM, e.g., duty cycling and dynamic voltage scaling (see section 1.5.2.2) [44]. Conversely, HAPM methods can be used to minimize the energy consumption of battery powered devices [49].

3.2.2 Topologies

There are three relevant topologies for EHSs. It is important to establish the peculiarities of each since the HAPM design goals need to be adjusted according to the characteristics of each system.

3.2.2.1 Secondary Harvesting System

If a battery is the main source of energy, the harvesting device plays a secondary but important role. A HAPM policy for this configuration should limit battery energy usage in order to increase the system's lifetime—i.e., by making external recharging or replacement of batteries less frequent [43]. A primary or secondary (rechargeable) battery can be employed, and the harvested energy can directly or indirectly energize the load or specific subsystems. An example can be found in [54].

3.2.2.2 Autonomous Harvesting System

Autonomous harvesting systems are battery-less. Their energy requirements are entirely met by the energy harvesting subsystem [35]. An autonomous harvesting system can operate (only) when the energy source is available, but the system's lifetime and performance are not limited by battery inefficiencies—i.e., aging, self-discharge, and round-trip efficiency. The energy neutrality principle (see section 1.4) is inherent since the system can never consume more energy than the harvesting device is able to deliver. The HAPM strategy for autonomous systems should ensure that the purpose of the system is met while it operates within a variable energy environment [55].

3.2.2.3 Autonomous Hybrid Harvesting System

In the most common scenario, the battery plays an important role as an energy reservoir and the harvesting device collects energy for system

operation and battery recharging [20, 30, 34, 44, 47, 49-53, 55-59]. This topology can dramatically increase the system's lifetime and can offer a 0% dead time operation when proper HAPM techniques are implemented [56]. The battery and the energy harvesting device are sized to satisfy the system's energy needs, and the enforcement of the energy neutrality principle (see section 1.4) is recommended [55]. The system can sometimes consume more energy than the harvesting source provides (using battery reserves), but the production/consumption rates have to be balanced over the long run. This can be the most successful implementation, since it can cope with battery deficiencies and at the same time with the unpredictability of the harvesting source [43]. AWSs that use solar panels for electricity generation are autonomous harvesting systems, and a special accent on this topology is given in the next sections.

Finally, autonomous harvesting systems have three design considerations: *lifetime extension*, *energy-neutral operation*, and *maximum performance* [43]. These design considerations reflect the fact that the performance of a harvesting system closely depends on both the energy usage and the profile of the energy source.

3.2.3 Subsystems

Figure 3.2 shows the main components of an energy harvesting system. Although a harvesting system does not necessarily include all the components that are shown in the scheme, the HAPM strategy should be strongly tied to the hardware configuration. In this section, a description of the different subsystems of an EHS is provided.

3.2.3.1 Harvesting Source

Possible harvesting sources and energy transducers for AWSs and their main properties were identified in section 3.1.3. The energy harvester refers to the device that extracts environmental energy (electromagnetic, thermal, or mechanical) and converts it to electrical energy [43]. One energy harvesting

system can extract energy from different sources and use distinct transducers for this purpose. This can lead to higher system performance but it increases the HAPM complexity. For example, two different transducers can be used to harvest energy from the same vibrational source [52], or solar and wind energy can be used to energize a single system.

Some examples of energy transducers are piezoelectric generators, photovoltaic panels, magnetic generators, and thermopiles. These components deliver either AC or DC signals (*cf*. Table 3.4), which often need conditioning before they can energize electronic circuits. Usually, the conversion efficiency of energy harvesters is very low and the recovered electrical energy needs to be wisely employed.

3.2.3.2 Harvesting Subsystem

The harvesting subsystem is composed of several modules. Some distinctive components of this subsystem are described in [57], and an extended list is provided here.

3.2.3.2.1 Harvesting Aware Power Management

The HAPM module is the core of the harvesting subsystem [30, 43]. It gathers information provided by the energy monitor, and decides whether to use environmental energy or energy reserves to feed the load; it also controls energy routing. Naturally, both the harvesting source and the load have distinct production and consumption profiles. Energy production will not always match consumption, hence the need for HAPM. The main goal of HAPM is to "satisfy the energy consumption profile from the available generation profile" [43].

The HAPM subsystem sends control signals to the load through the energy switching module so that the energy consumption can be matched to the production profile (using techniques such as duty cycling). It can also take in charge active energy converters and energy storage management.

Frequently, resources of the main CPU (load) are reserved for HAPM tasks [57]. Alternatively, a dedicated circuit can be used for this purpose [55].

3.2.3.2.2 Energy Monitor

The energy monitor measures and analyzes key parameters of the power source, the energy storage, and the load. The data collected help to make energy routing and scheduling decisions and can be used to create a model of the environment [55], which is exploited by the HAPM algorithms.

3.2.3.2.3 Energy Switching

As described in [57], this module distinctively energizes or deenergizes some of the load's components, depending on the energy profile. This allows energy savings by shutting down submodules that do not need to be in continuous operation. For example, duty cycling a sensor can significantly reduce energy consumption [49].

3.2.3.2.4 Energy Converters

Energy harvesting systems use energy converters to generate electric signals that are required by different electronic modules or devices. As they represent another source of energy loss, care must be taken in their choice and design. Power conditioning is required to convert AC signals into DC signals, to scale DC signals up or down, to regulate unstable signals, and to implement maximum energy point tracking systems that actively match impedances [47].

Energy conditioners can be used to recharge a battery and to provide an adequate electric signal to the load (electronic circuitry). There are two ways to transfer energy to the load: direct and indirect. Direct feeding occurs when the energy produced by the transducer is conditioned and used to power the load; indirect feeding refers to the conditioning of the electric signal coming from an energy storage device.

Active energy converters can improve the efficiency of the energy harvesting process—to obtain the most energy possible from the source. In this case, the HAPM module can generate control signals that efficiently convert energy according to the system status [60]. For example, [34] used charge pumps and a MPPT-based energy management strategy to maximize energy transfer from the source to the load.

3.2.3.2.5 Energy Routing

The energy routing module directs energy from the environmental source to the load and/or to the storage device, and from the storage device to the load. The HAPM module provides the control signals that achieve these tasks.

3.2.3.2.6 Energy Storage

In most situations, scavenged energy is of a discontinuous nature, and two distinct operation modes are possible: (1) If the harvesting power source produces more energy (on average) than the load can use, then the operation can be continuous. (2) If the source produces less energy than the load's consumption, the operation *has* to be discontinuous [20]. In both cases, a storage device might be required to supply energy when it is needed. Most harvesting systems can rely on a battery for energy storage purposes (as mentioned in section 3.2.2, harvesting systems that do not use a storage device are a special case). The HAPM should take into account factors such as the chemistry, the energy rating, and the capacity of the storage element.

Rechargeable batteries are the most popular energy storage devices. They are suitable for long term storage but have problems such as aging and rate capacity effects [47]. Another choice can be ultracapacitors or supercapacitors. They can buffer transient energy but have limited energy capacity, high leakage rates, and are expensive [47].

3.2.3.2.7 Charging and Overcharge Protection

Batteries are more efficient when they are charged and discharged using appropriate protocols that depend on the chemistry of the battery. For

example, overcharge can lead to premature aging or damage to the storage device [57]. For harvesting systems that rely on batteries, preventing battery degradation is essential, as a worn-out battery will have an impact on the operational life of the entire system.

3.2.3.2.8 Undercharge Protection

The charge of the battery should be prevented from decreasing below a critical limit. For some battery chemistries, such as lead-acid, deep discharge cycles will lead to premature or permanent damage of the cell [55].

3.2.3.3 Load

The load is the heart of the application, while the power source is formed by the harvesting source and the harvesting subsystem. A typical load consists of a processing unit, transducers, and actuators that interact with the environment. To implement HAPM schemes that achieve the required goals, the load must be harvesting aware designed, e.g., a sensor that supports low energy modes (idling or sleeping) is a good candidate for a power management strategy based on duty cycling.

The load can operate continuously or discontinuously, depending on the nature of the energy source and on the configuration of the system. The load is the system that is powered by the harvesting source. It is mainly composed of electronic circuits, transducers, and actuators. Low-energy devices are suitable for these applications, since the amounts of energy that can be harvested are normally very low. Examples of loads not related to AWSs are security devices, medical implants, HVAC (heating, ventilation, air conditioning) control systems, and automatic metering systems [61].

The energy management strategy is also closely related to the profile of the load. The main goal of the HAPM is to keep the system (load) running at peak performance and in compliance with the energy neutrality principle; that is, the load cannot consume more than the harvesting device can produce, and

the source should not produce electrical energy in excess of the load's requirements.

3.2.4 Applications

It is now clear that AWS powered by local sources of energy can be studied from the perspective of an energy harvesting system. The AWS has a load (data logger, sensors), and the power source is typically a solar panel and a secondary battery system. Hence, the design of an AWS can benefit from the use of HAPM philosophy. Energy systems from ultra low power devices (medical implants) to high power applications (energy efficient buildings) share the same structure overall, and can be classified as EHSs.

Most HAPM research publications deal with wireless sensor networks. Some applications include structural health monitoring, embedded test and evaluation, and condition based maintenance [49]. However, HAPM can successfully be applied to systems that share similar hardware architectures and that use an energy harvesting power supply. Actually, battery powered systems can be redesigned to benefit from energy harvesting sources. Some examples mentioned in the literature include wearable devices[20] and computers [30], radio-frequency-identification (RFID) tags [54], biomedical implants [47, 62], sensor-actuator [17] and wireless networks [59], mobile devices [17], embedded systems, and microelectromechanical systems (MEMS) [51].

Currently, there are several energy harvesting systems on the market or under research and development, such as passive RFID systems, personal digital assistants (PDAs), radios, chargers for cell phones, flashlights, and watches. They use electromagnetic, photovoltaic, thermoelectric, and piezoelectric energy harvesting principles. The energy sources can be human active or passive (such as kinetic or thermal), thermal gradients, radio signals, sunlight, and ambient vibrations [17].

3.3 Energy Harvesting Theory

Energy harvesting theory is a valuable tool in energy harvesting design. Several energy harvesting theories have been suggested [43, 53, 55], and the one presented here is based on a flexible approach that can be used to model a wide range of energy systems and provide a basic level of understanding about them. The theory serves as an introduction to the energy-neutral operation theory described in section 3.4. Both energy harvesting theory and energy neutrality theory can be used to model AWS systems.

The analytical model described below represents a harvesting device (transducer) and a storage device. It is a simple model that can be adapted to power sources of very different natures, from stochastic to periodic. A consumption model is also presented along with two important theorems [55].

3.3.1 Sources

$P(x)$ is a continuous and bounded function of a continuously varying parameter x. $P_S(x)$ is a $(\rho, \sigma_1, \sigma_2)$ – source if and only if, for any finite real number X it satisfies [55]:

$$\int_0^X P_S(x)dx \geq \rho T - \sigma_1 \tag{3.1}$$

and

$$\int_0^X P_S(x)dx \leq \rho T + \sigma_2. \tag{3.2}$$

A method to determine σ_1 and σ_2 from practical measurements is given in [55]. The *Sustainable Performance at Eternity Theorem with Constant Power Consumption* is presented next.

If a device is supplied energy by a $(\rho, \sigma_1, \sigma_2)$ – source, operates at constant energy ρ, and has an energy storage capacity of $\sigma_1 + \sigma_2$, then the device fully utilizes the energy source and can operate forever [55].

3.3.2 Consumers

A device is said to be a (ρ', σ) – consumer if its power consumption $P_C(x)$ satisfies the constraint:

$$\int_0^X P_C(x)dx \leq \rho' X + \sigma, \tag{3.3}$$

for any value of X [55].

The *Sustainable Performance at Eternity Theorem with Variable Consumption Profile* is formulated as follows: If a (ρ', σ) – consumer device is powered by a $(\rho, \sigma_1, \sigma_2)$ – source, has an energy storage capacity of $\sigma + \sigma_1 + \sigma_2$, and

$$\rho' < \rho, \tag{3.4}$$

then the device can operate forever [55].

3.3.3 Discussion

Note that the capacity of the storage element is derived directly from theory. As stated in [55], harvesting theory can help "to determine performance levels given the energy source classification." Furthermore, the authors maintain that their work can be useful to answer some fundamental questions of HAPM, such as:

- What is the minimum latency for a particular application in a given energy environment?
- What performance level can a system achieve if it must survive eternally from environmental sources?
- What additional resources may be needed if a particular quality of service must be achieved?

Answers to those questions are outlined in the next paragraphs [55]. The average available energy can be predicted from ρ. If P is the maximum energy that the load can draw, then two possible scenarios where the device can operate indefinitely are possible:

1) If $P > \rho$ and the system has a storage device of capacity $\sigma_1 + \sigma_2$.
2) If $P < \rho$ and the load can be *forced* to behave as a (ρ', σ) – consumer, thus matching the average power consumption with ρ'.

Power consumption reduction can be obtained by duty cycling the load. In the case that the maximum achievable duty cycle would not be able to yield the expected benefit from the system, this theory can be used to find an adequate "performance – resource" balance. A simple application example is proposed in [57].

3.4 Energy Neutrality Theory

Energy neutrality [43, 44, 47, 50, 56, 63], also called balancing of the "energy check book" [49], means that in order to operate indefinitely, a system cannot consume more energy than the harvesting source can provide (on average). If consumption exceeds production, the system will deplete its energy resources and stop working. This situation reduces the performance of the system.

The *energy-neutral operation theory* [43] is an extension of the energy harvesting theory [55] presented in section 3.3. This updated theory has been published in [44, 47, 50] and referenced in [53, 56, 63, 64]. The main improvement is that the nonidealities of energy storage devices are considered, leading to a more robust tool. Both sources and consumers are modeled using the same mathematical model. The notation from the original publications has been changed to provide a uniform version of both the energy-neutral and the energy harvesting theories, and to avoid confusion.

3.4.1 Conditions for Energy-Neutral Operation

The following three conditions guarantee an energy-neutral operation in terms of power output from an energy source $P_S(x)$ and power consumption $P_C(x)$ [43]. Refer to sections 3.1.3 and 3.1.4 for information on the energy sources.

- Autonomous harvesting system: This is the simplest case. A disadvantage is that if the consumed energy is less than the energy produced, the excess energy will be lost. The condition for energy-neutral operation requires that:

$$P_S(x) \geq P_C(x). \tag{3.5}$$

- Autonomous hybrid harvesting system *with ideal energy storage device*: The difference from the previous case is that excess energy is stored in an ideal energy storage device with a round trip efficiency of one and null leakage. The initial stored energy is B_0 and the energy-neutrality condition is satisfied if (for $X \geq 0$):

$$\int_0^X P_C(x)dx \leq \int_0^X P_S(x)dx + B_0. \tag{3.6}$$

- Autonomous hybrid harvesting system *with nonideal energy storage device*: The storage device has limited capacity, its round-trip efficiency (η) is less than one and leakage is considered. The function $[x]^+$ is the Heaviside function of x multiplied by x— i. e. , $H(x) \times x$. The condition, without taking into account the energy storage device capacity, is:

$$B_0 + \eta \int_0^X [P_S(x) - P_C(x)]^+ dx - \int_0^X [P_C(x) - P_S(x)]^+ dx - \int_0^X P_{leak}(x)dx \geq 0. \tag{3.7}$$

In addition to this condition, if excess energy cannot be wasted and storage capacity is considered, the following condition must be met:

$$B_0 + \eta \int_0^X [P_S(x) - P_C(x)]^+ dx - \int_0^X [P_C(x) - P_S(x)]^+ dx - \int_0^X P_{leak}(x) dx \leq B. \tag{3.8}$$

Using the same notation as for the energy harvesting theory presented earlier, the *energy-neutral operation theorem* can be summarized as follows: if a (ρ', σ) – consumer device is powered by a $(\rho, \sigma_1, \sigma_2)$ – source, the energy storage device has a capacity B, an initial stored energy B_0, a round-trip efficiency η, and a leakage ρ_{leak}, and if:

$$\rho' \leq \eta\rho - \rho_{leak}, \tag{3.9}$$

$$B_0 \geq \eta\sigma_2 + \sigma, \tag{3.10}$$

$$B \geq B_0, \tag{3.11}$$

then, the device is able to operate in an energy-neutral mode [43].

This theory can help to determine the energy storage device characteristics and the achievable performance level [43]; it is also a valuable design tool for EHSs. Energy management strategies for EHSs are introduced in the following section; the energy-neutral operation theorem can assist in the design of robust energy management strategies for energy harvesting systems.

3.5 Energy Management

HAPM is an emerging research field, and is a key feature in harvesting aware design. Harvesting aware design is the fourth step in the development of energy optimization techniques, after low power design, power aware design, and battery aware design [30]. The design and operation of harvesting powered devices differ in several aspects from the design of

battery powered devices. This is mainly due to the energy harvesters' low power output [25, 30], and to the irregular nature of energy harvesting sources [30, 53, 54, 56, 57]. In this thesis, the concept of HAPM is extended to energy management since this approach is aligned with the operation of AWSs in arctic regions. In most chapters both concepts are used without distinction.

A good HAPM strategy allows a system to operate in an energy-neutral mode [44]. This means that the system has neither excess nor shortage of energy—i.e., the "energy check book" is balanced [49]. Indeed, a system that satisfies this property can operate "indefinitely": as long as it is necessary or as long as the system's hardware lifetime permits. The energy-neutral operation theory was discussed in section 3.4.

3.5.1 Hardware Requirements

Typically, an electronic system consumes more instant energy than an energy harvesting source is able to deliver. Following the energy harvesting theory presented earlier, a device can operate continuously only when power production is equal to or superior to power consumption. When consumption is higher than production, the system might fail to operate at the desired utility level. Thus, matching average energy production with average energy consumption is an essential issue. This can be achieved with the help of energy storage devices and with the use of energy management techniques. A harvesting-friendly hardware environment facilitates the implementation of energy management schemes. For example, the popular technique called "duty cycling" requires the use of hardware that supports sleeping modes. Besides the CPU, some supporting circuitry (analog-to-digital converters), sensors, and actuators (like radio frequency transmitters) can also be duty cycled [49, 59]. HAPM applications are usually based on duty cycling techniques; hardware with advanced features, such as dynamic voltage scaling (DVS) (see section 1.5.2.2) and dynamic frequency scaling

(DFS), opens the door to energy management strategies that can increase the functionality of the harvesting system.

3.5.2 HAPM Strategies

As implied earlier, a successful HAPM is not trivial, as it must take into account all aspects of the system. This starts with the problem of predicting future energy availability, and includes efficient power conversion algorithms, scheduling, duty cycling, etc. The energy management strategy has to be closely tied to the hardware configuration, e.g., in a system with high-end and low-end processors, the energy management algorithm should be designed to exploit this architecture in order to reduce energy consumption [59]. Table 3.5 summarizes some harvesting power management strategies found in the literature.

Table 3.5 Harvesting aware power management strategies.

Perspective	Strategy
System	Duty cycling Adaptive duty cycling Dynamic voltage scaling (DVS) Dynamic frequency scaling (DFS) Dynamic voltage and frequency scaling (DVFS) Maximum energy point tracking
Peripherals [53]	Adaptive sensing rate Adaptive memory management
Sensors [49]	Turn on energy to the sensor only when sampling Turn on energy to the signal conditioning only when sampling a sensor Sample the sensor(s) only on event Reduce the sensor sample rate to the minimum required by the application Sleep between samples Scalable fidelity
RF transceivers [49]	Reduce the amount of wireless data transmitted through data compression/reduction Lower the transceiver duty cycle and frequency of data transmissions Implement strict energy management – use energy down and sleep modes Implement an event-driven transmission strategy – transmit only on sensor event(s)

3.5.2.1 Duty Cycling

Duty cycling is the energy management technique most commonly cited in the energy harvesting literature [44, 47, 50, 53, 56, 65, 66]. This can be

attributed to the fact that embedded systems (or some of their components) frequently support *sleeping* modes, making duty cycling a direct approach. The simplest, static implementation of this technique is to set a fixed duty cycle so that average energy consumption matches average energy production.

A dynamic energy management scheme can improve overall system performance, compared to the static approach. Assume that the system has a fixed duty cycle. If the power source is providing abundant energy (more than the energy consumed), excess energy will be stored until the storage element has reached a full charge. In the opposite scenario, if energy production is less than energy consumption, the system will eventually deplete the storage reserves and stop working. A dynamic approach can cope with both scenarios, extending the device's functionality. When the source is able to provide excess energy, a dynamic algorithm can increase energy consumption by allowing a high duty cycle. The system's workload will be higher during this period: this is a good time to process data, to transmit data, or to increase the sampling rate. When the energy availability is low, the system should be kept working at a slow pace to avoid a power shortage.

Similar remarks apply to the voltage and frequency scaling presented in the next section. A dynamic (or adaptive) energy management strategy is a good choice for energy harvesting systems. Such systems rely on variable energy sources and the dynamic strategy can match energy consumption and generation in real time, while assuring the highest possible workload.

One of the first publications to present a duty cycling algorithm in a HAPM environment departed from the simple harvesting theory (without accounting for storage inefficiencies), calculated a sustainable duty cycle, and showed that the system could operate without depleting its energy storage during a trial period of time [55].

This work is extended in [44], where an adaptive duty cycling algorithm is presented using the updated energy neutrality theory (accounting for storage inefficiencies). This approach allows the achievement of an energy-neutral mode of operation. The performance of the system is maximized and the adaptation to the dynamics of the energy source is made in real time. The energy management strategy predicts the energy availability and adjusts the duty cycle accordingly. The adaptive algorithm makes use of the available energy at almost the same level as the proposed theoretical optimum. A naive approach is shown to perform poorly, especially when the round-trip efficiency of the storage device is low.

Systems described in [44, 55] require up-front characterization of the energy environment, which is not valid once the environment changes [55]. In addition, the adaptive algorithm used in [44] relies on a model of the energy source, making this approach hard to extend to other energy scenarios, e.g., different transducers or energy sources. To overcome this problem, a model-free adaptive duty cycle algorithm supported by adaptive control theory is proposed in [56]. The algorithm can handle periodic and aperiodic energy sources, requires modest computational resources, provides a 0% dead time, and is able to reduce the duty cycle variance.

An adaptive duty cycling technique that allows the efficient detection of events while maximizing the system's lifetime is proposed in [65]. Based on probability theory, the system uses a wakeup protocol that can be used in wireless sensor nodes that form part of a sensing network. The duty cycle of every sensor is reduced without compromising the efficient detection of events.

3.5.2.2 Dynamic Voltage and Frequency Scaling

Dynamic voltage scaling (DVS) and dynamic frequency scaling (DFS) are often depicted as advanced energy management techniques in the HAPM literature. However, to our knowledge, no research has been published on

these topics. The apparent lack of popularity of these techniques is due to the fact that they require hardware specifically designed to support their particular modes of operation. Despite this added effort, both scaling techniques can be useful in HAPM design. A brief review of these approaches is presented below.

The basic premise of DVS is that increasing a circuit's voltage allows it to switch faster, albeit with an increase in energy consumption. The opposite holds when voltage is decreased. An increase or decrease in clock frequency has a similar effect. A combination of DVS and DFS (DVFS) is also possible. The advantage of these techniques is that when the energy availability is low, they allow the system to keep running at a low pace and with reduced energy consumption, without compromising the execution of important tasks. In comparison, duty cycling completely stops all tasks during the sleeping mode. In some cases, all three techniques can be used together.

DVS and DFS can be used as a means to reduce energy consumption of biomedical devices powered by harvested energy [62]. An example of dynamic energy management using DVS for battery powered systems can be found in [67]. A similar approach can be used for harvesting systems. For example, a DFS-based energy management strategy has been used to reduce the energy consumption of a computing system [68]. These techniques can also be used at an AWS, provided the data logger supports these advanced functions. A general view of DVFS can be found in [69].

3.5.2.3 Maximum Power Point Tracking

Maximum power point tracking (MPPT) allows the maximum energy to be transfered to the load. Energy transducers, such as solar panels, have a dynamic voltage-current characteristic, where the optimal load for maximum energy usage depends on the operation point. MPPT requires monitoring of the incoming energy to determine the optimal operation point, and an adaptive load. Several strategies can be used to provide the optimal load. For

example, the HAPM module can decide to route more or less energy to the battery, to adjust the duty cycle or the workload.

An MPPT energy management system for solar energy harvesting devices is proposed in [34]. The energy converter is a charge pump with operation frequency adjusted in order to deliver maximum energy to the load (battery or electronic circuitry). Related work is presented in [35]. To operate at the maximum energy point, a power management unit determines the operation point and adjusts the load accordingly. To "generate" the required load, the energy management module can make use of one of two different strategies or can combine both. The first strategy adjusts the duty cycle of the system so that the average energy production "matches" the desired load. The second strategy turns on and off different modules of the system; the modules that are on will be equivalent to the targeted load, e.g., turning on the satellite transmitter and using it to transmit buffered data will increase the load of the system.

3.5.2.4 Energy Management for Peripherals

Energy management for peripherals can also be referred to as dynamic power management (DPM) [70]. A rich list of strategies that can be applied to sensors and RF transceivers for the purpose of reducing energy consumption is presented in [49] and some approaches relevant to HAPM are described in Table 3.5. The importance of sensor energy management is pointed out in [59]: some sensor subsystems consume considerable amounts of energy, e.g., sensors that need high rate and high resolution A/D converters, sensor arrays, and active transducers. Two methods are proposed to reduce energy consumption of such sensors: scalable fidelity and shutdown. The main idea behind these approaches is that sampling should be done "only if needed, when needed, where needed, and with the right level of fidelity" [59].

A power management strategy for peripherals that is able to adapt to the parameters of a system is presented in [53]. In particular, the algorithm is

shown to dynamically manage the sensing rate and the memory management (data transmission) of a sensor node. Approaches like this can be exploited by automatic weather stations whose ultimate goal is data sampling.

3.6 Simulation Tools

The purpose of the systems, theories, and techniques discussed in this chapter is to assist in the design of factual energy harvesting systems. Whether it is an AWS or another kind of application where an energy harvesting approach can be applied, the use of simulation tools is an important step. Simulations can provide important information about the feasibility and reliability of a system before it is actually built. For example, sizing of the power source, testing of energy management algorithms, and assessment of worst case scenarios can all be done through simulations.

A simulator is built on models of the different components of the harvesting system, which include but are not limited to energy sources, energy modules, and loads. Creating a simulator from scratch is a difficult task, but sometimes it is the only way to deal with specialized systems or uncommon scenarios—such as AWSs deployed in arctic regions.

Several simulation platforms can be used to perform model-based simulations of EHSs and to assess the performance of HAPM algorithms. In the HAPM-related literature, it is common to find simulation results that were obtained with custom simulators: MATLAB®/Simulink® and PSPICE® or HSPICE for embedded systems; other platforms can be used as well.

However, some specialized simulators already offer the tools required by energy systems. For example, a power aware simulator for wireless sensor networks is presented in [71]. The simulation framework is based on the OMNeT++ discrete event simulator and has energy subsystem simulation capabilities. This framework appears to handle energy harvesting scenarios. With a proper understanding of the framework, the creation of custom models is possible, simplifying the construction of a working simulator.

A custom simulator is likely the best way to deal with energy systems in the arctic, as the equipment is subject to extreme weather conditions (e.g., very low temperatures) that seldom occur in other situations. Models that take into account these special considerations are normally not included with general purpose simulators.

Natural Resources Canada developed a flexible and modular MATLAB®/Simulink® library for photovoltaic systems: PV Toolbox [72]. The PV Toolbox was designed for research and development purposes and can be customized to suit the researcher's needs. It takes into account relevant phenomena for cold regions such as temperature dependencies and includes models of batteries, solar panels, energy converters, and controllers (among other items). However, it is only available for internal use at Natural Resources Canada [73].

Chapter 4 presents modeling aspects for different energy harvesting subsystems, with a focus on AWSs. In chapter 5, a simulator based on these models is outlined and simulation results are provided for an AWS with an intelligent energy management strategy.

3.7 Conclusion

Most of the research on HAPM is related to wireless sensor networks. A wireless sensor node is an embedded system, often subject to specific hardware, size, and energy constraints. However, the concepts presented in this chapter can be applied to any EHS. More specifically, the energy neutrality theory can be “scaled up” and applied to AWSs or other energy harvesting systems. When midpower or high power generation is considered, EHSs are commonly known as *renewable energy systems*.

Distinct technologies can be exploited to power stand-alone EHSs in arctic regions. They range from fuel generators to energy harvesting generators. EHSs work unsupervised and under harsh climatological conditions. Access to the areas where they are deployed is seasonal and expensive. Fuel

generators require refueling every season and harvesting devices can fail due to special weather occurrences, e.g., snow accretion. Therefore, there is no obvious choice between a fuel generator or a harvesting generator.

In section 3.2 energy harvesting generators were described with a focus on solar and wind approaches. A discussion on energy harvesting systems and theories was elaborated, energy management issues were considered, and simulation tools and simulation issues for EHSs were addressed.

Research opportunities in the field of HAPM include the nonntrivial combination and integration of several energy management techniques. Duty cycling, maximum energy point tracking, and DVFS can increase the performance of an energy harvesting system. Although solar energy harvesting recurrently appears in the energy harvesting literature, there are few studies on other energy sources (e.g., thermal) for which commercial generators are readily available. Multisource harvesting is another area of research worthy of further exploration. When two or more sources are used to extract energy from the environment, the energy management scheme has to be designed considering the intrinsic attributes of each energy source and the properties of the transducers used to generate electricity. Characteristics of the energy storage device and the load need to be taken into account as well.

Chapter 4 - Models of Monitoring Station Components

Application-specific hardware models are useful to design and validate HAPM strategies. Energy system models include information from energy sources, energy transducers, energy storage devices, and energy converters. The energy harvesting source can be modeled using real or synthetic data, and a model of the energy transducer is needed to estimate the power output. Transducers usually employ complex energy conversion mechanisms and they are hard to model. Empirical or mathematical models are used for modeling purposes and it is important to consider that the accuracy of the model will have an impact on simulation results.

Static models of the load are generally sufficient for HAPM purposes, unless the load presents special characteristics such as very high power requirements at start-up. In this thesis, energy generators are simulated using average hourly climatological data, and the effect of transients is not considered. Furthermore, in chapter 5, it is demonstrated that the AWS has an energy flow cycle of one year; hence modeling the dynamics of the system with high accuracy is not required, and the use of static models is a convenient way to shorten development and simulation times.

Models for generators and loads are covered in the literature related to HAPM. Although many of them are related to wireless sensor networks, these models are a good starting point for general energy harvesting purposes. For example, models for photovoltaic and thermoelectric generators are provided in [74] and [75], respectively. Models for electromagnetic and

piezoelectric transducers are provided in [52], and a general electrical model for energy harvesters is developed in [60]. Information on load modeling, particularly sensor node consumption, can be found in [49]. Problems specific to wireless communication subsystems are treated in [76].

AWSs in arctic regions face very different operation conditions than equipment operating in warmer regions. Commonly, models and simulators are obtained and designed with disregard of harsh environments. Specifically, solar irradiation models are not optimized for high latitudes, and battery models for very low temperatures are rare or non-existent [1]. This chapter describes the models that were used to program the simulator.

4.1 Wind Generators

Wind turbine generators are used for arctic applications [1], although they suffer from ice riming and ice accretion. Whenever the generator is affected by such phenomena it will malfunction or stop working. The smallest energy generators available on the market are oversized for the energy requirements of weather monitoring stations (50 W vs. 5 W). Although the recently developed wind flutter generators can also be affected by climatological issues, their use in cold environments should be studied. They are simple devices that can produce electrical energy at low wind speeds. To date, there is limited information on wind flutter generation issues, and models are non-existent in the literature. A first attempt to characterize these devices is accessible in [77]. This section presents a complete experimental study of a 50 cm wind flutter generator and proposes a linear model for electrical power generation.

4.1.1 Wind Energy

Wind carries kinetic energy that is transformed by the energy generator into electrical energy. Wind energy per unit of area (W/m^2) is calculated as

$$P_{W,T} = 0.5 \times \rho \times W_S^3, \tag{4.36}$$

where $P_{W,T}$ is the total wind energy (watts), ρ is the air density (1.225 kg/m^3 at sea level), and W_S is the wind speed (m/s).

Taking into account the active area of the generator and its efficiency, the output power delivered by a wind generator is given by

$$P_W = \eta_W \times g_{area} \times P_{W,T}, \tag{4.37}$$

where P_W is the power output of the generator (watts), η_W is the power conversion efficiency, and g_{area} is the active area of the wind generator (m^2).

4.1.2 50 W Wind Turbine Generator

A commercially available 50 W turbine generator (Rutland 503) for marine applications was selected for comparison purposes [78]. According to the manufacturer, the Rutland 503 turbine can be used for professional applications [79]. Although this generator is oversized for the reference AWS, a model is suitable to determine the generator's efficiency, which is later compared with the efficiency of the wind flutter generator.

The Rutland 503 generator has a swept area of 0.2 m^2 (blade diameter of 0.51 m) and delivers a 12–14 V signal, suitable to charge 12 V lead-acid batteries. A power curve based on the manufacturer's data is provided in Figure 4.1. The plot also shows a curve of the mathematical model (polynomial regression) represented by equation 4.38. For wind speeds lower than 3.6 m/s, the output power is 0 W and for wind speeds higher than 18 m/s, the generator will deliver a maximum energy of 55 W.

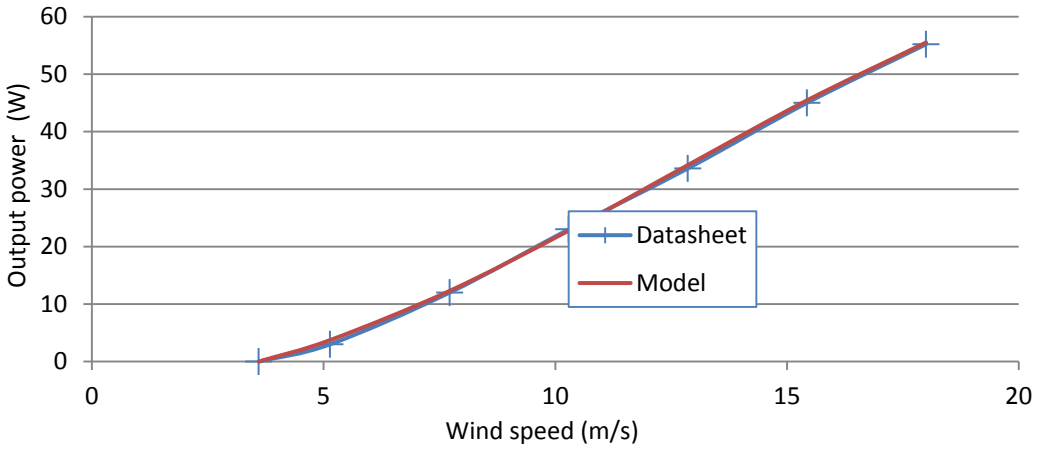

Figure 4.1 Rutland 503 generator energy curve.

$$P_{W,t} = -0.0103 \times W_S^3 + 0.3866 \times W_S^2 - 0.3578 \times W_S - 3.2417, \quad (4.38)$$

where $P_{W,t}$ is the energy generated by the turbine generator (watts) and W_S is the wind speed (m/s).

4.1.3 Wind Flutter Generator

The "windbelt" is a recently developed wind generator that relies on the aeroelastic flutter phenomenon. Unlike generators based on turbines, flutter generators are direct conversion machines and do not have a rotor, bearings, or gears. While scaling down a wind turbine generator is a nontrivial task, aeroelastic flutter generators appear to scale down easily. According to the developer, flutter generators can be manufactured for energies ranging from 1 mW to a few megawatts, and the manufacturing cost of a low power device could be as low as a few dollars [38]. Currently, the smallest low power commercial wind turbines are rated at 50 W, and their cost is around $600 [78].

To date, there is only one known scientific publication related to the wind flutter generator: the design and fabrication of a microscale aeroelastic flutter generator, along with experimental results, is presented in [80]. For macroscale flutter generators, the only source of (limited) information is the developer [38].

The design of harvesting systems powered by aeroelastic flutter generators requires accurate models. No sources of information regarding modeling of wind flutter generators other than [77] are known so far. In [77], an experimental approach is used to study a 50 cm prototype aeroelastic flutter generator. Characteristic plots obtained from experimental data are provided and a wind flutter generator model is developed.

4.1.3.1 Wind Flutter Background

In aeronautic and civil engineering fields, aeroelastic flutter effects are studied to avoid them [81], since they can cause catastrophic damage to structures such as airplane wings, suspension bridges, tall buildings, etc. However, the otherwise undesirable aeroelastic flutter can be used to generate electricity. The use of wind flutter generators in practical applications requires the study and characterization of the flutter effect and the surrounding energy conversion phenomena.

Flutter is a self-sustained oscillatory instability. For an airfoil that has both flexural and torsional degrees of freedom, flutter occurs when there is a phase change in both components. The simplest case involves one critical flutter speed, occurring where the airfoil oscillates with steady amplitude. For wind speeds above a critical value, the airfoil flutters. When the wind speed decreases below the critical value, oscillations will be dampened until the airfoil stops fluttering [4]. Figure 4.2 depicts the flexural and torsional components of an airfoil that is supported at both ends.

Figure 4.2 Flexion (a) and torsion (b) of an airfoil.

4.1.3.2 Wind Flutter Generator Prototype

A 50 cm flutter generator prototype was purchased from its developer, Humdinger Wind Energy, LLC [38]. The device is supported by a Plexiglas®

frame. The flutter generator consists of a Mylar® ribbon tensioned between two bolts and an electromagnetic transducer coupled to one end of the ribbon. The ribbon has one rough side and one smooth side, creating a simple airfoil. The transducer consists of two small neodymium magnets and an electromagnetic transducer. When the ribbon flutters, the magnets oscillate, inducing a current to a static coil located beside the magnets, as shown in Figure 4.3. The specifications of the generator as provided by the manufacturer [6] are listed in Table 4.1.

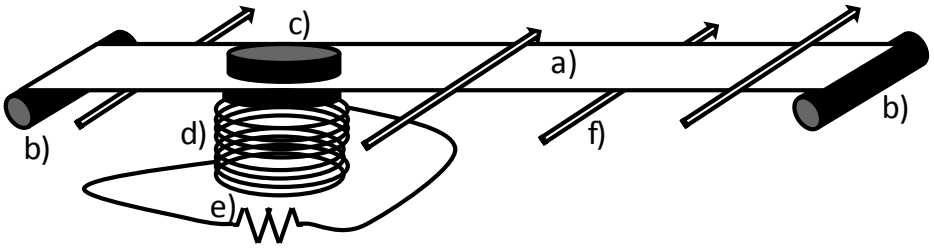

Figure 4.3 Wind flutter generator. (a) aeroelastic ribbon; (b) supports; (c) magnets; (d) electromagnetic transducer; (e) load; (f) wind flow.

Table 4.1 Wind flutter generator—manufacturer's specifications.

Parameter	Specifications
Cut-in wind speed (m/s)	< 3
Energy (mW)	10mW to 100mW
Output (VDC, after rectification)	0 to 6
Frequency	80 to 110
Membrane length (cm)	50
Membrane tension (N)	Around 44
Gearing	None
Overall dimensions (cm, original frame)	54 x 5.2 x 4.4
Transduction	Electromechanical

4.1.3.3 Experiment Setup

4.1.3.3.1 Wind Tunnel

To characterize the flutter generator under different wind speeds and with various orientations with respect to wind, it was tested using a recirculating wind tunnel [7]. Specifications of the wind tunnel are listed in Table 4.2.

Table 4.2 Wind tunnel specifications.

Parameter	Specifications
Test section (m, w × h × l)	2.4 × 1.2 × 11
Wind speed (m/s)	Min: 0.2, Max: 35 m/s

4.1.3.3.2 Wind Flutter Generator Test Bed

The flutter generator was removed from its original frame and mounted into a new support that was specifically designed and constructed for testing purposes. This new support allowed free flow of wind around the ribbon. Adjusting the tension of the ribbon was possible with the use of weights, and the angle of attack could be adjusted between -90 and 90 degrees. The frame was mounted inside the wind tunnel, and carefully centered and aligned (the default angle of attack was zero degrees, with the sides of the ribbon aligned with the direction of the wind). A single bolt was used to fix the frame to the floor, allowing manual rotation of the frame (z-axis) and adjustment of the angle of attack. The lower end of the ribbon snugly entered through a slot in the box-shaped lower part of the frame. This end of the ribbon was clamped using two small metal brackets that support a basket where weights were placed. This simple system allowed tensioning of the ribbon. If friction forces and the weight of the ribbon were neglected, then the ribbon tension was proportional to the weights placed in the basket. The minimum tension was 6.2 N and the maximum (tested) was 60 N. Higher tensions could be reached, but were not tested because the ribbon would not flutter at low speeds if high tensions were applied. A three dimensional rendering of the wind flutter generator test frame is provided in Figure 4.4, a picture is presented in Figure 4.5, and specifications are provided in Table 4.3.

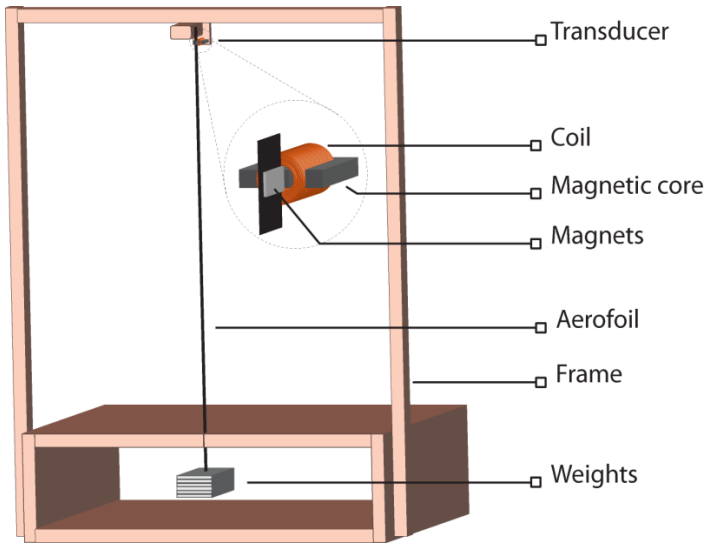

Figure 4.4 Three-dimensional rendering of the flutter generator test bed.

Figure 4.5 Picture of the wind flutter generator test bed.

Table 4.3 Test bed specifications.

Parameter	Specifications
Overall dimensions (cm, w × h × l)	62 × 29 × 75
Distance from the ribbon to the inner border of left and right posts (cm)	30.5
Length of ribbon exposed to wind (cm)	50
Ribbon width (cm)	1.3
Distance from the upper end of the ribbon to the center of the magnets (cm)	3.5
Distance from the border of the magnets to the electromagnetic transducer (mm)	2

4.1.3.4 Experimental Setup

The wind speed ranged from 3 to 20 m/s. Although the wind tunnel was able to produce lower and higher wind speeds, it was expected that no energy would be produced with very low wind speeds, and the device might be damaged if it were tested at higher wind speeds. For this reason, most experiments were performed with speeds ranging from 3 to 10 m/s, and only some with speeds from 11 to 20 m/s. A Tektronix wind flow meter based on the Pitot tube principle was used to measure the wind speed inside the wind tunnel.

The load was resistive, with values ranging from 10 to 220 Ω, in 10 Ω increments. Additionally, open circuit RMS voltage (infinite load) was measured and recorded. The load was connected directly to the electromagnetic transducer, and no power conditioning was used. The signal produced was an alternating current. A digital oscilloscope was used to measure the RMS voltage and the frequency of the signal at the load. Energy was calculated using the value of the load (resistance) and the measured RMS voltage ($P = v^2/R$). The tension of the ribbon could be adjusted from 8.4 to 53 N with 2.13 N increments. The angle of attack was set from 0 to 90 degrees in 10 degrees increments. Cut-in and cut-out angles were determined with a resolution of 5 degrees.

Figure 4.6 illustrates the test bed mounted inside the wind tunnel. The wind speed, the ribbon tension, the angle of attack, and the load were the key parameters used to determine the generator's output power and frequency characteristics. Table 4.4 summarizes the test bed capabilities.

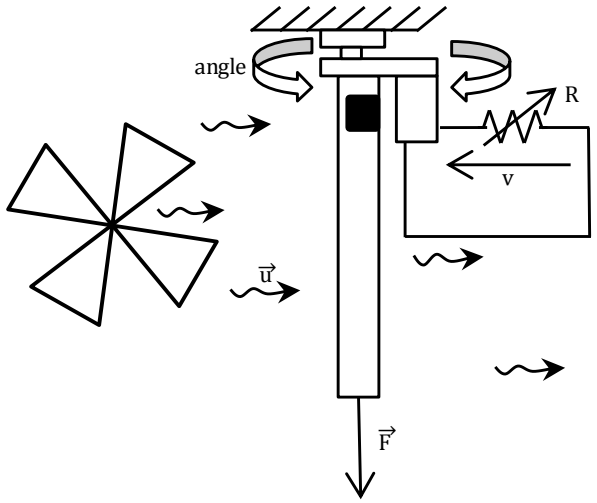

Figure 4.6 Test bed diagram.

Table 4.4 Test bed capabilities.

Parameter	Units	Range	Step
Wind speed	m/s	3 to 20	1[a]
Ribbon tension	N	6.4 to 59.4	2.13
Resistive load	Ω	10 to 220	10
Angle of attack	Degrees	-90 to 90	5[b,c]

[a]Infinite resolution can be achieved.
[b]The angle of attack was incremented in 10 degrees steps.
[c]The cut-in and cut-out angles were determined using a resolution of 5 degrees.

4.1.3.5 Experiment Protocol

For each wind speed tested, a series of steps was followed in order to obtain the optimal tension, the optimal load, and the influence of the angle of attack.

1. The wind tunnel wind speed was adjusted until the desired wind speed reached steady conditions. Starting with the lowest ribbon tension, the open circuit RMS voltage and frequency were measured and manually recorded. The tension was incremented by 2.13 N and measurements were taken and recorded. The process was repeated

until the ribbon tension impeded fluttering. The tension that yielded the highest open circuit RMS voltage was identified as the optimum.

2. With the optimal tension applied to the ribbon, and keeping the same wind speed setting, a 10 Ω load was connected; RMS voltage and frequency were recorded. The load was incremented by 10 Ω and the resulting RMS voltage and frequency were measured, until the load reached 220 Ω. Using the recorded RMS voltages and their respective loads, output power was calculated. This allowed identification of the optimal load (the one from which maximum energy can be extracted from the generator).
3. Using the optimal tension and load previously obtained, the angle of attack was changed from 0 to 90 degrees, in 10 degree increments. Due to the symmetry of the frame and the generator, it was not considered necessary to experiment with angles from -10 to -90 degrees. The wind speed was kept at the same, previously adjusted value. The RMS voltage and signal frequency were recorded for each angle of attack and the experimentation continued until the cut-out angle was reached (sudden fluttering stop). This procedure allowed assessment of the influence of the angle of attack on the generated energy.
4. The cut-out angle reached during the last step was noted. The frame was rotated back in the direction of the 0 degrees position, until power generation started. This was recorded as the cut-in angle.

For all experiments, measurements were averaged over 16 datasets before the value was recorded, using the oscilloscope built-in averaging function. Sometimes, a given system condition would produce a self-sustained but unsteady oscillation, e.g., at low wind speeds and/or low ribbon tensions. In those cases, the RMS voltage and frequency measurements were averaged over 64 datasets.

The goal of the first experiment was to determine the cut-in and cut-out wind speeds for the aeroelastic flutter generator. The range of wind speeds was from 3 to 3.9 m/s. To determine the cut-in wind speed, the wind speed inside the wind tunnel was gradually increased (starting at 3 m/s), until a self-sustained oscillation was obtained (with a load of 10 Ω connected to the transducer). The same approach was used to determine the cut-out speed, this time lowering the wind speed until the fluttering ceased. Once the cut-in and cut-out speeds were determined, the experimentation protocol defined in the last paragraphs was followed. Using the same experimentation protocol (steps 1–4), experiments were made for wind speeds ranging from 4 to 10 m/s. The wind speed was incremented by 1 m/s at a time.

The last set of experiments followed a simpler protocol. The goal was to complete the output power characteristic curve with wind speeds higher than 10 m/s. A fixed tension of 38.1 N and a load of 110 Ω were used and wind speeds were changed from 11 to 20 m/s in 1 m/s increments. The RMS voltage at the load was recorded.

4.1.3.6 Experimentation Results

Figure 4.7 shows the relationship between the ribbon tension and the RMS open circuit voltage, for different wind speeds. For each wind speed, only tensions that would give a self-sustained oscillation are presented. For example, at 3.6 m/s, only a tension of 8.4 N would produce continuous fluttering. The output voltage vs. ribbon tension relationship is nonlinear and there are local maxima. This might be due to the fact that in an airfoil system there might be several critical flutter speeds [4]. Whenever the maximum open circuit RMS voltage occurs near the cut-out ribbon tension this was discarded as the optimal point and the next point was selected (with lower tension). This way, when a load was connected to the generator, the output tension was at the highest point and the output power was maximized.

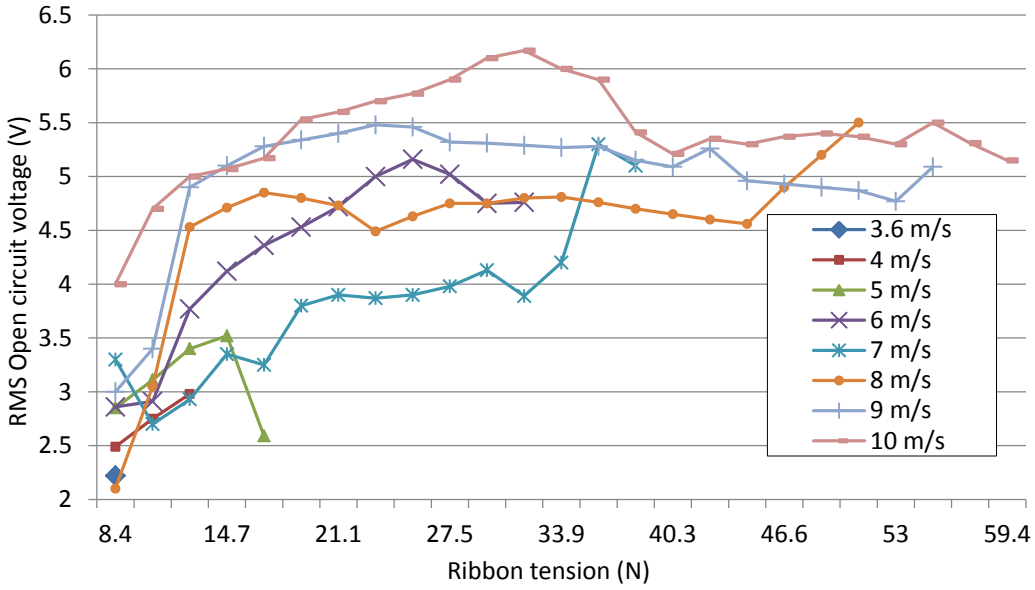

Figure 4.7 Open circuit voltage vs. ribbon tension for different wind speeds.

The relationship between the optimal ribbon tension and the wind speed is nonlinear. Generally, lower wind speeds did not induce fluttering when high tensions were applied to the ribbon. High wind speeds produced more energy at higher tensions, and they produced much less energy at lower tensions. Unless a dynamic tensioning system was implemented, the only way to produce energy in a wide range of wind speeds was by setting the ribbon tension to a low value.

The optimal load was in the range of 90 to 130 Ω, with 100 and 110 Ω being typical values. Since the optimal load had little variation, the use of maximum energy tracking point techniques with this generator was not necessary.

Output power decreased slowly with the increase of the angle of attack. The only exceptions were 3 and 4 m/s, where a slight increment of the attack angle maximized the output power. After a steady decline of the output power, there was a critical point where fluttering abruptly stopped. This was the cut-out angle and it varied from 55 to 65 degrees. The cut-in angle was found to be between 40 and 55 degrees. For the range of wind speeds tested, power generation could be guaranteed as long as the angle of attack was lower than the minimum cut-in angle obtained (40 degrees). Once there was

a steady power generation, it continued as long as the angle of attack was lower than the minimum cut-out angle (55 degrees).

The frequency of the generated signal was a function of the wind speed and the tension of the ribbon. Low wind speeds produced low frequencies. The frequency increased with the tension of the ribbon, until the tension was too high to maintain the oscillations and it became zero. When loads of different values were connected, the change of frequency was negligible.

Figure 4.8 shows the characteristic energy curves of the wind flutter generator under different operating conditions. When an optimal ribbon tension and an optimal resistive load were used, the output power increased with wind speed. The same was true when a load of 110 Ω and a tension of 38.1 N were used. Under these conditions, wind speeds below 7 m/s did not produce fluttering. The output power characteristic changed when a tension of 8.4 N and a load of 110 Ω were applied to the system. Energy generated at speeds from 6 to 9 m/s was less than the energy generated at 5 m/s. This was due to the nonlinearity of the system. Note: it is likely that the optimal ribbon tension had a value not reproduced by the resolution of 2.13 N that was used for testing. This would explain why power generation was sometimes higher at lower wind speeds. Unfortunately, testing of the flutter generator device proved to be resource-consuming; therefore, testing with lower ribbon tension resolutions would be difficult.

Table 4.5 summarizes the results obtained with wind flutter generator experiments. Maximum and minimum values are given for each of the studied parameters. Energy, voltage, frequency, and membrane tension have the same order of magnitude as the manufacturer's specifications in Table 4.1. However, a peak output power of 171 mW was reached with a wind speed of 20 m/s (compared to the nominal specification of 100 mW). Adjusting the ribbon tension and the electrical load to optimal values for a wind speed of 20 m/s, would likely result in higher power output.

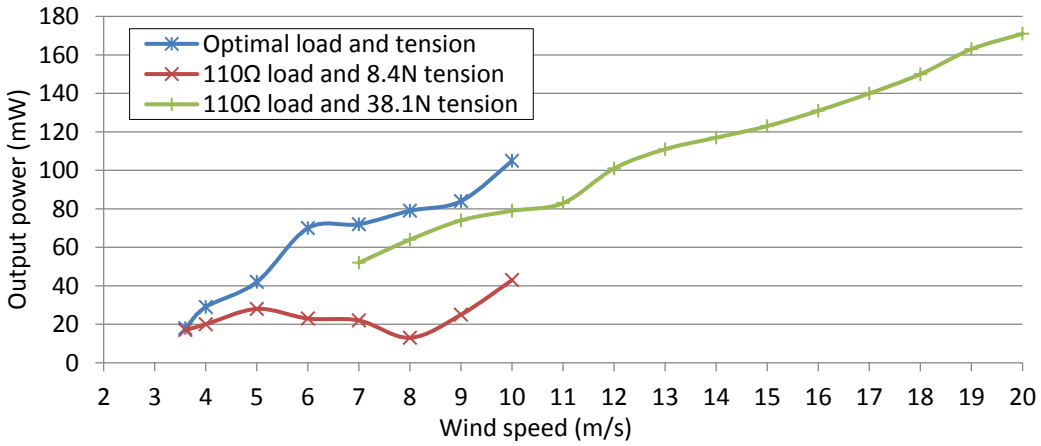

Figure 4.8 Output power curve of the wind flutter generator.

Table 4.5 Experimentation results summary.

Parameter	Units	Minimum[a]	Maximum[a]
Cut-in wind speed	m/s	3.6 (10Ω load)	N/A
Cut-out wind speed	m/s	3.6 (10Ω load)	N/A
Optimal ribbon tension	N	8.4 @ 3.6 m/s	36 @ 7 m/s
Optimal resistive load	Ω	90 @ 3.6 m/s, 5 m/s	130 @ 10 m/s
Cut-in angle of attack	degrees	40 @ 3.6 m/s, 4 m/s	55 @ 10 m/s
Cut-out angle of attack	degrees	55 @ 4 m/s, 7 m/s	65 @ 7 m/s, 8 m/s, 10 m/s
Open circuit RMS voltage[b]	V	2.22 @ 3.6 m/s	6.17 @ 10 m/s
Frequency[b]	Hz	54 @ 3.6m/s, 10Ω	142 @ 10m/s, 59.4N, open circuit
Output power	mW	5 @ 3.6m/s, 10Ω	171 @ 20m/s, 38.1N, 110Ω

[a]Other parameter values are optimal unless otherwise noted.
[b]For these parameters, experiments were made up to 10 m/s.

The manufacturer's specifications state that the cut-in speed is lower than 3 m/s. In our experiments, we could obtain a self-sustained oscillation with a wind speed of 3 m/s and no wind speeds below this threshold were tested. However, the oscillations stopped when a load (220 Ω) was connected. This speed (3 m/s) was discarded as the cut-in speed, since it was not able to power a load. The obtained values of 3.6 m/s cut-in and cut-out wind speeds allowed the connection of a 10 Ω load at start-up.

4.1.3.7 Enhanced Wind Flutter Generator

During the first part of the experimentation process it was noted that a different frame configuration could boost the response of the generator (self-sustained oscillations starting at lower wind speeds and lower tensions, and stopping at larger cut-off angles and under higher tensions). The test bed was modified according to the observations collected during the testing of the original device. A second set of experiments was performed to determine the characteristics of the "enhanced" wind flutter generator.

The experiment setup was the same as in section 4.1.3.4, with the noticeable difference that the test bed used the "enhanced" prototype. The protocol described in section 4.1.3.5 was also used with minor modifications. The wind speed ranged from 2 to 15 m/s (1 m/s increments), the ribbon tensions varied from 7.5 to 60 N (2.5 N increments), the angle of attack was tested every 10 degrees (-60 to 60 degrees) and the load took values of 30 to 210 Ω (20 Ω increments). A comparative study between the "original" and the "enhanced" flutter generators is developed in section 4.1.3.8.

4.1.3.7.1 Wind Flutter Generator Output Voltage Waveforms

A set of screenshots from load voltage waveforms was recorded during the experimentation with the enhanced wind generator. They allowed the comparison of signal waveforms generated under different operating conditions. Load voltages took forms ranging from quasisinusoidal (Figure 4.9a) to signals with unstable amplitudes and frequencies. These unstable waveforms typically occurred when the generator operated near or at boundary conditions, e.g., cut-in or cut-out wind speeds (Figure 4.9f, 15 N). Quasisinusoidal waveforms were frequent when the system oscillated steadily. But for most operating conditions the voltage was an irregular waveform with steady amplitude and frequency. See Figure 4.9.

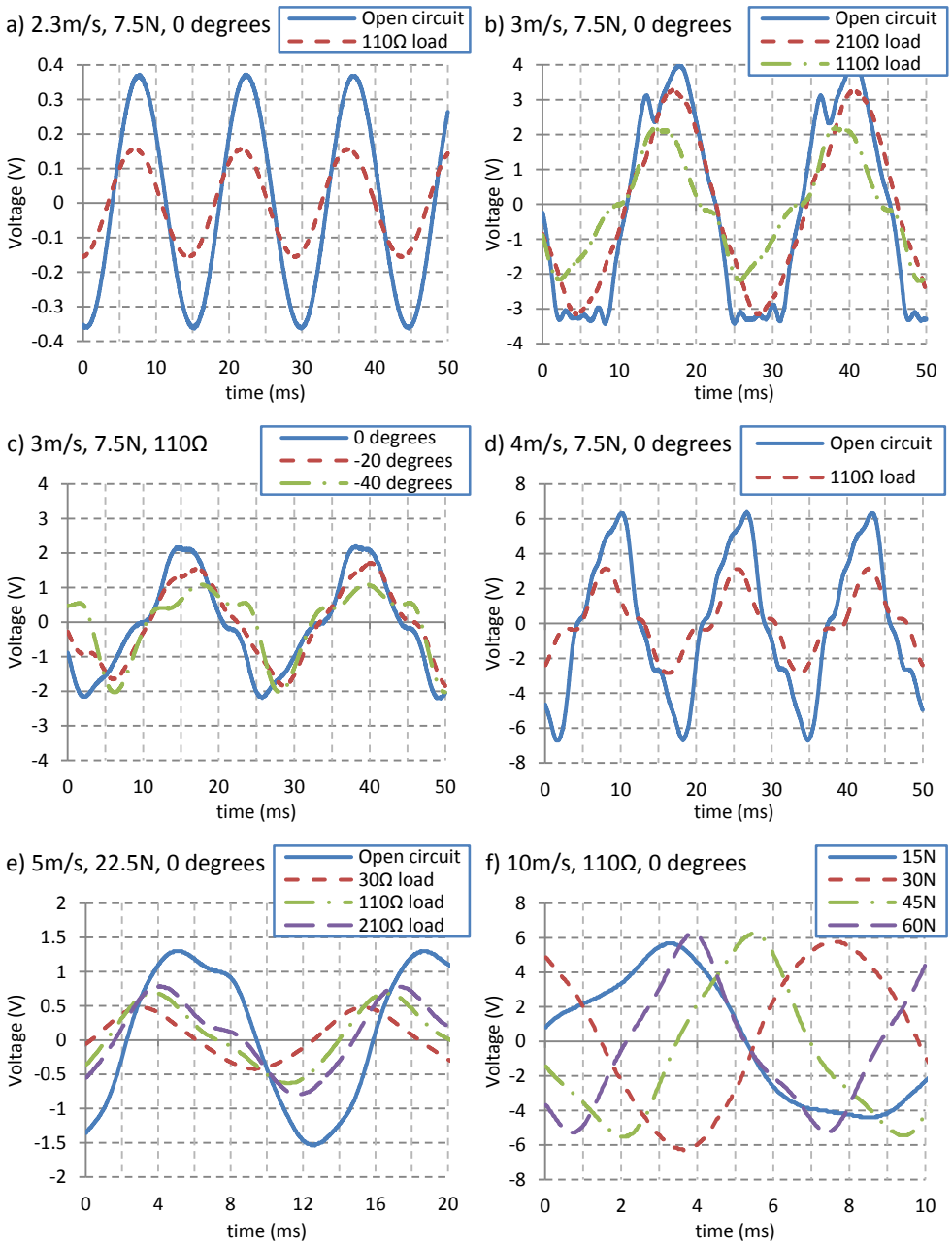

Figure 4.9 Wind flutter generator voltage waveforms.

4.1.3.8 Comparative Study

This section develops a study of the original and the enhanced versions of the wind flutter generator. The parameters of interest are output power, cut-in speeds, ribbon tension, load (resistive), angle of attack, frequency, efficiency, and performance. Finally, a 50 W commercial wind turbine and both versions

of the flutter generator are compared in terms of total energy, average energy, and efficiency over a period of one year, for different arctic locations.

4.1.3.8.1 Output Power

The advantage of the enhanced wind flutter generator over the original wind flutter generator is clearly demonstrated in this section's figures. Figure 4.10 provides a power output comparison for low ribbon tensions and equal loads. At these tensions, the enhanced version had a cut-out speed of 9 m/s and the original version had a cut-out speed of 10 m/s. At 6 m/s, the output of the enhanced generator was triple that of the original version. Both plots present an initial linear behaviour followed by an interval where the output power drops. After this interval, the response seems to be linear again. This is further discussed in section 4.1.3.8.2.

Figure 4.11 corresponds to the energy curve obtained with the use of high ribbon tensions. For these operating conditions, the enhanced version had a cut-in speed of 5 m/s, while the original version started generating electricity at 7 m/s. Both situations present a linear trend. Note that experiments with the enhanced version were conducted with wind speeds up to 15 m/s due to the high fluttering frequencies that were attained above this speed.

Finally, both flutter generators exhibit a linear trend when optimal loads and ribbon tensions are used at each wind speed (Figure 4.12). The cut-in speed for the original version is 3.6 m/s, noticeably higher than the 2.3 m/s obtained with the enhanced version. The advantage of a higher output power for the enhanced generator is less obvious when optimal tensions and loads are considered. Still, the enhanced version provided more energy under all circumstances and had a lower cut-in speed. The energy curve of the enhanced flutter generator with optimal loads and tensions is used to develop a linear model in section 4.1.3.9. Section 4.1.3.8.7 presents estimations of energy and power generation using real meteorological data for four locations across the arctic.

Note: optimal ribbon tensions and loads above 10 m/s were not obtained for the original wind flutter generator.

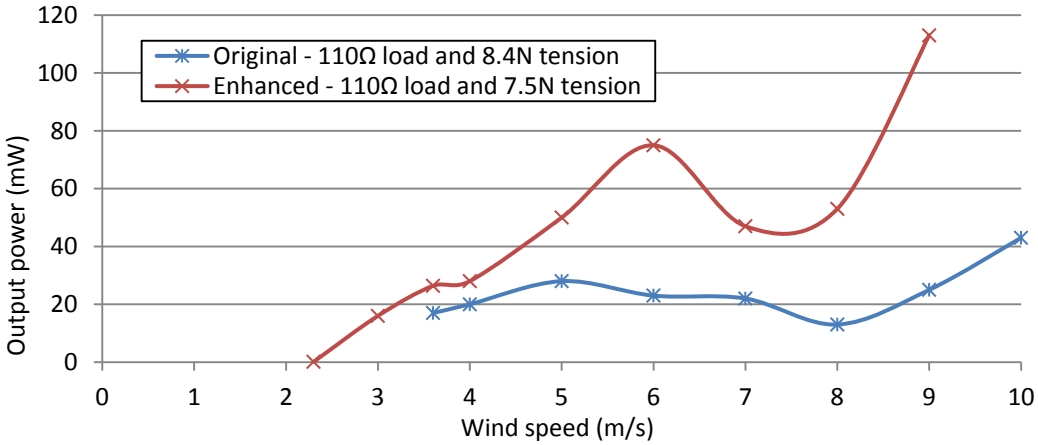

Figure 4.10 Output power vs. wind speed, with low ribbon tensions.

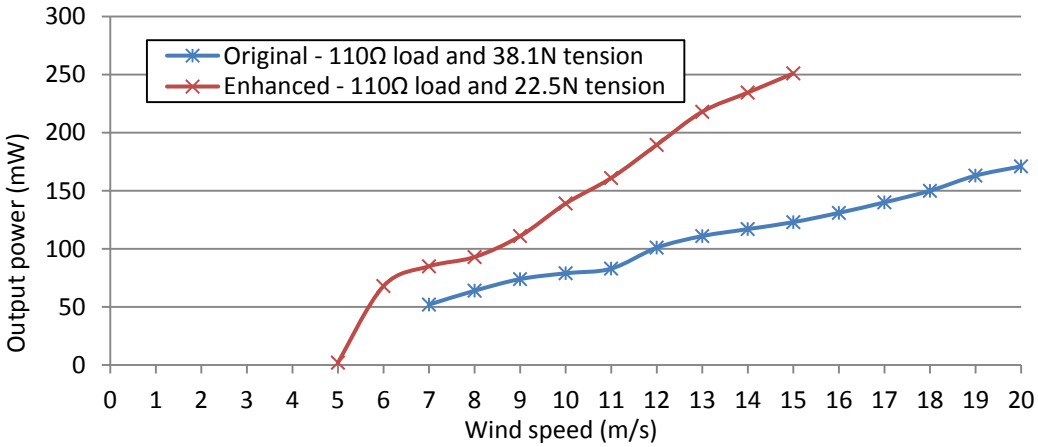

Figure 4.11 Output power vs. wind speed, with high ribbon tensions.

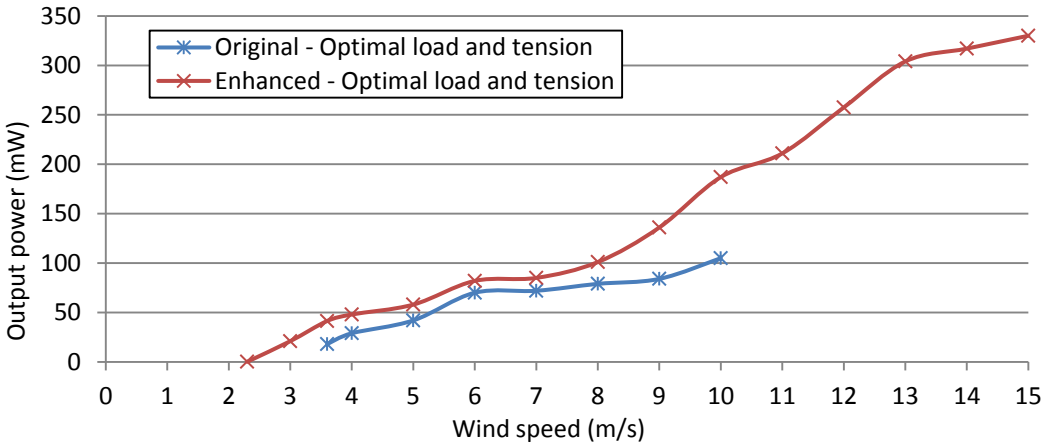

Figure 4.12 Output power vs. wind speed, with optimal loads and optimal ribbon tensions.

4.1.3.8.2 Ribbon Tension

Ribbon tensions were incremented using 2.13 N steps for the original generator and 2.5 N steps for the enhanced generator. Figure 4.13 shows a nonlinear optimal tension trend for both cases. However, some intervals of the curves present high linearity. It is very likely that optimal tension drops are due to the use of suboptimal ribbon tensions. For the original version, the drop comes just after the higher ribbon tension resolution attained the maximum (tested) of 53 N (wind speed of 8 m/s).

For experimentation with the enhanced flutter generator, the ribbon tension range was lowered from 8.4 to 7.5 N and raised from 53 to 60 N. Figure 4.13 shows that optimal tension drops at 11, 13, and 15 m/s. The explanation seems to be the same, the optimal tensions for wind speeds higher than 10 m/s were above the 60 N testing limit. For wind speeds up to 5 m/s, the optimal tension was the same (7.5 N). Lower tensions and higher resolutions are probably required to determine the optimal ribbon tensions at these low wind speeds.

The effect of the use of suboptimal ribbon tensions is observed in other curves as well (Figure 4.10).

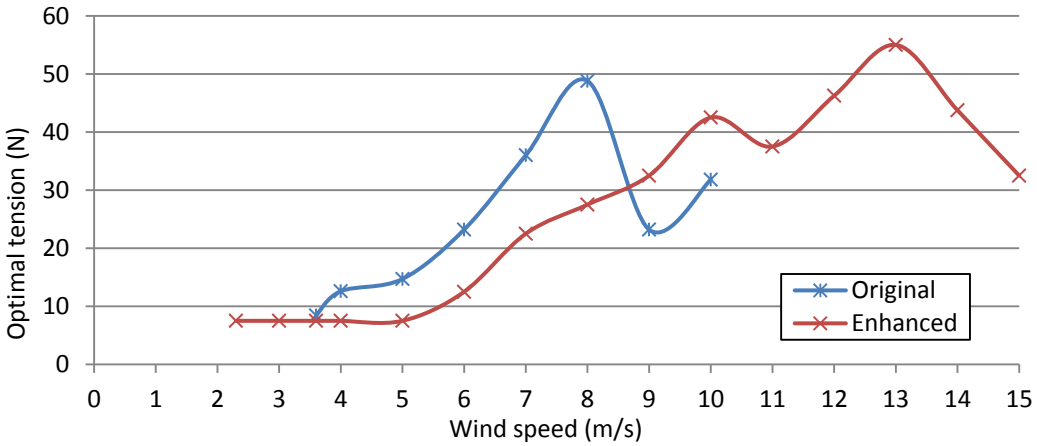

Figure 4.13 Optimal tension vs. wind speed.

4.1.3.8.3 Resistive Load

The optimal loads are those at which power output is maximized. The optimal load for the original flutter generator was almost constant and settled around 100 Ω. For this system, no maximum energy point tracking was necessary (Figure 4.14).

The enhanced version followed a very different trend. For wind speeds up to 4 m/s, the optimal load was around 200 Ω. At 5 m/s it decreased to 70 Ω and for higher wind speeds the optimal load increased almost linearly (the testing step for the original generator was 10 Ω, while the enhanced system was tested using 20 Ω steps). The high optimal loads at low wind speeds can be explained in two ways: (1) the use of suboptimal ribbon tensions or (2) low power levels were unable to sustain high loads—i.e., at the same energy, lower resistance implies higher currents.

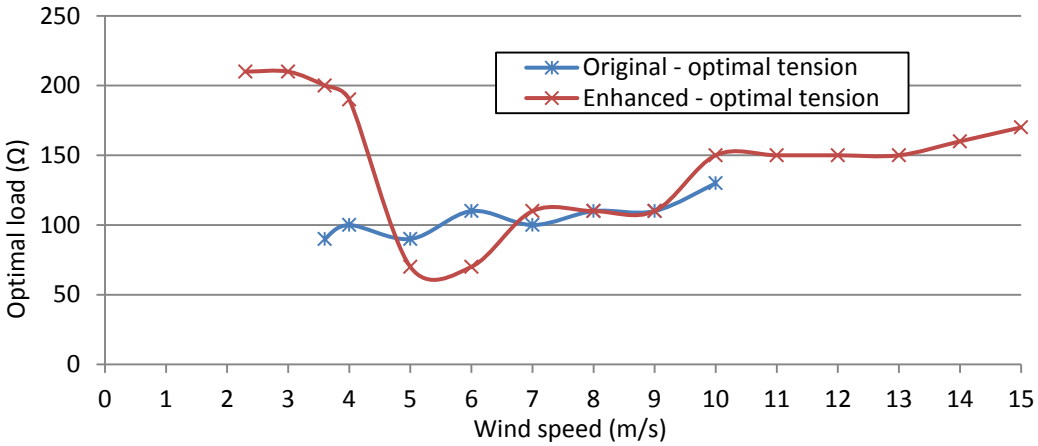

Figure 4.14 Optimal load vs. wind speed, with optimal ribbon tensions.

4.1.3.8.4 Frequency

The same remarks about the use of suboptimal ribbon tensions for some tests apply to the output voltage frequency characteristics – see Figure 4.15. A linear trend can be seen in both the original and the enhanced generators. For the original device, the voltage frequency goes from 60 to 120 Hz, and it increases with wind speed. The enhanced system has a wider frequency span, which goes from 40 to 150 Hz.

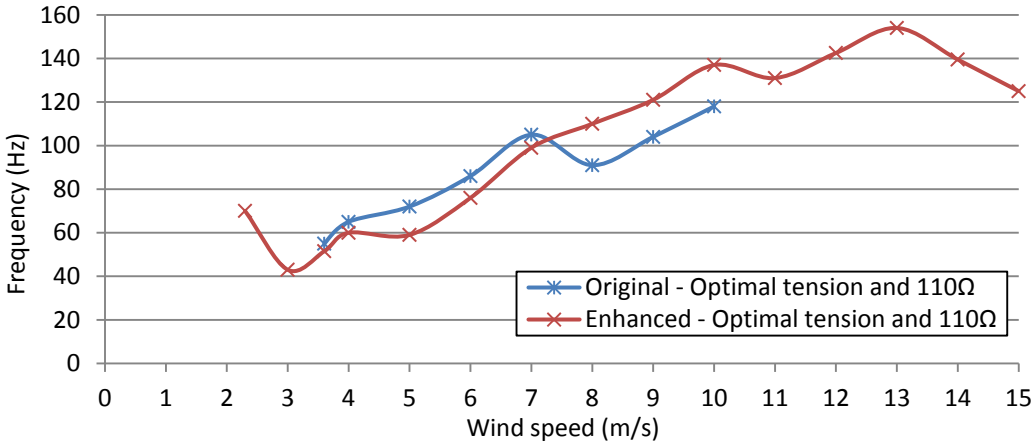

Figure 4.15 Frequency vs. wind speed, with optimal ribbon tensions.

4.1.3.8.5 Angle of Attack

The angle of attack was studied to determine the impact of the wind direction with respect to a fixed orientation of the flutter generator. However, maximizing the amount of energy extracted from the wind requires the use of a device that is able to track the wind.

For the original generator, mounted on an open frame, the effect of the angle of attack was considered to be symmetrical and the experiments were done for positive angles (0 to 90 degrees; at 0 degrees the device is facing the wind and maximum power generation is expected). The curve corresponding to the negative angles in Figure 4.16 is a mirror of the positive counterpart.

The enhanced generator used a modified, nonsymmetrical frame that obstructed wind flows coming at high angles. The angles of attack were obtained for both positive and negative angles. The curve in Figure 4.16 shows a dissymmetry with respect to 0 degrees that is explained by the geometrical configuration of the frame.

As expected, the original device had a relatively wide operating range (-60 to 60 degrees) and started generating electricity at higher angles of attack. In comparison, the range of the enhanced generator was narrower (-50 to 40 degrees). Neglecting the dissymmetry of the enhanced system, the overall trend of both generators with respect to the angle of attack was similar.

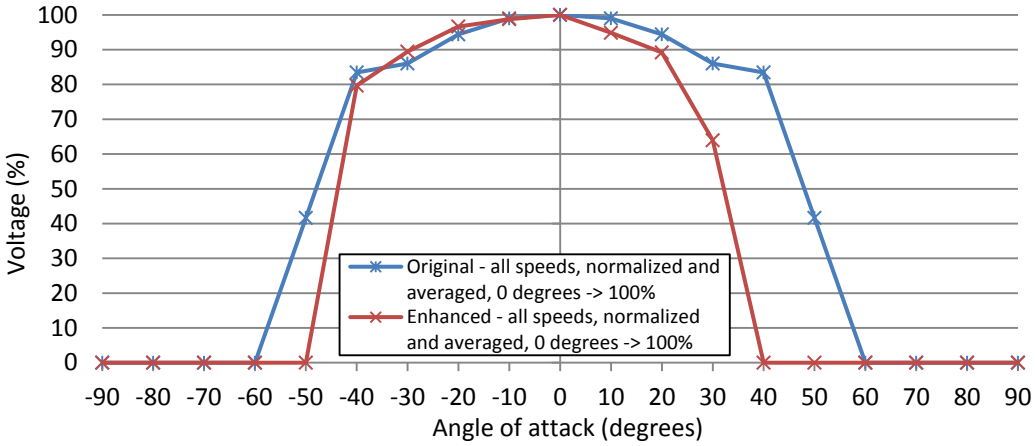

Figure 4.16 Averaged and normalized voltage vs. angle of attack. The average voltage was obtained using measurements from each tested wind speed.

4.1.3.8.6 Performance

Table 4.6 presents a summary of the experimentation results for both original and enhanced wind flutter generators. Two relevant parameters are the cut-in wind speed and the output power. The cut-in speed was noticeably lower for the enhanced version (2.3 vs. 3.6 m/s). Lower cut-in speeds were obtained when the load was disconnected (open circuit), but in such cases the system was not able to produce any energy.

The second parameter of interest is the output power. The enhanced prototype was able to deliver low power (0.15 mW) at very low wind speeds; the original wind generator started power generation at 5 mW, but the output abruptly dropped to zero at lower wind speeds. The advantage of the enhanced generator was that power generation started at 2.3 m/s and it increased steadily.

Table 4.6 Wind flutter generator specifications for wind speeds up to 10 m/s.

Parameter	Units	Original	Enhanced
Cut-in wind speed - with resistive load attached	m/s	3.6	2.3
Optimal resistive load	Ω	90 to 130	70 to 210
Oscillating frequency	Hz	54 to 118	43 to 137
Output power - optimal operating conditions	mW	5 to 105	0.15 to 187

The performance improvement of the enhanced wind flutter generator with respect to the original device depended on the mode of operation (Figure 4.17). The enhanced version performed at least 20% better than the original; the improvement increased up to 350% with the use of low ribbon tensions. Again, the effect of the utilization of suboptimal ribbon tensions can be seen in these plots. Probably, a higher performance could be reached with the use of optimal ribbon tensions.

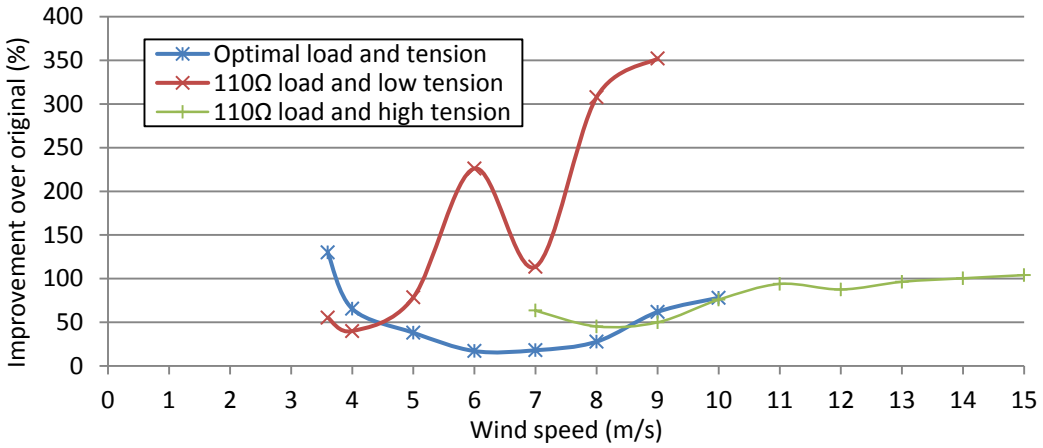

Figure 4.17 Performance improvement of enhanced flutter generator vs. wind speed.

Table 4.7 shows simulation results based on one typical climatological year for four arctic locations. On average, the enhanced generator performed 133% better than the original. The rate of improvement depended on the combination of load and ribbon tension used. The results show that the best outcome was obtained when an adequate (fixed) tension and load were used,

rather than optimal parameters that did not take into account the wind speed profile of the location.

Finally, Figure 4.18 offers plots of the characteristic energy curves of both flutter generators for speeds up to 10 m/s and the use of optimal ribbon tensions and optimal resistive loads (*cf*. Figure 4.12). Linear models were obtained from these plots.

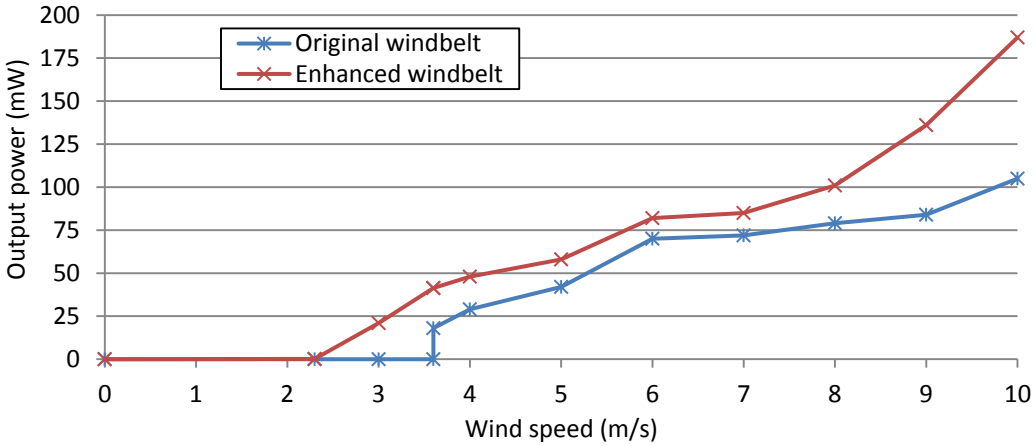

Figure 4.18 Characteristic output power curves of the wind flutter generator.

Table 4.7 Improvement of enhanced flutter generator with respect to original flutter generator (%).

	Optimal tension & load	110Ω, 7.5N	110Ω, 22.5N
Barrow	65	142	140
Inuvik	52	94	360
Resolute	74	192	111
Whitehorse	61	123	185
Average		**133**	

4.1.3.8.7 Comparison of Wind Flutter Generators and Commercial 50 W Wind Turbine

The efficiency of a wind generator varies with wind speed. A 50 W wind turbine (Rutland 503) is compared with the original and enhanced versions

of the wind flutter generator in Figure 4.19. The curves follow the same trend in all cases: as the wind speed increases, there is a rapid increase in efficiency to a maximum followed by a decrease in efficiency at high wind speeds. When the flutter generators are adjusted with a fixed tension, it is probably a good idea to adjust the ribbon tension to match the maximum efficiency point.

The original fluttering generator had a maximum efficiency of 4.6% at a wind speed of 4 m/s and it reached 8.8% when the enhanced version was used. Both values are low compared to the efficiency of the wind generator that goes up to 23%. However, this value was estimated from the manufacturer's data [81] and practical efficiency values could be lower.

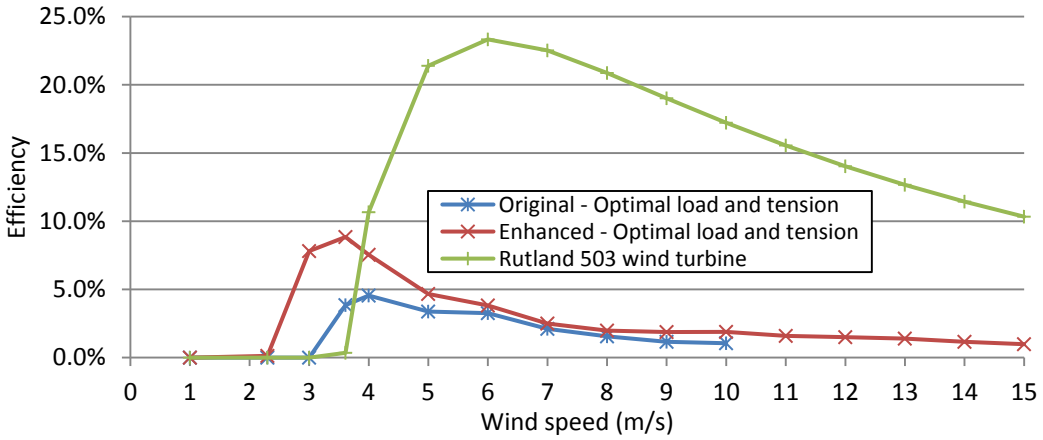

Figure 4.19 Efficiency vs. wind speed for optimal load and tension.

Table 4.8, Table 4.9, and Table 4.10 summarize simulation results for different arctic locations, based on one typical meteorological year. Table 4.8 contains yearly energy calculations, Table 4.9 provides the equivalent average energy, and Table 4.10 estimates the corresponding efficiencies. It is important to note that the final efficiency of each device changes with respect to the arctic location. This is normal, since each location has a particular wind speed profile and the efficiency of the generators depend on the wind speed.

To corroborate Figure 4.19, Table 4.10 shows that the efficiency of the original wind fluttering generator is always lower than the efficiency of the enhanced version. The datasheet model (windbelt), obtained using the

manufacturer's data [38], exhibits values between the original and the enhanced generators' results. The enhanced device achieves higher efficiencies than those of the datasheet-based model.

We conclude that the wind turbine has a higher efficiency than the fluttering generators, but it is oversized for EC's reference station and it is costly. The advantages of the flutter generators over the small wind turbine are (1) they can be sized to match the wind profile and the load requirements, (2) they are simple mechanisms with one moving part and direct energy conversion, (3) they are lightweight, and (4) they are reasonably priced.

Table 4.8 Yearly energy converted by different wind generators at selected arctic locations – one typical meteorological year. All values in watt-hours unless otherwise noted.

	Available wind energy (Wh/m²)	Datasheet models		Experimentation models					
				Original			Enhanced		
		Rutland 503 turbine	Windbelt	Optimal tension & load	110Ω, 8.4N	110Ω, 38.1N	Optimal tension & load	110Ω, 7.5N	110Ω, 22.5N
Barrow	1494	54838	543	416	171	153	687	413	367
Inuvik	327	11651	149	150	79	16	228	153	74
Resolute	3376	90578	850	508	174	278	883	507	588
Whitehorse	615	24265	254	220	98	58	354	219	164

Table 4.9 Average energy produced by different wind generators for one typical meteorological year. All values in milliwatts unless otherwise noted.

	Available wind energy (W/m²)	Datasheet models		Experimentation models					
				Original			Enhanced		
		Rutland 503 turbine	Windbelt	Optimal tension & load	110Ω, 8.4N	110Ω, 38.1N	Optimal tension & load	110Ω, 7.5N	110Ω, 22.5N
Barrow	171	6300	62	47	19	17	78	47	42
Inuvik	37	1300	17	17	9	2	26	17	8
Resolute	385	10300	97	58	20	32	101	58	67
Whitehorse	70	2800	29	25	11	7	40	25	19

Table 4.10 Efficiency (%) of different wind generators – one typical meteorological year.

	Datasheet models		Experimentation models					
			Original			Enhanced		
	50 W turbine	Rutland 503 turbine	Optimal tension & load	110Ω, 8.4N	110Ω, 38.1N	Optimal tension & load	110Ω, 7.5N	110Ω, 22.5N
Barrow	18	2.2	1.7	0.7	0.6	2.8	1.7	1.5
Inuvik	18	2.8	2.8	1.5	0.3	4.3	2.9	1.4
Resolute	13	1.5	0.9	0.3	0.5	1.6	0.9	1.1
Whitehorse	20	2.5	2.2	1.0	0.6	3.5	2.2	1.6

4.1.3.9 Wind Flutter Generator Model

The model of the wind flutter generator was based on experimental data published in [77]. Although the physics of a wind fluttering device are quite

complex, a linear model for power generation vs. wind speed can be obtained if the device is subject to a fixed operational mode. The model assumed that the wind generator was able to track the direction of the wind, and that the load and ribbon tension were kept constant at all times. This is a conservative approach (*cf.* Table 4.7). A mathematical description of the model for a single 50 cm flutter generator is provided in equation 4.39, and a related energy characteristic is shown in Figure 4.20.

$$P_{W,f} = \begin{cases} 0, & W_S < 2.3 \\ 25 \times W_S - 56, & 2.3 \leq W_S < 12, \\ 319, & W_S \geq 15 \end{cases} \tag{4.39}$$

where $P_{W,f}$ is the energy generated by the flutter generator (mW) and W_S is the wind speed (m/s).

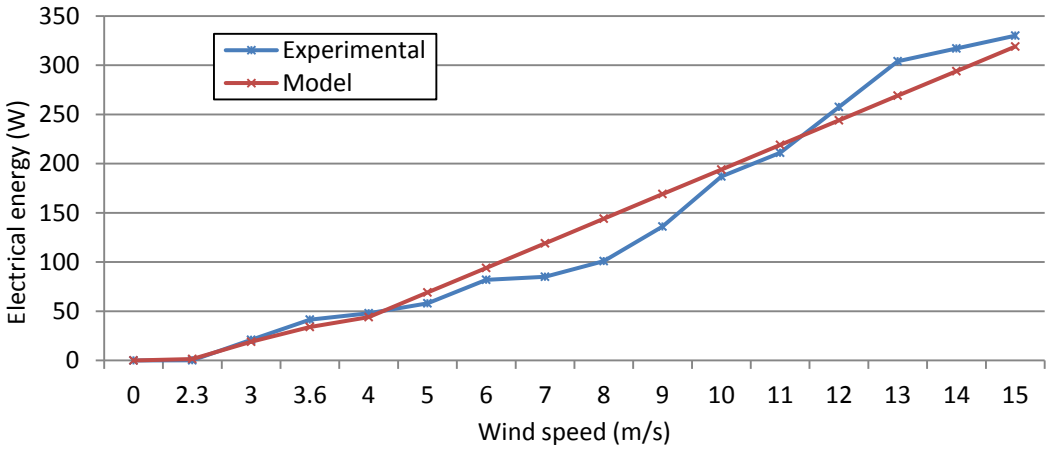

Figure 4.20 Linear model of the wind flutter generator vs. experimental measurements.

4.2 Solar Generator

It is common to find data regarding direct normal irradiation and diffuse horizontal irradiation on climatological databases [1]. However, databases rarely include calculations of total solar irradiation on inclined surfaces. Estimating the amount of irradiation striking a solar panel (inclined surface) with acceptable accuracy requires the use of a model. There are models that allow computation of diffuse reflected rays and beam components of solar irradiation on an inclined surface, departing from direct normal and diffuse

horizontal irradiation data [82]. The solar energy irradiation model for inclined surfaces presented in this section is based on the latest version of the Perez model [32], as cited in [82].

Additionally, the energy conversion efficiency of the solar panel varies with irradiation levels and the temperature of the panel. The final stage of the model deals with estimation of conversion efficiency and computation of the solar panel's output power.

4.2.1 Diffuse Irradiation on an Inclined Surface

The first part of the algorithm consists of estimating the angle of incidence of the direct component of the sun on an inclined surface, as described below. All the trigonometric functions have arguments in degrees.

$$B = \frac{360}{d_y}(n_d - 1), \tag{4.1}$$

$$E_t = \frac{229.2}{60} \times (0.000075 + 0.001868 \times \cos(\mathrm{B}) - 0.032077 \times \sin(\mathrm{B}) - 0.014615 \times \cos(2\mathrm{B}) - 0.04089 \times \sin(2\mathrm{B})), \tag{4.2}$$

$$t_{solar} = t_{standard} + \frac{4}{60} \times (\lambda - M_{lst}) + E_t, \tag{4.3}$$

where n_d is the day of the year (1 to 365 or 366 for leap years), d_y is the number of days in a year (365 or 366 for leap years), E_t is a parameter called "equation of time" (hours), $t_{standard}$ is the local standard time (hours), λ is the longitude of the location (degrees), M_{lst} is the local standard time meridian (degrees) and t_{solar} is the local solar time (hours). The equation of time estimates the difference between the true solar time and the local solar time for a particular location at any given point in time.

The local solar time is used to calculate the declination and the hour angle, which represents the displacement of the sun referenced west of the local

meridian (-15 degrees per hour before noon, +15 degrees per hour after noon).

$$\delta = 23.45 \times \sin\left(360\frac{284 + n_d}{d_y}\right), \tag{4.4}$$

$$\omega = (t_{solar} - 12) \times 15, \tag{4.5}$$

where δ is the declination (angular position of the sun, degrees) and ω is the hour angle (degrees).

The simulator (chapter 5) makes use of hourly databases, where a data point represents an average measurement taken during the hour ending at the recorded time stamp. Thus, a "midpoint" hour angle is appropriate for the model. When sunrise (equation 4.6) or sunset (the negative of the sunrise hour) occurs during the hour of the average measurement, the midpoint hour is the average between the hour angle and the sunrise hour (equation 4.8) or the sunset hour (equation 4.9). Otherwise, the midpoint hour angle is given by equation 4.10 (7.5 degrees equals half an hour).

$$\omega_R = \tan(\varphi) \times \tan(\delta), \tag{4.6}$$

$$\omega_S = -\omega_R, \tag{4.7}$$

$$\omega_{m,R} = \frac{\omega + \omega_R}{2}, \tag{4.8}$$

$$\omega_{m,S} = \frac{\omega + \omega_S - 15}{2}, \tag{4.9}$$

$$\omega_m = \omega - 7.5, \tag{4.10}$$

where ω_R is the sunrise hour angle (degrees), φ is the latitude (degrees), ω_S is the sunset hour angle (degrees), $\omega_{m,R}$ is the midpoint hour angle at sunrise, $\omega_{m,S}$ is the midpoint hour angle at sunset, and ω_m is the midpoint hour angle for all other cases.

The following equations give the solar altitude angle and the solar zenith angle.

$$S_\alpha = \cos(\varphi) \times \cos(\delta) \times \cos(\omega) + \sin(\varphi) \times \sin(\delta), \tag{4.11}$$

$$\alpha_s = \arcsin(S_\alpha), \tag{4.12}$$

$$\theta_z = 90 - \alpha_S, \tag{4.13}$$

where S_α is the solar altitude, α_S is the solar altitude angle (degrees), and θ_Z is the solar zenith angle (degrees).

The terrestrial variables required to calculate the sun's direct irradiation angle of incidence on an inclined surface are described in equations 4.1 to 4.13. The inclination of the surface with respect to the horizontal plane and the azimuth of the surface (zero if the surface faces south) are two additional variables. The equation of the angle of incidence is given below.

$$\begin{aligned}\cos(\theta) = S_\alpha \cos(\beta) \\ + \sin(\beta)\,(\cos(\delta)\,(\sin(\varphi)\cos(\gamma)\cos(\omega_m) \\ + \sin(\gamma)\sin(\omega_m)) - \sin(\delta)\cos(\varphi)\cos(\gamma)),\end{aligned} \tag{4.14}$$

where θ is the angle of incidence (degrees), β is the inclination of the surface (degrees), and γ is the surface azimuth (degrees).

The second part of the algorithm allows the computation of the diffuse components of the solar irradiation: sky diffuse (isotropic conditions), circumsolar diffuse, and horizon diffuse, see equations 4.15 to 4.17.

$$I_{S,d} = I_{d,h} \times \frac{(1 - F_1)(1 + \cos(\beta))}{2}, \tag{4.15}$$

$$I_{C,d} = I_{d,h} \times F_1 \times \frac{a}{b}, \tag{4.16}$$

$$I_{H,d} = I_{d,h} \times F_2 \times \sin(\beta), \tag{4.17}$$

where $I_{S,d}$ is the sky diffuse irradiation, $I_{d,h}$ is the diffuse horizontal irradiation (from database), $I_{C,d}$ is the circumsolar diffuse irradiation, $I_{H,d}$ is the horizon diffuse irradiation, and F_1, F_2, a, and b are coefficients, as described below.

The parameters a and b are computed according to equations 4.18 and 4.19.

$$a = \begin{cases} 0, & \cos(\theta) < 0 \\ \cos(\theta), & \cos(\theta) \geq 0' \end{cases} \tag{4.18}$$

$$b = \begin{cases} \cos(85), & \cos(\theta_Z) < \cos(85) \\ \cos(\theta_Z), & \cos(\theta_Z) \geq \cos(85)' \end{cases} \tag{4.19}$$

$$\cos(\theta_Z) = \sin(\alpha_S). \tag{4.20}$$

Obtaining the brightness coefficients F_1 (circumsolar) and F_2 (horizon) involves several steps. First, a sky clearness coefficient is calculated as,

$$\epsilon = 1 + \frac{I_{D,n}}{I_{d,h} \times (1 + 5.535 \times 10^{-6} \times \theta_Z^3)}, \tag{4.21}$$

where ϵ is the sky brightness coefficient and $I_{D,n}$ is the direct normal irradiation (database). The sky brightness coefficient allows the determination of a set of brightness coefficients (f_{11}, f_{12}, f_{13}, f_{21}, f_{22}, f_{23}), according to Table 4.11 [32].

Table 4.11 Perez model coefficients.

ϵ (lower limit)	f_{11}	f_{12}	f_{13}	f_{21}	f_{22}	f_{23}
1	-0.008	0.588	-0.062	0.06	0.072	-0.022
1.065	0.130	0.683	-0.151	-0.019	0.066	-0.029
1.23	0.330	0.487	-0.221	0.055	-0.064	-0.026
1.5	0.568	0.187	-0.295	0.109	-0.152	0.014
1.95	0.873	-0.392	-0.362	0.226	-0.462	0.001
2.8	1.132	-1.237	0.412	0.288	-0.823	0.056
4.5	1.060	-1.6	-0.359	0.264	-1.127	0.131
6.2	0.678	-0.327	0.25	0.156	-1.377	0.251

Three additional parameters are required to compute the coefficients F_1 and F_2. They are the air mass (equation 4.22), the extraterrestrial normal irradiation (equation 4.23), and a brightness parameter (equation 4.24).

$$m = \frac{1}{S_\alpha + 0.5057 \times (96.08 - \theta_Z)^{-1.634}}, \tag{4.22}$$

$$I_{E,n} = 1367 \times \left(1 + 0.033 \times \cos\left(\frac{360 \times n_d}{d_y}\right)\right), \tag{4.23}$$

$$\Delta = m \times \frac{I_{d,h}}{I_{E,n}}, \tag{4.24}$$

where m is the air mass, $I_{E,n}$ is the extraterrestrial normal irradiation, and Δ is the brightness parameter. The coefficients F_1 and F_2 are given in equations 4.25 and 4.26, respectively.

$$F_1 = \begin{cases} 0, & f_{11} + f_{12} \times \Delta + f_{13}\dfrac{\pi \times \theta_Z}{180} < 0 \\ f_{11} + f_{12} \times \Delta + f_{13}\dfrac{\pi \times \theta_Z}{180}, & f_{11} + f_{12} \times \Delta + f_{13}\dfrac{\pi \times \theta_Z}{180} \geq 0 \end{cases}, \tag{4.25}$$

$$F_2 = f_{21} + f_{22} \times \Delta + f_{23}\frac{\pi \times \theta_Z}{180}. \tag{4.26}$$

4.2.2 Ground-Reflected Irradiation on an Inclined Surface

The ground-reflected irradiation on an inclined surface is directly obtained from the direct normal irradiation, the diffuse horizontal irradiation, the albedo, and the inclination of the solar panel.

$$I_{D,h} = I_{D,n} \times S_{\alpha}, \tag{4.27}$$

$$I_{G,r} = A \times (I_{d,h} + I_{D,h}) \times \frac{1-\cos(\beta)}{2}, \tag{4.28}$$

where $I_{D,h}$ is the direct horizontal irradiation, $I_{G,r}$ is the irradiation reflected by the ground, and A is the albedo (isotropic ground).

4.2.3 Direct Irradiation on an Inclined Surface

The component corresponding to the direct irradiation on an inclined surface (equation 4.29) makes use of the direct horizontal irradiation and a "ratio of beam radiation" (equation 4.30).

$$R_b = \frac{\cos(\theta)}{\cos(\theta_Z)}, \tag{4.29}$$

$$I_D = I_{D,h} \times R_b, \tag{4.30}$$

where R_b is the ratio of beam radiation and I_D is the direct irradiation on an inclined surface.

4.2.4 Total Irradiation on an Inclined Surface

The total irradiation on an inclined surface is obtained with the addition of the five components previously described: the sky diffuse irradiation ($I_{S,d}$), the circumsolar diffuse irradiation ($I_{C,d}$), the horizon diffuse irradiation ($I_{H,d}$), the irradiation reflected by the ground ($I_{G,r}$), and the direct irradiation on an inclined surface (I_D).

$$I_T = I_{S,d} + I_{C,d} + I_{H,d} + I_{G,r} + I_D, \tag{4.31}$$

where I_T is the total irradiation on an inclined surface.

4.2.5 Solar Panel Efficiency

The solar panel efficiency model considers two separate issues: the effect of the temperature and the effect of the irradiation level. The temperature of the solar panel cell is computed according to equation 4.32 [83].

$$T_{cell} = I_T \times (e^{-3.56-.075 \times W_S} + 0.003) + T_{air}, \quad (4.32)$$

where T_{cell} is the temperature of the solar panel cell (degrees Celsius), W_S is the wind speed (database, m/s), and T_{air} is the temperature of the air (database, degrees Celsius). The constants are for an open rack, glass/cell/polymer solar panel. For other configurations, these constants need recalculation, refer to [83].

A nominal solar panel efficiency of 14% at 25 °C is considered, and the rate of efficiency change is -0.4% per degree Celsius [1]. The resulting efficiency equation is noted below.

$$\eta_T = 0.155 - 0.0006 \times T_{cell}, \quad (4.33)$$

where η_T is the efficiency accounting for the temperature of the cell.

The efficiency of the solar panel is also influenced by irradiation levels. At low irradiation levels, the efficiency greatly decreases [1] – see Figure 4.21. This effect is modeled using an interpolation table (Table 4.12). The global efficiency of the solar panel is obtained by multiplying η_T and η_I.

$$\eta_g = \eta_T \times \eta_I, \quad (4.34)$$

where η_g is the global efficiency of the solar panel and η_I is the efficiency accounting for the irradiation level (computed according to Table 4.12).

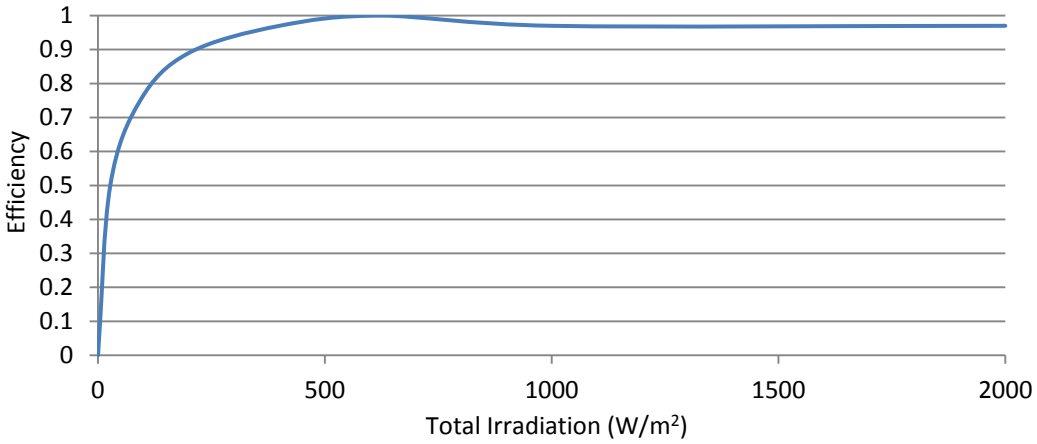

Figure 4.21 Solar panel efficiency vs. irradiation level.

Table 4.12 Interpolation model for the solar panel efficiency vs. irradiation level.

I_T	0	27	93	200	400	625	1000	2000
η_I	0	0.5	0.75	0.89	0.97	1	0.97	0.97

4.2.6 Solar Panel Output Power

The model equations previously introduced estimate energy flows, but it is convenient to estimate average energy in watts for electrical simulation purposes. Fortunately, the conversion is straightforward. When watt-hours are used as units of energy and the calculations are done on an hourly basis, the numerical value of the solar energy estimated by the model equals the electrical energy in watts. Equation 4.34 describes the electrical output power of the solar panel in terms of the total radiation, the panel area, and the efficiency.

$$P_S = \eta_g \times I_T \times p_{area}, \tag{4.34}$$

where P_S is the electrical energy delivered by the solar panel (watts when the inputs of the simulator are in watt-hours and the simulation step is one hour) and p_{area} is the area of the panel.

4.3 Energy Converters

A power converter is also required by the energy subsystem. This module is considered to be a single energy converter that integrates a maximum energy point tracker and a battery charger that automatically adjusts voltage levels to achieve an adequate charge of the battery. The efficiency of this device is 90%. Equation 4.40 relates the power output of the converter to the energy generated by the harvesting devices.

$$P_C = \eta_C \times (P_S + P_W), \tag{4.40}$$

where P_C is the converter's output power, η_C is the efficiency of the converter, P_S is the energy generated by the solar panel, and P_W is the energy coming from the wind generator.

4.4 Energy Storage

The lead-acid battery is modeled around the state of charge (SOC) of the battery. Incoming and outgoing currents are used to estimate the SOC of the battery at any given time. It is assumed that charging efficiency is 90%, and efficiency is 95% during the discharge. Self-discharge is also accounted for, at a rate of 2% per month. The hourly discharge rate is 0.00003%. This is a very low value, but the cumulative battery discharge over a period of three months is over 6% and cannot be neglected.

The battery is placed inside an insulated enclosure with a phase change material that keeps the internal temperature of the battery above 0 °C. For ambient temperatures above 0 °C, the internal temperature of the battery follows the ambient temperature within a reasonable margin of error [84]. The capacity of the battery is estimated using a linear relationship that makes the capacity drop to 85% of its nominal value when the internal temperature reaches 0 °C (see equation 4.41 and Figure 4.22).

$$Q = \begin{cases} 85, & T_{air} < 0 \\ \frac{3}{5} \times T_{air} + 85, & 0 \leq T_{air} < 25, \\ 100, & T_{air} \geq 25 \end{cases} \quad (4.41)$$

where Q is the capacity of the battery (percentage) and T_{air} is the ambient temperature (degrees Celsius).

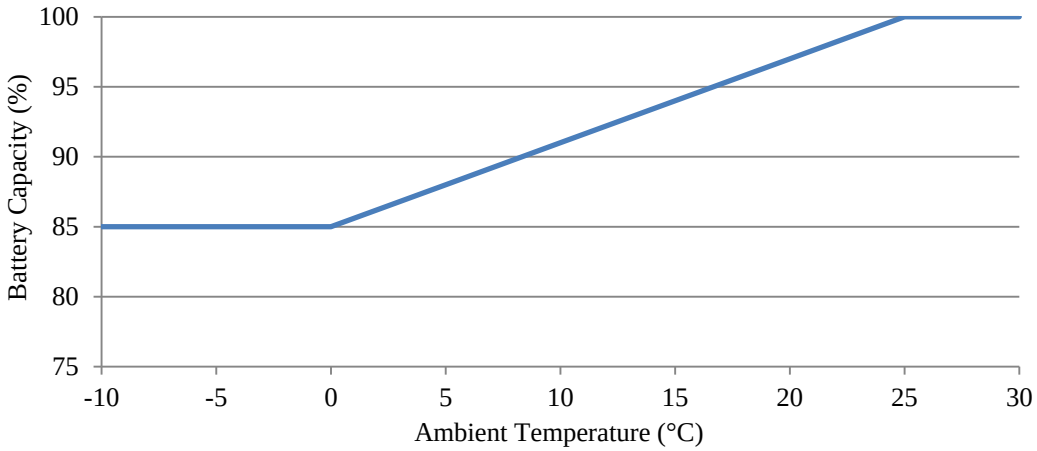

Figure 4.22 Battery capacity vs. ambient temperature.

4.5 Loads

The load is subdivided into three categories: data logger, satellite transmitter, and sensors. Average power consumption values provided by EC are used to estimate the current required to feed the load (Table 2.1). The load can be duty cycled by the energy management module, increasing or decreasing energy usage according to the system's status. To adapt the energy consumption profile to the electrical energy production profile, distinct duty cycles can be applied to each load (logger, satellite, or sensors. For example, individual duty cycles can be used to develop energy management strategies that transmit data (activate the satellite module) whenever there is excess energy coming from the transducers. This excess energy would otherwise be unexploited.

Equation 4.42 models the consumption profile.

$$C_L = d_{dl} \times C_{dl} + d_s \times C_s + d_{st} \times C_{st}, \quad (4.42)$$

where C_L is the consumption of the load; d_{dl}, d_s, and d_{st} are data logger, sensors, and satellite transmitter duty cycles, respectively, and C_{dl}, C_s, and C_{st} represent the maximum average consumption of these devices. This relation is valid for energy or current.

4.6 Conclusion

A 50 cm wind flutter generator was tested in a wind tunnel and plots of the test results are provided in this chapter. Parameters taken into account are wind speed, ribbon tension, angle of attack, and load. Experiments were made with different combinations of these parameters, and the resulting output RMS voltage and signal frequency were recorded. RMS voltage and load values were used to calculate output power under different system conditions. This allowed the identification of maximum energy points, optimal tensions, and optimal loads for diverse operating conditions. The effect of the angle of attack on the output power was also characterized.

An enhanced version of the wind flutter generator was developed and tested under similar conditions. This enhanced version provided higher efficiencies than the original (manufacturer's) version. The relative performance of both devices was established and both were compared with a small commercial wind turbine. Although the wind turbine worked at higher efficiencies than the flutter generators, it is costly and oversized for Environment Canada's weather station requirements.

A linear model for the wind flutter generator was proposed and it was used within the simulator as described in chapter 5. It is worth mentioning that there are several design parameters that can be considered for optimization of the flutter generator. These include the position of the magnets along the ribbon, the distance from the magnets to the electromagnetic transducer, the relative position of the magnets, the weight (and magnetic force) of the magnets, the length and width of the ribbon, and the characteristics of the

electromagnetic transducer, among others. The development of a mathematical model of the generator based on aeroelasticity theory is possible and requires a deep knowledge of the field.

A power generation model for solar panels is introduced afterwards. The model uses solar irradiation data to estimate the incident radiation on an inclined surface (solar panel) and includes relations that permit the computation of the temperature-dependant solar panel efficiency and the corresponding output power. The solar model is far more complex than the models used for other subsystems of the automatic weather station, and special attention was put into the creation of a functional model.

Finally, models of the energy converter, battery, and load were provided. In Chapter 6 - these models are used as a basis for the design, testing, and validation of energy monitoring stations powered by solar panels and aeroelastic flutter generators.

Chapter 5 - Simulation Model of Monitoring Station

5.1 Simulation Framework

Figure 5.1 depicts the simulation process. First of all, climatological datasets (section 5.1.2) for different arctic locations were used as an input for the simulator. The datasets included several fields for variables that are of general interest in engineering applications. For the solar and wind energy models developed in Chapter 4, only some fields from the datasets were required: time stamp, solar irradiation, air temperature, and wind speed. Datasets from different sources were parsed and reformatted to generate uniform subsets to be used by the simulator.

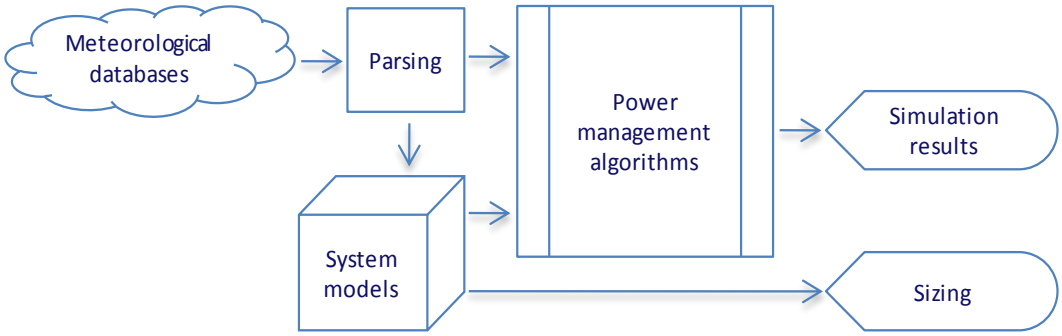

Figure 5.1 Simulation process.

System models were used to estimate power generation and to establish load consumption profiles. Once a complete model of the system was obtained and the requirements of the load had been estimated, real or synthetic meteorological data could be input to the system. The following step consisted of sizing of the harvesting power source for a specific location and

load. Additional simulations were performed to evaluate different energy management strategies.

Energy management algorithms were designed and introduced into the simulation process. Their goal was to guarantee the continuous operation of the system with minimal energy loss. Different approaches were tested and their performance compared (fuzzy controller vs. simple controller). Worst case scenarios were simulated to assess the performance of the algorithms and the robustness of the resulting control systems. Climatological datasets usually span more than two decades and smaller subsets were used for simulation purposes.

The models introduced in Chapter 4 were used as the foundation of an energy simulator for AWS. The simulator was built using the Matlab®/Simulink® platform (Figure 5.2 and Appendix 2). The main subsystems of the simulator: data input, solar, wind, energy converter, energy management, battery, load and data output are described in the following section.

5.1.1 Simulator Architecture

1) *Data input and output*. Simulator inputs included climatological data and a set of parameters that described the properties of each module. For example, the estimation of incoming solar energy made use of the size, azimuth, and inclination of the solar panel. The outputs of the simulator consisted of performance metrics, energy, and energy estimations. Table 5.1 provides the list of inputs and outputs of the simulator. SI units are used.

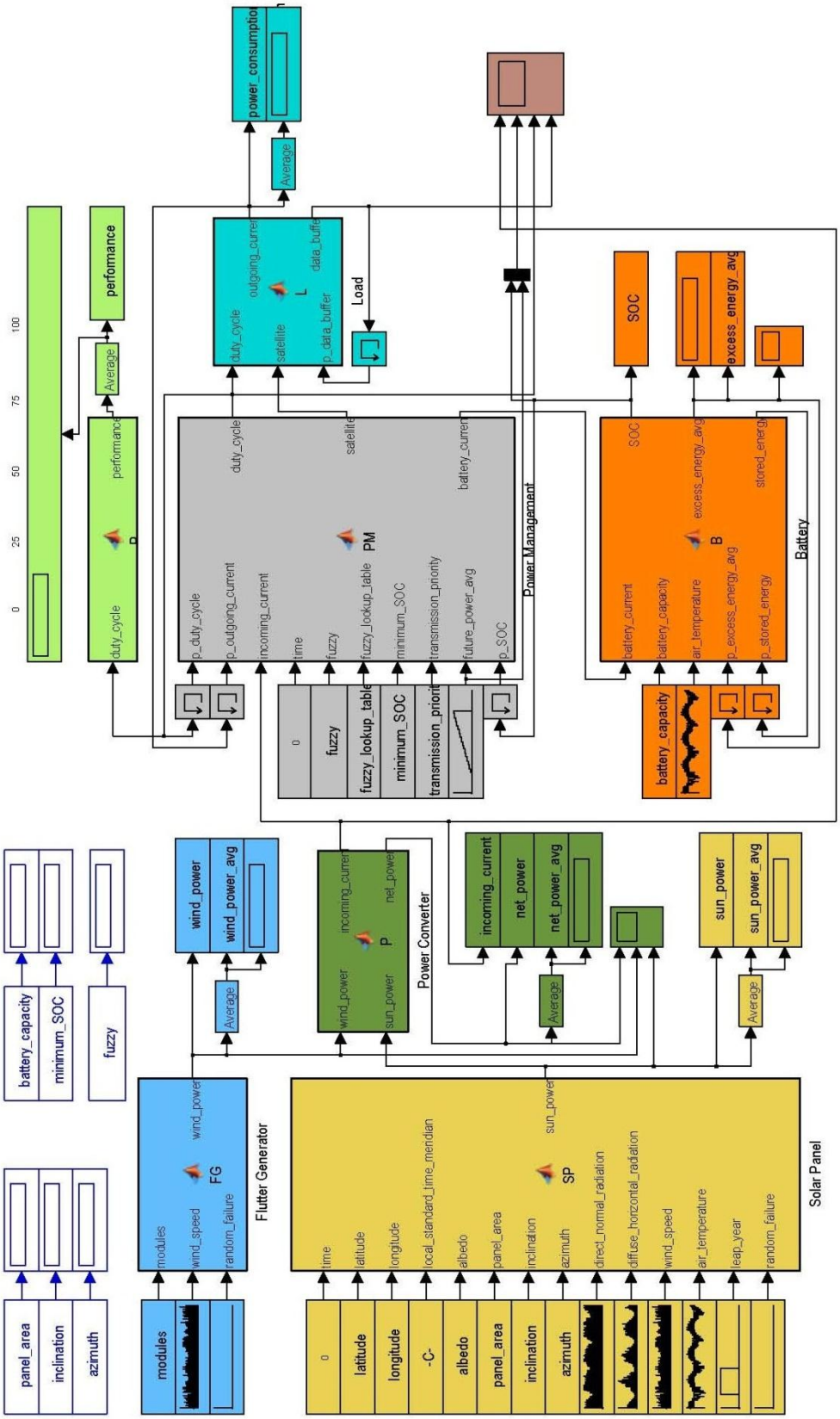

Figure 5.2 Simulink® Simulator Model.

Table 5.1 Simulator variables.

Parameter	Type	Subsystem	Comments
ETR	Input	N/A	Extraterrestrial radiation
GHI	Input	Solar	Global Horizontal Insolation
DNI	Input	Solar	Direct Normal Insolation
DHI	Input	N/A	Direct Horizontal Insolation
Temp	Input	Solar, Battery	Ambient temperature
Wdir	Input	N/A	Wind direction
Wspd	Input	Wind	Wind speed
Azimuth	Input	Solar	Solar panel azimuth
Inclination	Input	Solar	Solar panel inclination
Panel_area	Input	Solar	Area of the solar panel
Latitude	Input	Solar	Latitude of the location
Longitude	Input	Solar	Longitude of the location
Albedo	Input	Solar	Albedo
Time	Input	Solar	Elapsed time, hours
Modules	Input	Wind	Number of wind modules
Solar	Input	Energy Converter	Incoming solar energy
Wind	Input	Energy Converter	Incoming wind energy
Incoming	Input	Energy Routing	Total incoming current
Outgoing	Input	Energy Routing	Total outgoing current
SOC	Input	Energy Routing	Battery State of Charge
Q	Input	Battery	Battery Capacity
Logger	Input	Load	Data logger load profile
Satellite	Input	Load	Satellite comm. load profile
Sensors	Input	Load	Sensors load profile
Senergy	Output	Solar	Solar panel energy
Senergy_avg	Output	Solar	Average solar panel energy
Senergy_avail	Output	Solar	Available solar energy
Wenergy	Output	Wind	Wind generator energy
Wenergy_avg	Output	Wind	Avg. wind generator energy
Wenergy_avail	Output	Wind	Available wind energy
Load control	Output	Energy Routing	Load control signals
Battery current	Output	Energy Routing	Current from / to battery
SOC	Output	Battery	State of charge
Current	Output	Load	Load consumption

2) *Solar Panel*. Estimation of the energy generated by the solar panel was performed using the Perez model [32] (section 4.2). This was the most complex part of the simulator, as computing the amount of solar radiation received by a tilted surface with specific azimuth involves several algorithms. This module took into account the location of the AWS, the characteristics of the solar panel, the local standard time,

and several meteorological variables. The output was an hourly average of the electrical energy produced by the solar panel.

3) *Flutter Generator*. This module was based on a wind flutter generator model developed from experimental results. A simple linear model was used (section 4.1.3.9). The number of discrete wind generators and the wind speed were the inputs of this system. Additionally, generator failures can be simulated using a binary input provided for this purpose (the solar module offered this functionality as well). The flutter generator module output was an hourly average of the energy produced.
4) *Energy Converter*: An electronic energy converter with an efficiency of 90% was considered. The output power estimated by the wind and solar modules was used to estimate the energy and current that exited the converter. The current was calculated on the basis of a 12 V bus.
5) *Energy Management*. This module was used for two purposes: energy routing and energy control (energy management). In a real setting these submodules would be represented by two separate entities: a piece of software run by a microcontroller (energy management) and a hardware module capable of directing electrical energy in three different ways: source to load, source to battery, and battery to load. For simplicity, the simulator used a unique representation of both modules. Two energy management strategies were considered within this module and a flag selected one or the other. The first one was a simple energy management algorithm based on the state of charge of the battery (SOC). Preliminary testing of the simulator was conducted using this algorithm and is discussed in section 5.1.4. The second strategy is an advanced intelligent energy management scheme that is presented in sections 6.5 and 6.7.
6) *Battery*. A model employed to estimate the state of charge of a battery was discussed in section 4.4. This module used the battery capacity, the current that flows in and out of the battery, and the air

temperature to provide an estimation of the state of charge. Self-discharge, round-trip efficiency, and low temperature effects were taken into account.

7) *Load*. Hourly energy consumption of the sensors, data logger, and satellite transmitter were considered. The data logger and the sensors were grouped together and operated according to a duty cycle established by the energy management module. This provided a way to adjust energy consumption and avoid system shutdowns. The satellite transmitter followed a different mode of operation. The duty cycle of the data logger and the sensors affected the quality but not the quantity of gathered data. Hence, the amount of hourly data to be transmitted was always the same, unless the system was dead and data were lost. A technique that increased the energy efficiency of the AWS with an appropriate control mode for the satellite transmitter is presented in section 6.8.

5.1.2 Datasets

The output power estimation of the energy harvesting generators depended on meteorological conditions that could be derived from climatological datasets. Four databases fit for renewable energy studies in Canadian and U.S. arctic locations were used: CWEEDS, CWEC [13], NSRDB, and TMY3 [14] (Table 2.5). The focus of this thesis is on wind and solar power generation and not all variables included in the databases were of interest. Parsing and reformatting allowed the creation of custom and uniform datasets that contained information relevant to the energy estimation needs (Table 5.2). The parsing scripts used for this purpose were programmed in Python™ and are provided in Appendix 1.

Table 5.2 Variables obtained from datasets.

Variable	Module
Wind speed	Flutter generator and solar panel
Direct normal radiation	Solar panel
Diffuse horizontal radiation	Solar panel
Air temperature	Solar panel and battery
Leap year*[1]	Solar panel
Future average incoming energy*[2]	Energy management

*These entries are not included in the original databases.
[1]Leap year is a binary variable that indicates whether the data corresponds to a leap year (1) or not (0).
[2]Future average incoming energy is estimated with the simulator and integrated into the custom dataset.

Four locations were selected based on the high quality of the data they provided: Resolute, Inuvik and Whitehorse (Canada), and Barrow (United States). The location of the data sources is shown in

Figure 5.3, and pertinent details about these locations and their datasets are provided in Table 5.3.

Table 5.3 Information about the locations and datasets used for simulation.

	Barrow	Inuvik	Resolute	Whitehorse
Country	USA	Canada	Canada	Canada
Location with respect to the Arctic Circle	North	North	North	South
Latitude (degrees North)	71.32	68.32	74.72	60.72
Longitude (degrees West)	156.62	133.53	94.98	135.07
Local Standard Time Meridian (degrees West)	135	105	90	120
Typical meteorological year dataset	Yes	Yes	Yes	Yes
Full dataset span (years)	44	17	27	37
Data frequency	Hourly	Hourly	Hourly	Hourly

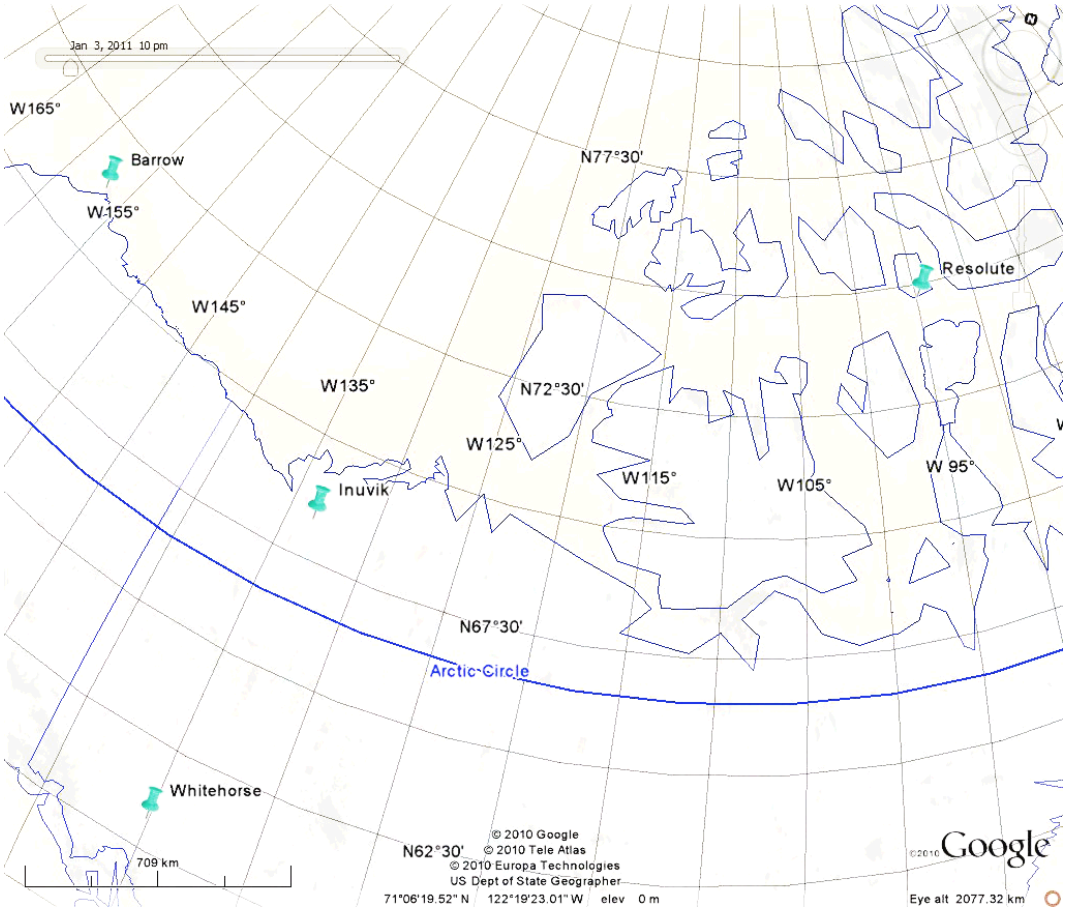

Figure 5.3 Location of arctic data sources.

5.1.3 Simulation Parameters

Table 5.4 provides a list of the parameters used to configure the simulator. Some of these parameters appear as inputs of one or more modules. Climatological entries such as temperature and wind speed were introduced in the last section and are not included in this table. Variables that correspond to the parameters and were represented by vectors or matrices are shown in Table 5.5. These variables were updated according to the needs of the simulation, e.g., a new control surface was obtained after optimization of the fuzzy controller.

Table 5.4 Parameters of the simulator.

Parameter	Module	Description
Modules	Flutter generator	Number of discrete generators
Time	Solar panel and energy management	Simulation time, in hours.
Latitude	Solar panel	Latitude of the AWS location.
Longitude	Solar panel	Longitude of the AWS location.
Local standard time meridian	Solar panel	Local standard time meridian of the AWS location.
Albedo	Solar panel	Albedo at the AWS location, isotropic ground conditions.
Panel area	Solar panel	Surface of the solar panel.
Inclination	Solar panel	Inclination of the solar panel.
Azimuth	Solar panel	Azimuth of the solar panel.
Fuzzy	Energy management	(1) – fuzzy control mode; (0) – simple control mode.
Minimum SOC	Energy management	Minimum allowed state of charge of the battery. If the SOC falls below this limit, the station is shutdown.
Battery capacity	Battery	Nominal capacity of the battery.

Table 5.5 Variables represented by vectors or matrices.

Variable	Module	Description
Random failure	Flutter generator and solar panel	Binary vector: (1) indicates that the generator is failing and the output power is zero; normal operation corresponds to (0).
Fuzzy lookup table	Energy management	Fuzzy control surface look-up table.

5.1.4 Simulator Testing

A simple energy management algorithm was used to test the simulator. The use of a deep discharge battery was assumed, with a maximum allowed depth of discharge of 80%. When this condition occurred and the environmental energy sources were unable to power the load, the system shut down. Under all other scenarios, the load was fully powered; the battery was charged or discharged depending on the availability of environmental sources. Excess energy was wasted. Figure 5.4 shows a plot of the simulation

spanning over one typical meteorological year. Simulation parameters are provided in Table 5.6.

Starting on January 1, the battery was fully charged and the polar night impeded solar power generation. The wind modules slowed battery discharge. Solar generation started in mid-February and peaked by the end of May. The efficiency of the solar panel was higher during the cold months (spring) than under warmer conditions (summer and autumn).

With the aid of incoming solar energy, the battery slowly recharged. From May to August, the battery was fully charged and excess environmental energy was discarded. In October, solar energy production greatly declined and the system started to depend heavily on the stored energy. In December, the battery reached an SOC of 20% and the system started to operate intermittently.

Preliminary testing of the simulator revealed the need to size the power source according to the location and the characteristics of the load. Additionally, the simulation started with an unlikely state of charge of 100% in the middle of the winter. For this reason, subsequent simulations started in July. Finally, a properly sized power source was able to power the load as long as its operational conditions were within the boundaries used to define the characteristics of the power source. The power source failed to power the load continuously whenever the system operated outside these boundaries (Figure 5.4), e.g., worst case scenarios.

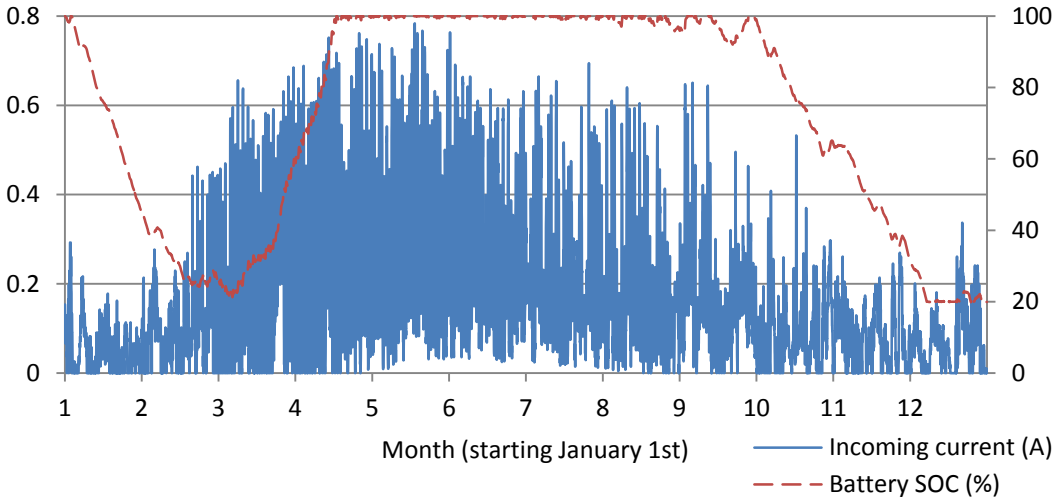

Figure 5.4 Simulator test results.

Table 5.6 Simulator test parameters.

Parameter	Value
Time	1 typical year (CWEC)
Location	Resolute, Nunavut, Canada
Latitude	74.72°
Longitude	94.98°
Solar panel azimuth	0°
Solar panel inclination	45°
Solar panel area	0.07 m^2
Albedo	0.7
Wind modules	15
Battery SOC (initial)	100%
Battery voltage	12V
Battery capacity	100Ah
Data logger avg. consumption	0.039A
Satellite module avg. consumption	0.054A
Sensors avg. consumption	0.036A

Chapter 6 - Intelligent Energy Management

Most recent studies related to harvesting aware power management are related to sensor networks. Energy and power management concepts share the same principles but AWS deployed in cold regions are subject to special operational conditions (section 2.1). Specifically, when solar panels are used as the main component of the power source, the energy production cycle of these unmonitored stations is too long (one year) and an unusually large backup battery is required. In such system, the energy neutrality principle (section 3.4) is hard to enforce because incoming excess energy is normally wasted during the summer and during the winter the system can be faced with energy shortages. An ideal energy-neutral management strategy will match energy production with energy consumption and minimize energy losses.

Ideally, harvesting aware energy management (HAEM) algorithms that are to be implemented in hardware-limited embedded systems, such as data loggers, should have low computing complexity. In addition, the energy overhead created by the real-time processing of an HAEM algorithm should be as low as possible, and the net energy gain obtained by the algorithm must be higher than the gain obtained by the use of naive energy management strategies. The design of energy management algorithms based on computational intelligence techniques must abide by these rules.

Intelligent algorithms (based on fuzzy logic, neural networks, or genetic programming, to mention some) normally require lots of computing resources and can hardly be handled by modern data loggers (not to mention

legacy data loggers). This problem can be solved if the energy management strategy is mostly computed off-line, e.g., creation of precompiled controllers [85] (look-up tables) and parameter optimization prior to implementation into the logger's microcontroller.

Some reasons that justify the use of computational intelligence techniques for energy harvesting purposes are listed below:

- Environmental energy sources can be unpredictable and several internal and external factors affect the performance of the energy transducers.
- Storage elements suffer from aging and behave differently when they are used at low temperatures.
- When a variable duty cycle approach is employed, a careful scheduling of the loads can lead to improved system performance and some energy savings.

Hence, the use of algorithms that are able to adapt to stochastic and changing system conditions is suggested. Genetic algorithms (GA) and fuzzy logic (FL) are used throughout this chapter for control and system optimization. This chapter describes a simulator that was developed with the purpose of designing and testing intelligent energy management algorithms. The chapter describes the design, optimization, and simulation of a fuzzy energy management strategy, with one section dedicated to the optimization of power source components. Fragments of this chapter are presented in [86].

6.1 Energy Management and Power Management

The line that divides energy management and power management is not clear in the literature. There are many references to power management and only a few to energy management. Although the boundary between the terms is hard to define, it can be put in terms of time and energy magnitude. Immediate, high power requirements are best handled by power

management, while energy management is a better approach for long term, high energy needs. Most systems are in between these extremes and will benefit from power and/or energy management strategies at different levels.

The peculiarities of AWSs operating in arctic regions were described in chapter 2; these systems operate in one year cycles, their immediate energy requirements are very low, but they require a considerable amount of long term energy. Therefore, they mainly benefit from energy management strategies. These strategies are similar to the power management techniques that commonly appear in the literature (HAPM).

6.2 Energy Management in Harsh Environments

Equipment deployed in the arctic displays unusual operational peculiarities due to standalone operation (isolation), low temperatures, extreme weather, and the polar night (solar panels). As mentioned in section 6.1, AWSs in the arctic can benefit from energy management strategies. This is especially true when solar panels are used to harvest electromagnetic radiation from the sun, as the polar night and the long winters create a natural, yearly (solar) energy cycle. Long energy cycles are not common to most applications, and it is hard to compare AWSs with systems that operate on daily energy cycles.

As a reference, rovers are vehicles designed to explore extraterrestrial bodies such as Mars [87]. This is an extreme case where the reliability of the system is paramount and the exposure to extreme environments is very high, e.g., temperature changes and dust [88]. The application of energy management strategies to experimental rovers has been shown to reduce the energy/performance gap [70]. But rovers differ from AWSs in that their missions are relatively short, they use moving mechanisms and heating elements that consume lots of energy, and they are subject to daily energy cycles when they are energized with the use of solar panels.

The energy management strategies described in Chapter 3 can be applied to energy harvesting systems such as rovers, as stated in [70]. For instance,

NASA's Mars Pathfinder used a very simple energy management strategy that consisted of task sequencing. The main goal was to prevent going over the energy capacity of the source (a primary battery and a solar panel) [89]. Therefore, the challenge is not which strategies are used, but how to implement them in a manner that will be beneficial (increase efficiency and/or system utility) for the application of interest. The same applies to the automatic weather stations located in northern regions (from an energy perspective).

6.3 Energy Management and Computational Intelligence

Computational intelligence (CI) can be defined as "the study of making computers do things that the human needs intelligence to" [90]. In our case, human-level intelligence would be needed to manage power in an arctic monitoring station or in any other system that relies on harvested energy. Few publications deal with the use of CI techniques for harvesting aware energy management applications, and no references concerning intelligent energy management for AWSs or intelligent energy management for arctic regions were found in the literature. The CI algorithms presented in the following sections make use of two particular techniques: fuzzy logic and genetic algorithms (GA).

Most of this chapter deals with the design, optimization, and simulation of a compiled fuzzy controller (FC) for energy management purposes. Fuzzy controllers use linguistic membership functions (e.g. "high", "low") to describe their inputs and outputs. The three main steps in fuzzy control are fuzzification, fuzzy inference and defuzzification. Fuzzification is the process of assigning a degree of membership between 0 and 1 in each input fuzzy set, for each input parameter. Fuzzy inference combines this fuzzy description of the inputs with a knowledge encoded in the form of fuzzy IF-THEN rules. Defuzzification takes the fuzzy product of this composition and converts it to a specific, crisp value. In a compiled controller, the control surface of a fuzzy controller is represented using a look-up table. This table, which can be

programmed into a microcontroller memory, implements the fuzzy control algorithm with little overhead—i.e., the inputs of the controller point to a memory location where the precomputed output is stored. Once the input values have been established, the output is obtained using memory read-out operations.

FCs do not require a model of the system to operate. Instead, the controller's output is obtained using a set of rules that describe the desired operation of the system. FCs are very useful when a model of the system is not available or is hard to obtain, and when expert knowledge about the system is available. For these reasons, FCs are well known for their ability to control systems that are very difficult to control using traditional control methods.

One problem that arises with the use of compiled FCs is that the control surface is precomputed and it might fail to correctly control a system when unexpected statuses occur. Updating the look-up table in real time usually requires a fuzzification-inference-defuzzification process to update every entry on the table. This is difficult to implement and resource-consuming when low-end microprocessors are used. One solution is updating the look-up table entries without resorting to the use of the fuzzy process, as described in [85]. Using this method, adaptive compiled FCs that are able to deal with unknown situations in real time can be programmed in simple microprocessors.

Expert knowledge is required to establish the rules that define the operation of the system and the fuzzy sets that describe the inputs and outputs of a fuzzy system. Once fuzzy sets and rules have been outlined, tuning of the FC to obtain an acceptable performance is required. Tuning can be achieved through optimization of the parameters that describe the fuzzy sets and/or the rules. The optimization process is normally nonlinear and the combinations of all possible parameters' values can be infinite. With these constraints, a direct search optimization is not practical or feasible.

Optimization strategies that aim to find a set of suboptimal solutions (parameters) can be used instead. They will not search over all the space and they will focus searching efforts to specific areas, saving time. Some examples of intelligent optimization algorithms are hill climbing, swarm, genetic and simulated annealing.

Genetic algorithms and genetic programming are part of the family of evolutionary computing [90]. These techniques are inspired by evolutionary processes. Genetic programming can be used to obtain time-series models for energy management applications. This technique can be used to obtain models of solar and wind speed time-series, which can be employed to forecast incoming energy. The estimation of future incoming energy can be used to establish load profiles accordingly. Genetic programming is successfully applied to forecast energy consumption in [91], where it is demonstrated that a model obtained with genetic programming is able to forecast time series with a lower sum of squares due to error than polynomial and energy equation models.

The typical flow of an evolutionary algorithm is described below. A random population is created and each individual (candidate solution) is evaluated against a fitness function. Individuals with high fitness "survive" and become the parents of the next generation. Children are generated using one or both of these approaches: crossover and mutation. For crossover, two parents are randomly selected and randomly recombined. The mutation operator replaces a randomly selected gene of the parent with a random value. A new generation is obtained; parents and children compete (fitness) and the process starts again. The algorithm iterates until a stopping condition occurs, such as finding an individual with better fitness than that of a preestablished threshold.

As described in section 6.5.1, a genetic algorithm was used to search for combinations of solar panel configurations and battery capacities that

minimize energy waste and system shutdowns. Since distinct geographical locations provide unique solar and wind energy profiles, the algorithm was applied to every arctic location considered to be within the scope of this dissertation. Genetic algorithms were used again in section 6.7 to optimize the parameters of the fuzzy energy management strategy.

CI techniques such as reinforcement learning, hill climbing, and bargaining games have been used for energy management of energy harvesting devices. Hill climbing algorithms are iterative processes where parameters are updated in the direction that moves the solution one step closer to the goal. The algorithm ends when a change in the parameters will not produce an output that is closer to an optimal value. The main disadvantage of this algorithm is that it does not provide a way to escape from local minima (which more sophisticated search algorithms are able to do), but it can be implemented with great simplicity. In [34], a hill climbing algorithm is used to track the optimal output power point of a solar energy harvesting system. The control strategy based on this method adjusts the frequency of operation of a charge pump, allowing optimal energy transfer to the load.

An interesting application of CI to the field of harvesting aware energy management is the use of a bargaining game approach. It is used to establish optimal sleep and wakeup probabilities for solar-powered wireless sensor nodes in [58]. A sensor node can read and buffer data, or receive and transmit data from and to other sensor nodes. Three different modes of operation for the transceiver (active, listen, and sleep) have their respective energy consumptions and the data buffer has a finite capacity. Data packets can be blocked if the receiving node is sleeping or whenever its buffer is full. The bargaining game aims at establishing a convenient trade-off between energy conservation and blocked or dropped data packets.

Reinforcement learning is an unsupervised learning approach that builds a map of the system. To face unknown or stochastic states, the algorithm is

able to update the map online by means of exploration. Otherwise, it uses the map to determine an optimal policy to follow, according to the system status. Reinforcement learning is used to implement a dynamic energy management strategy for wireless sensor networks in [92]. Experimentation results reveal that the reinforcement learning strategy has an overall better performance than an adaptive duty cycling method. Reinforcement learning is also used as the core of an adaptive controller that maximizes transferred energy from a vibrational energy harvester to the load; this adaptive method increases the efficiency of the harvesting system [93]. Although these publications show that reinforcement learning methods can be applied to energy management tasks, they are probably too complex to allow straightforward implementation in a data logger setting. However, following the same idea of compiled fuzzy logic controllers, reinforcement learning can be used to produce control surfaces for HAEM routines.

6.4 Estimation of Average Electrical Energy

The first task of the simulator was the estimation of annual average energy produced by solar and wind flutter generators at different arctic locations (Barrow, Inuvik, Resolute, and Whitehorse). Typical meteorological years from CWEC and TMY3 datasets were used for the estimation. The flutter generators were supposed to have wind tracking capabilities and the solar panels had an inclination of 45 degrees and an azimuth of 0 degrees. The conditions of operation were ideal and the generators were free of snow, frost, or rime. The results are summarized in Table 6.1.

Wind and solar energy generation profiles greatly differed from location to location. This reinforced the need to optimize the power source on a case per case basis. The optimization of the power source involved several parameters: capacity of the battery; number of wind flutter modules; size, inclination, and azimuth of the solar panel.

Table 6.1 Average power generation for different arctic locations (one typical meteorological year).

	Barrow	Inuvik	Resolute	Whitehorse
Annual average energy per 100 cm² solar panel (watts)	0.13	0.16	0.19	0.28
Annual average energy per 50 cm flutter generator (watts)	0.08	0.03	0.10	0.04

6.5 Fuzzy Energy Management

6.5.1 Power Source Sizing

According to the developer [38], wind flutter generators can be arranged in arrays to increment the output power. An array of 20 discrete (one meter) generators fit inside a 1 m × 1 m × 0.05 m frame. With the aid of the simulator, it was determined that an array of 10 units of 50 cm, (combined with a solar panel), provided enough energy to prevent the complete discharge of the battery during the winter. The annual energy generated by this array was lower than the requirements of EC's weather station; hence, use of a storage battery and solar panel was necessary.

For sizing purposes, the solar panel was the most flexible component of the power source. Solar panels are manufactured in a wide range of sizes and capacities, and obtaining a solar panel array that matched the required energy production was not difficult. This flexibility was not offered by commercial lead-acid batteries, where the capacity variety is limited to a few different models, depending on the manufacturer. Whenever possible, the use of a single battery was preferred (fewer connections and straightforward installation). A deep discharge "Deka Solar" lead-acid battery for renewable energy applications was chosen as the storage device for the simulated monitoring station [94]. The manufacturer (Deka) offers a selection of gel batteries for solar applications with capacities ranging from 30 to 225 Ah @ C20, where C20 indicates the battery will fully discharge in 20 hours. A 225 Ah (70 kg) battery was selected. Note that the capacity of this

battery is lower than the 280 Ah that the reference station requires to operate for 90 days. Another important point is that although cold temperatures reduce the capacity of the battery, this is compensated by the low discharge rates made possible by the use of a solar panel and a wind flutter generator. The capacity of the same 225 Ah battery increases to 265 Ah @C100 and it can be expected to be higher at lower discharge rates. A complete charge and discharge cycle for this system takes one year, and estimating the "true" capacity of the battery under these circumstances is quite complex.

C20 is the most commonly used rate of discharge for batteries. It designates a rate of discharge that will completely discharge a fully charged battery in 20 hours. Similarly, a C100 rate will discharge a battery in 100 hours. The apparent capacity of a battery changes with the discharge rate; a battery that is rapidly discharged possesses a lower capacity than the same battery that is discharged at a low rate.

Finally, sizing of the solar panel was necessary. For the experiments described in this section, the area of the solar panel was set to 0.09 m^2. This value was obtained experimentally and is a compromise between energy waste in the summer (a panel so large that the harvested energy far exceeds the capacity of the battery), and energy shortage during the winter (an undersized panel that cannot keep the battery charged at 100 % by the end of the summer). Table 6.2 provides a summary of the configuration of the main components of the power source.

Table 6.2 Specifications of the power source.

Component	Properties
Lead-acid battery 8G8DLTP-DEKA	Voltage: 12 V Capacity @C20: 225 Ah Capacity @C100: 265 Ah Available capacity @0 °C: 85 % Self-discharge: 2 % per month
Wind Flutter Generator Array	Discrete unit length: 50 cm Number of units: 10 Array size (approx.): 50 x 50 cm
Solar panel	Panel area: 0.09 m2 Construction: Glass/cell/polymer Efficiency: 14 %
Energy converter	Efficiency: 90 % Maximum power point tracking capabilities

6.5.2 Fuzzy Controller

A FC was developed and its performance was compared to a simple energy management approach. The simple approach shut down the system whenever the state of charge of the battery fell below 20%. The AWS was powered on again when the incoming energy (wind and/or sun) was able to power the system and recharge the battery above 20%.

Data loggers have limited computational capabilities, and a design constraint for any energy management strategy is its simplicity. Complex algorithms require lots of computing energy and consume more energy than simple algorithms. In addition, the implementation of a complex algorithm in a data logger might be difficult (refer to section 6.9).

The initial fuzzy energy management approach had three goals: (1) to avoid system shutdowns (null duty cycle), (2) to maintain the duty cycle as high as possible, and (3) to keep the charge of the battery above 20 %. Other goals, such as minimizing data buffer overflows and reducing energy wastage were introduced as described in this chapter. The configuration of the system is described in the following paragraphs.

6.5.2.1 Fuzzy Controller Inputs and Outputs

The FC had one output (duty cycle) and two inputs (battery state of charge and future energy availability). The first input, recorded hourly, corresponded to the future energy availability and was determined by running a system simulation using a dataset for one typical year (for each location), and computing a 90 day moving average of the energy generated by the solar panel and the flutter generator. A table was generated and saved to memory. A real implementation of the algorithm would employ a "compressed" table with an estimate of the 90 day future energy availability for each day of the year (instead of every hour).

The second input represented the actual state of charge of the battery, while the output set the duty cycle of the system. In the FC, each input or output was represented by three fuzzy sets: low, medium, and high. Trapezoidal and triangular membership functions were used; parameters determined manually were based on experience and experiments. The resulting fuzzy sets are shown in Figure 6.1. Section 6.7 describes how these parameters were optimized to get better performance from the controller. The optimization was done using GAs but other optimization techniques can be used as well.

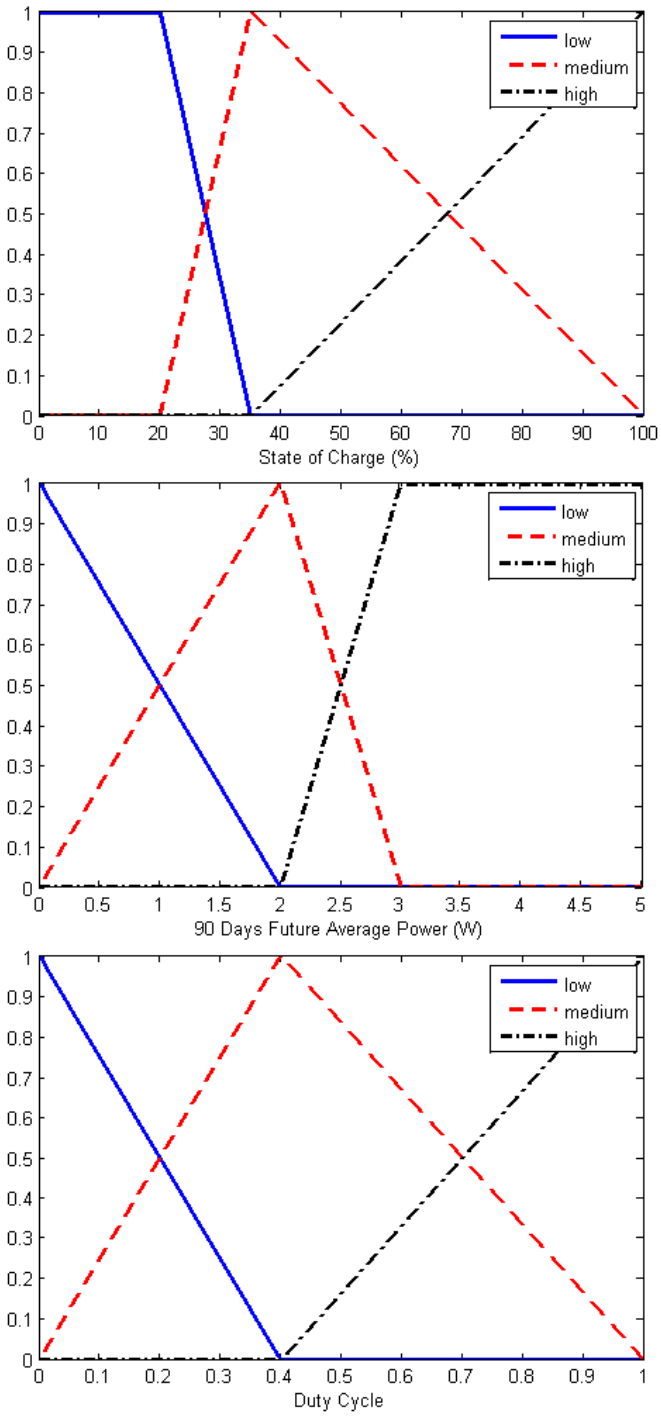

Figure 6.1 Fuzzy sets.

6.5.2.2 Fuzzy Controller Rules

As mentioned above, the fuzzy control system had two inputs and one output. Hence, nine fuzzy rules were needed to describe the fuzzy system. The initial

set of fuzzy rules was developed using expert knowledge, and tweaked until an acceptable system response was obtained. This set of rules is listed below.

1) If (energy is low) AND (SOC is low) THEN (duty cycle is low) ELSE
2) If (energy is low) AND (SOC is med) THEN (duty cycle is med) ELSE
3) If (energy is low) AND (SOC is high) THEN (duty cycle is high) ELSE
4) If (energy is med) AND (SOC is low) THEN (duty cycle is med) ELSE
5) If (energy is med) AND (SOC is med) THEN (duty cycle is high) ELSE
6) If (energy is med) AND (SOC is high) THEN (duty cycle is high) ELSE
7) If (energy is high) AND (SOC is low) THEN (duty cycle is high) ELSE
8) If (energy is high) AND (SOC is med) THEN (duty cycle is high) ELSE
9) If (energy is high) AND (SOC is high) THEN (duty cycle is high)

The input variable "energy" represents the future 90 day average energy, while "SOC" designates the battery's state of charge. To maximize the performance of the FC, this set of fuzzy rules can be optimized for different arctic locations.

6.5.2.3 Compiled Fuzzy Controller

A "continuous" FC, whose control surface is shown in Figure 6.2, was compiled. Since the duty cycle of the system represented measurements that were usually averaged and recorded hourly, "infinite" granularity of the duty cycle was not necessary. According to EC [95], some measurement instruments are programmed to operate at 15 minute intervals. Therefore, the granularity of the variable duty cycle can be reduced, taking as a reference the 15 minute interval standard and the one hour logging. The proposed set of duty cycles is presented in Table 6.3. Figure 6.3 shows the discretized version of the FC. This controller was saved as a look-up table and used in simulations. The resulting table is compact and suitable for programming on simple processors usually found in data loggers.

Table 6.3 Duty cycles.

Measurement interval (min)	Duty cycle (%)
15	100
20	75
30	50
60	25
-infinite-	0

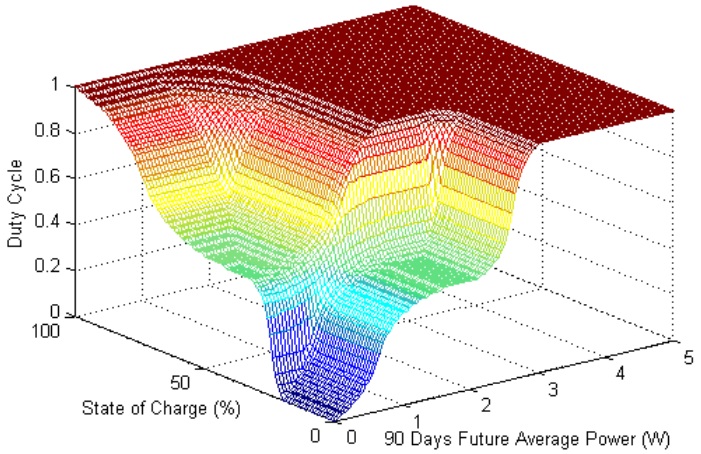

Figure 6.2 Continuous fuzzy controller.

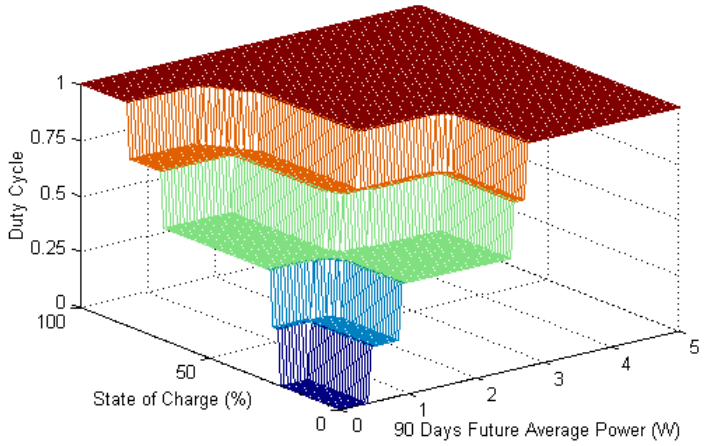

Figure 6.3 Discrete fuzzy controller.

6.5.3 Fuzzy Controller Testing

A set of simulations covering four arctic sites (Barrow, Inuvik, Resolute, and Whitehorse) was performed using simple and fuzzy energy management strategies. Recall that the first strategy shuts down the meteorological station

whenever the state of charge of the battery drops below 20%. The second strategy uses the compiled FC described in the previous section. No optimization procedures other than "trial and error" were used for sizing the power sources or to adjust the parameters of the controller. The same parameters (described in the previous section) were used for all simulations. Optimization of the power sources and the controller's parameters were performed for each arctic site and are presented in sections 6.6 and 6.7.

Figure 6.4 presents simulation results for Resolute, Canada. In this example, a typical meteorological year was used to compute the incoming energy (combined solar and wind energy generation), which is shown in Figure 6.4a. Figure 6.4b and Figure 6.4d show the state of charge of the battery for both strategies. Note that it never reaches 100%, since it is computed considering the effects of temperature on the nominal capacity of the battery: the temperature is always below 25°C, and the capacity never reaches its nominal value. However, the plots show long periods when the state of charge reaches an asymptotic level around 87%. During such times, the battery is fully charged and the energy harvested in excess is lost. This problem can be addressed with the use of a power management technique that adjusts the load of the system according to the incoming energy fluctuations. For example, data can be logged only when there is environmental energy available, and satellite communications can be postponed until there is an "excess" of energy (see section 6.8 – A Satellite Transmitter Strategy).

Figure 6.4c and Figure 6.4e illustrate the "simple" and the fuzzy energy management strategies, respectively. The simple strategy allowed the battery to discharge to a level of 20% over a long period of time (exceeding one month). During this interval, the system oscillated between active and inactive states. In several instances, the system was shut down for up to 10 hours in a row, leading to the non-recoverable loss of data. Furthermore,

keeping the state of charge at very low levels for long periods of time degrades battery performance and reduces its lifespan.

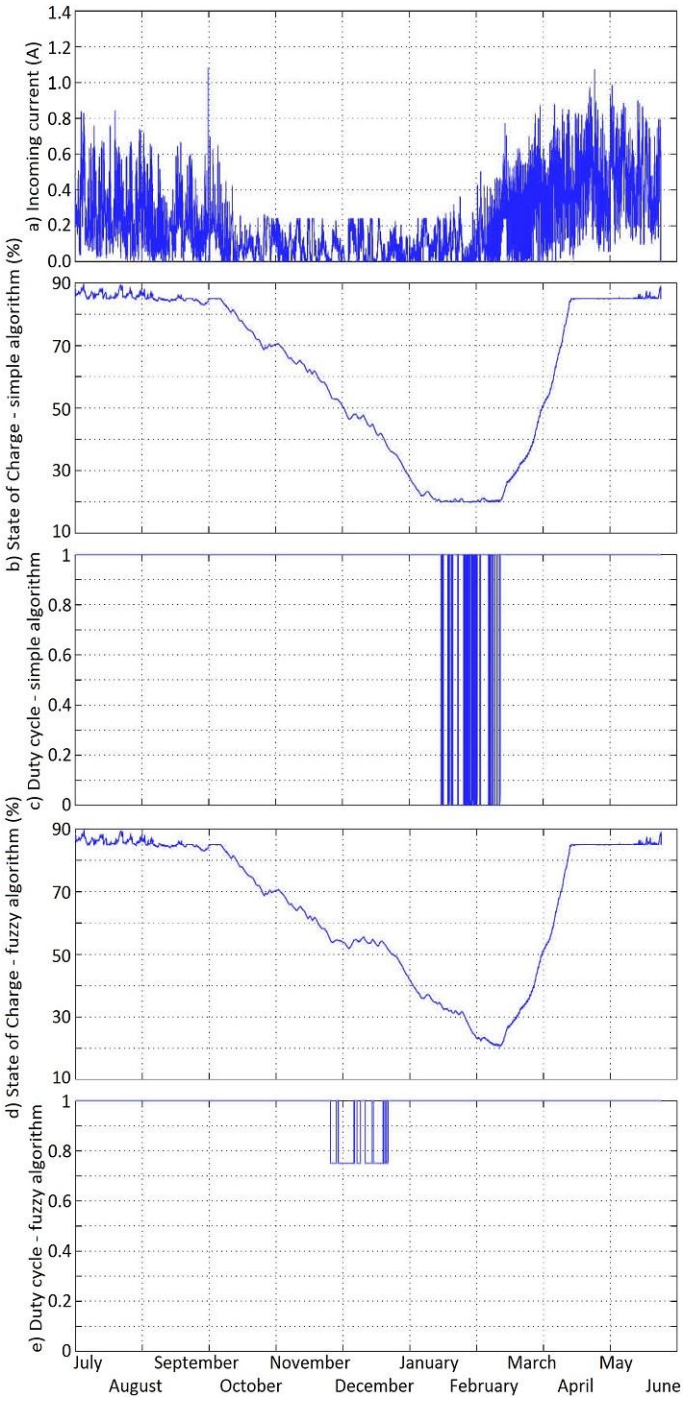

Figure 6.4 Sample simulation of a typical meteorological year for Resolute, Canada.

The fuzzy energy management strategy performed consistently better than the simple algorithm. The system operated most of the time at 100%, and the duty cycle never dropped below 75%. The algorithm anticipated the discharge of the battery with a lead time of several weeks, and acted accordingly. When it detected that the future energy availability was increasing, the duty cycle was again adjusted to 100%. Eventually, the battery's state of charge dropped toward (but never reached) 20%. At that time, the sunny season started, and the solar panels recharged the battery to its maximum level.

Figure 6.4 allows a visual inspection of the behaviour of the system. The performance of the algorithms were measured by the percentage of time that the system operated at each state (duty cycle). The simple system operated only at 0% or 100%, while the fuzzy algorithm based system used duty cycles of 25%, 50%, and 75 %.

The main advantage of the fuzzy energy management scheme was that it kept the duty cycle of the system at a high level (contrary to the simple method whose only way of reducing energy consumption was by shutting down the entire system). Unless a duty cycle of 0% is selected by the fuzzy algorithm, no hourly measurements are lost. Indeed, the only difference between duty cycles of 100% and 50% is that the second one will use 50% fewer samples to compute the hourly data average. For practical purposes an additional flag in the database can be used to mark these occurrences and relate them to the quality of the data: the higher the duty cycle the better the quality of the data (see Table 6.4).

Table 6.4 Simulation results – duty cycle occurrences (%) by arctic site and by energy management scheme (S - simple, F - fuzzy).

	Barrow		Inuvik		Resolute		Whitehorse	
Duty cycle	S	F	S	F	S	F	S	F
0 (shutdown)	6	0	22	0	3	0	8	0
0.25	-	0	-	0	-	0	-	0
0.5	-	3	-	26	-	0	-	6
0.75	-	17	-	14	-	8	-	15
1	94	80	78	60	97	92	92	79
Total	**100**	**100**	**100**	**100**	**100**	**100**	**100**	**100**

It is important to note that both the simple and the fuzzy strategies had access to the same energy resources. The differences in performance of these (or other) strategies are inherent to their design. None of these algorithms can reduce the annual average energy consumption of the system. They only provide different ways to schedule the utilization of the environmental energy by the energy harvesting devices.

The results in Table 6.4 were obtained using a power source and a control surface that were adjusted for Resolute, Nunavut. The best performance was obtained for this location, where the system operated with a duty cycle of 1 for 92% of the time and at 0.75 for 8% of the time. Lower performances were obtained at the other locations. This confirmed the need to optimize both the power source and the fuzzy control surface for each location. Sections 6.6 and 6.7 discuss the optimization and present simulation results.

6.6 Intelligent Power Source Sizing

As discussed in section 6.5.1, the power source components needed to be properly sized. The power source needed to produce enough energy to feed the load for one year and the availability of renewable energy varied with the location. Oversizing is a single, easy solution, but it involves higher costs and bulkier, heavier hardware. The challenge comes from the various parameters that are involved (location, weather, solar panel, wind generator, and battery

characteristics) and it increases with the amount of energy transducers and energy sources that are considered. This section introduces a genetic algorithm (GA) strategy that was used to find sets of power source parameters that guaranteed the yearly energy requirements of the AWS (no system shutdowns), minimized energy waste, and optimized the capacity of the battery.

The wind flutter generator was set to a fixed array consisting of 10 units of 50 cm. This put a cap on the electrical energy provided by this new device and let the solar panel and lead-acid battery act as the main components of the power source. The parameters to be optimized were the battery capacity and the solar panel's area, azimuth, and inclination (Table 6.5).

Table 6.5 Power source parameters.

Parameter	Values
Battery capacity (Ah)	200 to 320, 20 Ah increments
Solar panel area (m^2)	0.05 to 0.3, 0.01 m^2 increments
Solar panel inclination (°)	45 to 90, 5° increments
Solar panel azimuth (°)	-20 to 20, 5° increments

Optimization had multiple objectives: minimize system shutdowns, minimize excess (unused) energy, and minimize battery capacity. At the end of the optimization process, the GA optimization tool defined a set of parameters that represented different trade-offs between the objectives. The solution chosen was the one that presented fewer system shutdowns (ideally, 0). The Matlab®/Simulink® Optimization Toolbox was used to run the GA in the configuration shown in Table 6.6.

Note: the universe of solutions is finite and is represented by a set of vectors (one for each variable). The GA looks for positive integers that "point" to candidate solutions. The Matlab®/Simulink® GA solver does not include functions to handle integers. Therefore, custom initialization (population)

and mutation functions (Appendix A3.3) needed to be provided to the solver. Otherwise, an indexing error will occur.

An important part of the GA optimization strategy is the fitness function. The fitness function (equations 6.1 and 6.2) was designed to help meet the optimization constraints previously mentioned and the GA aimed to minimize it.

$$fitness_a = (system\_shutdowns + 1) \times annual\_excess\_energy \times \sqrt{\frac{\min(SOC)}{SOC_{min}}}, \quad (6.1)$$

$$fitness_b = -SOC_{final}, \quad (6.2)$$

where $fitness_a$ and $fitness_b$ are the multiobjective fitness functions, $system\_shutdowns$ is the number of hours that the system was off due to a lack of electrical energy, $annual\_excess\_energy$ is the amount of energy that was lost, SOC is a vector of hourly states of charge of the battery, SOC_{min} is the minimum SOC reached during the simulation period and SOC_{final} is the SOC at the end of the simulation.

The power sources' parameters were optimized for Whitehorse's typical meteorological year (Table 6.7). Similar results can be obtained for Barrow, Inuvik and Resolute. Note that the optimal solar panel inclination encourages winter energy harvesting as it is almost vertical (90°). This has the added advantage of preventing snow accumulation and facilitating water runoff. The solar panel azimuth is close to 0°, which means that the optimal orientation faces south.

Table 6.6 Intelligent power source sizing GA solver settings.

Parameter	Setting
Solver	Multiobjective optimization using genetic algorithm
Fitness function	energy_source_fitness
Number of variables	4
Lower bound	[1 1 1 1]
Upper bound	[7 26 10 9]
Population type	Double vector
Creation function/name	Custom / energy_source_population
Selection function	Tournament
Tournament size	4
Crossover function	0.5
Mutation function/name	Custom / energy_source_mutation
Crossover function	Scattered
Generations	30
Stall generations	15
Other parameters	Default values

Table 6.7 Power source optimization results.

Location	Battery capacity (Ah)	Solar panel area (m^2)	Solar panel inclination (°)	Solar panel azimuth (°)	Unused energy (%)
Whitehorse	320	0.06	85	-5	13

6.7 Intelligent Controller Optimization

Section 6.5.2 describes a compiled FC used for energy management purposes. The goal of the controller was to reduce or eliminate AWS system shutdowns due to a lack of electrical energy. This controller consists of a simple algorithm that turned the station off whenever the SOC of the battery dropped below 20% (or other predefined limit). The controller was shown to eliminate system shutdowns for a particular typical meteorological year (Resolute). The parameters of the FC were manually tuned, a time consuming process. Further experimentation with other datasets (several years of data and other locations) proved the need for optimization of FC parameters. This section describes the optimization of the FC using genetic algorithms. The

controller architecture described in section 6.5.2 and an extended set of rules were used. The rules presented below were obtained using expert knowledge.

1) If (time is low) AND (SOC is low) THEN (duty cycle is low) ELSE
2) If (time is low) AND (SOC is med) THEN (duty cycle is med) ELSE
3) If (time is low) AND (SOC is high) THEN (duty cycle is high) ELSE
4) If (time is med-low) AND (SOC is low) THEN (duty cycle is low) ELSE
5) If (time is med-low) AND (SOC is med) THEN (duty cycle is med) ELSE
6) If (time is med-low) AND (SOC is high) THEN (duty cycle is high)×$(time/101)^2$ ELSE
7) If (time is med-high) AND (SOC is low) THEN (duty cycle is low) ELSE
8) If (time is med-high) AND (SOC is med) THEN (duty cycle is low)×$(SOC/101)^2$×$(time/101)^2$ ELSE
9) If (time is med-high) AND (SOC is high) THEN (duty cycle is high) ELSE
10) If (time is high) AND (SOC is low) THEN (duty cycle is low) ELSE
11) If (time is high) AND (SOC is med) THEN (duty cycle is high) ELSE
12) If (time is high) AND (SOC is high) THEN (duty cycle is high)

One significant difference was the input variable "energy," which represented the 90 day average energy in the old FC; this was replaced with a simple ramp function that provides a time frame to the controller. This change avoided an early reduction of the duty cycle and allowed the controller to focus on the current energy status.

The FC was based on three distinct fuzzy sets: SOC (input), Time (input, ramp function) and Duty Cycle (output). Each fuzzy set had a discrete Universe composed of integers on the interval 0 – 100. The state of charge and the duty cycle were defined as percentages and fit directly into the 0 – 100 range. The parameters of the power source were determined using the procedure

described in section 6.6. The fuzzy sets and the resulting fuzzy controller are shown in Figure 6.5 (after optimization with the GA solver).

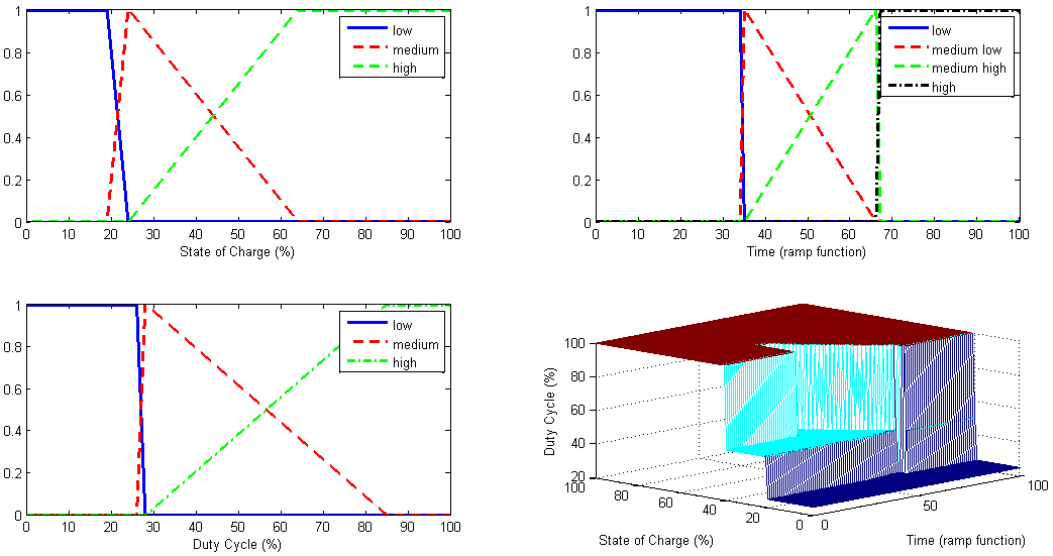

Figure 6.5 Optimized fuzzy sets and compiled fuzzy controller.

Table 6.8 provides the settings for the GA solver. Similar to its function in section 6.6, the GA looked for solutions within a finite universe. This greatly reduced simulation time and helped to converge to candidate solutions in an efficient manner. Once again, the Matlab®/Simulink® GA solver is designed to work with real numbers and dealing with integers required the use of custom population and mutation functions (Appendix A3.4). Additionally, the population was represented with an array of vectors (one vector for each parameter). The parameters that represented the fuzzy sets needed to be sorted and this had to be incorporated into the custom functions as well (population, mutation, and crossover).

The optimization function is a weighted sum:

$$fitness_{fuzzy} = 32d_0 + 2.5d_{25} + d_{50} - d_{100}, \qquad (6.3)$$

where d_0 is related to the number of hours that the system was shut down over the simulation period and d_{25}, d_{50} and d_{100} represent the number of hours where a duty cycle of 25, 50 and 100% were used.

The goal of the GA was to find a set of fuzzy controller parameters that minimized the fitness function. The term d_{100} has a negative sign because it is preferred to keep the system operating at 100% duty cycle for as long as possible. The rest of the terms carry positive signs and they are weighted according to their "undesirability." d_0 carries the highest weight since system shutdowns are heavily penalized.

Table 6.8 Fuzzy controller optimization GA solver settings.

Parameter	Setting
Solver	Genetic Algorithm
Fitness function	fuzzy_fitness
Number of variables	3
Population size	50
Creation function/name	Custom/fuzzy_population
Scaling function	Rank
Selection function	Remainder
Crossover fraction	0.5
Mutation function/name	Custom/fuzzy_mutation
Crossover function	Custom/fuzzy_crossover_single
Other parameters	Default values

6.7.1 Simulation Results

Figure 6.6 and Figure 6.7 show, respectively, the simulator output for the simple controller and the FC after optimization. The simple controller was described in section 6.5.2. Four years of data were used for these experiments. The only "real time" input for the simulator was the battery's SOC. The other input was a precomputed energy average (typical meteorological year). Still, the FC drastically reduced system shutdowns and was able to anticipate an energy outage without the use of complex techniques such as forecasting. The response of the controller was proportional to the energy environment: it provided lower duty cycles and maintained system operation for longer times when energy was scarce.

Figure 6.8 demonstrates the robustness of the controller when an additional (nontraining) sequence of 6 years was added to the set.

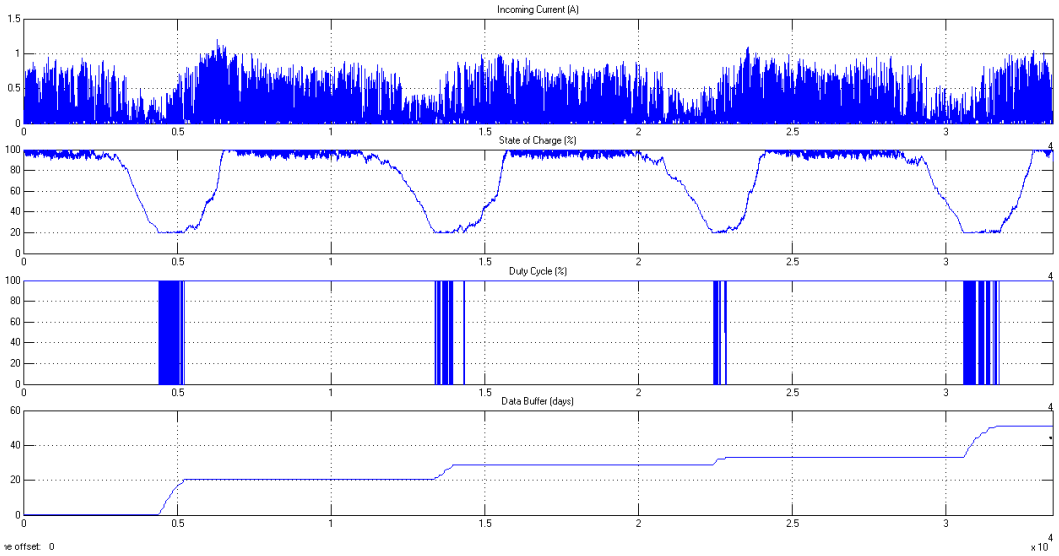

Figure 6.6 Simulation with simple controller. Whitehorse, July 1995 to June 1999.

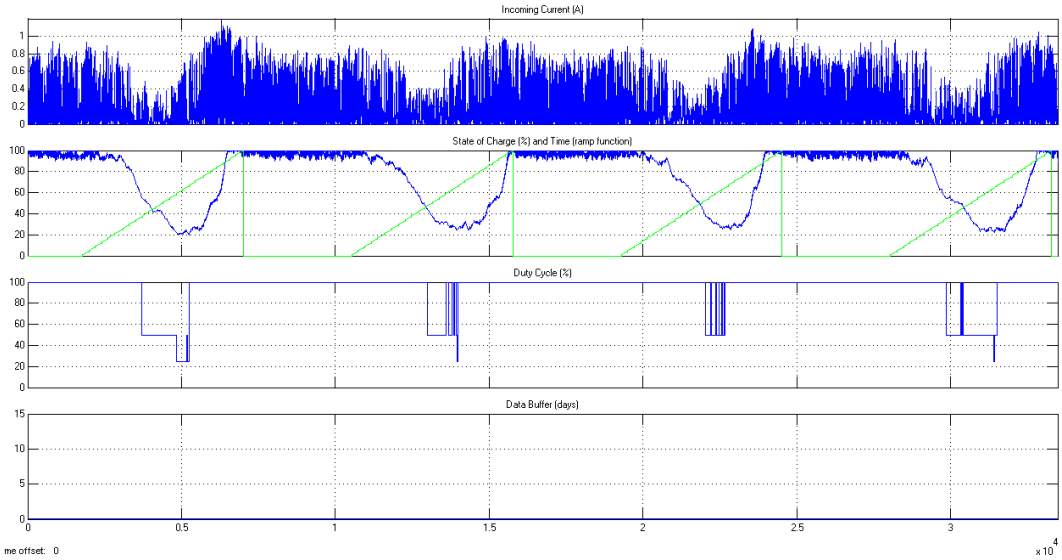

Figure 6.7 Simulation with optimized fuzzy controller. Whitehorse, July 1995 to June 1999 (training set).

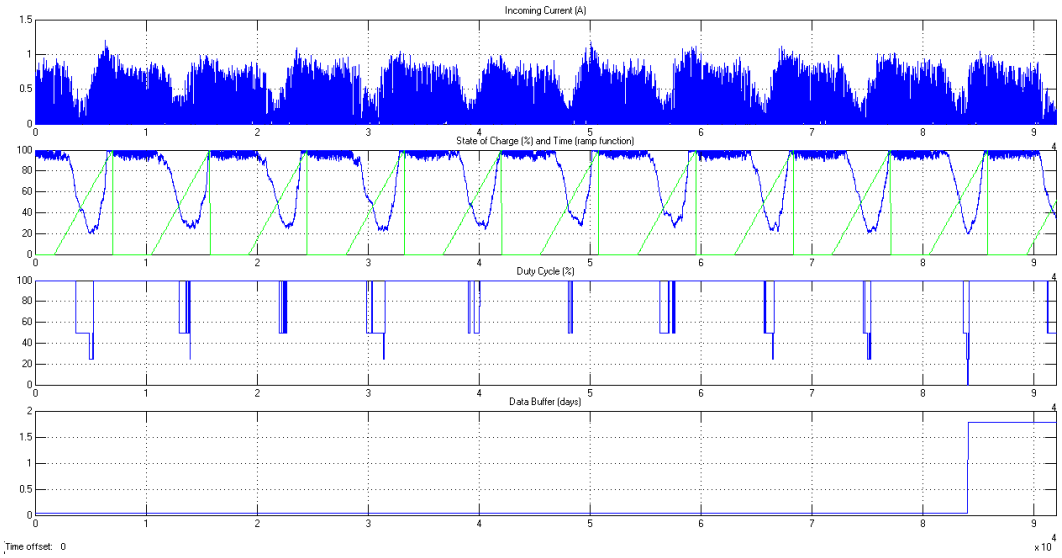

Figure 6.8 Simulation with optimized fuzzy controller. Whitehorse, July 1995 to December 2005 (complete set).

Table 6.9 Comparison between simple and optimized fuzzy controllers. Whitehorse, July 1995 to June 1999 (training) and Whitehorse, July 1995 to December 2005 (complete).

Controller	Lost Data – training dataset (days/4 years)	Lost Data – complete dataset (days/10 years)
Simple	51	99
Optimized fuzzy	0	2

Table 6.10 Simulation results – duty cycle occurrences (%) by energy management scheme (S - simple, F – optimized fuzzy). Training set.

	Whitehorse	
Duty cycle	S	F
0 (shutdown)	3.67	0
0.25	-	1.29
0.5	-	12.18
1	96.33	86.53
Total	**100**	**100**

6.8 A Satellite Transmitter Strategy

The AWS station's power source was designed to obtain most of the energy from the solar panels and to use the battery for both short term and long term energy storage. The wind generator provided a fraction of the energy

and was a secondary power source. Therefore, the AWS system had energy cycles that were heavily influenced by solar patterns (daily and yearly). As shown in Table 6.7, even optimized power sources were not able to harvest all the energy that was potentially available. This occurred when the battery was fully charged and energy consumption was lower than electrical energy generation. This unused energy was a significant portion of the total energy production over one year.

The main purpose of the data logger was to acquire and store data at regular intervals. Data were retrieved in different ways. A satellite module, similar to the one used by EC's reference station, was used to stream data in real time. This feature was convenient, as it eliminated long waits for data and the need to retrieve data at the time of servicing equipment (usually once a year). But the cost was high; the toll on the total energy budget was nearly 30% (Figure 2.4). Roughly, a power source (energy harvesters, energy converters, and storage) needs to have 30% more capacity if a satellite module is required.

Let's suppose that an AWS is equipped with a satellite transceiver, and that real time transmission of measured data is not a priority. Table 6.11 shows a comparison between a satellite transmission strategy that uses excess energy for this task, and a real-time transmission approach. Figure 6.9 illustrates two cases. The upper plots are the reference and represent a situation where satellite transmission is a priority and takes place in real time. The lower plots refer to the "transmit on energy availability" policy. The first scenario blindly uses available energy and eventually leads the system to failure (shutdowns) and the equivalent of three days of irrecoverable data loss. The second scenario (satellite transmission strategy) not only eliminates lack of energy issues, it keeps the SOC of the battery considerably above the minimum SOC of 20%. The toll is the accumulation of 60 days of data into the data logger's memory. But this data is transmitted (satellite) as soon as the incoming energy starts to rise. This simple satellite transmission strategy has a noticeable positive impact on the energy budget of the system, helps to

minimize system shutdowns, reduces the size of the power source (34% in Whitehorse), and relieves the seasonal energy changes. This algorithm can be combined with the fuzzy logic controller for further performance. The trade-off between energy savings and real time data transmission can be adjusted as required.

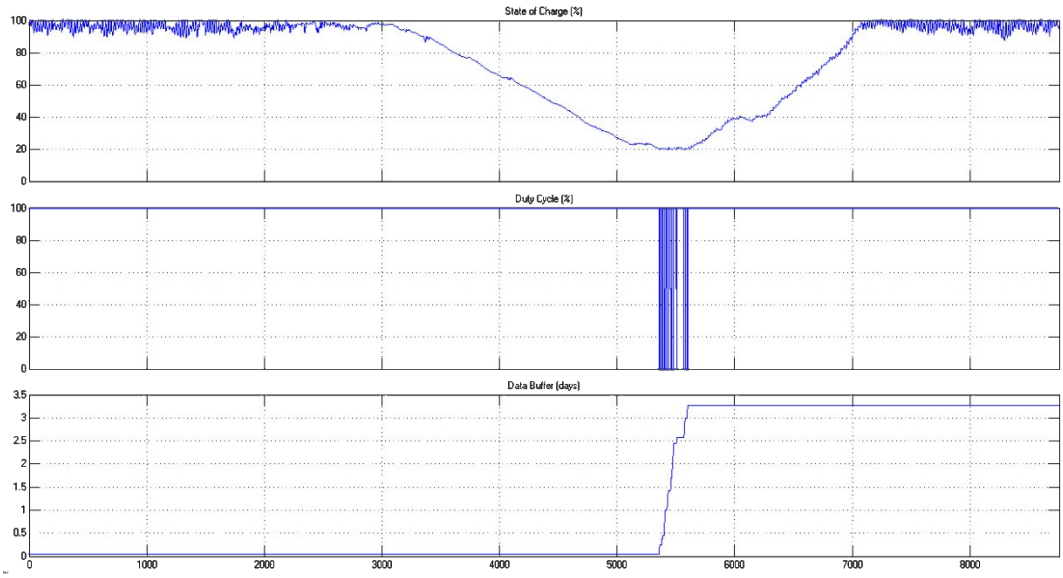

a)

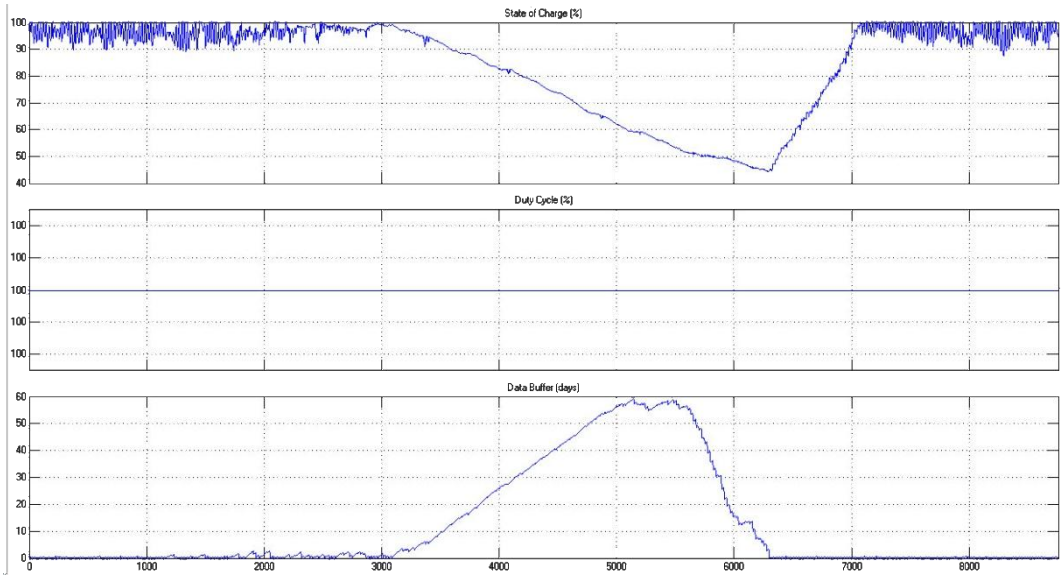

b)

Figure 6.9 Satellite transmitter strategy simulation (Whitehorse, one typical meteorological year). (a) Constant data streaming. (b) Energy-wise data streaming.

Table 6.11 Satellite transmitter strategy simulation results. One typical year; power source is undersized to force system shutdowns according to the simple control strategy.

	Constant transmission strategy		Energy-wise strategy	
	Lost data (days)	Minimum SOC (%)	Maximum stored data (days)	Minimum SOC (%)
Whitehorse	3.3	20	59	44

6.9 Data logger implementation

Most data loggers have limited computational capabilities. Hence, a design constraint for any energy management strategy is its simplicity in terms of the computational overhead created by the implementation of a data logger. Complex algorithms require lots of computing energy and consume more energy than simple strategies. In addition, the implementation of a complex algorithm in a data logger might be difficult and time consuming. The compiled fuzzy logic controller presented in this thesis requires few computing resources and can be implemented in most modern and some legacy data loggers.

Legacy and low-end data loggers have limited processing capabilities. However, the implementation of a compiled FC is possible with the inclusion of some lines of code. The controller and the precomputed estimation of future energy availability are saved to memory as tables. If there is an analog input port available, the state of charge can be estimated from a real-time reading of the battery voltage and with the use of another table that relates the state of charge with the voltage. Finally, the compiled controller's table outputs a duty cycle that corresponds to the actual system's status. This sequence is not harder to implement than a moving average algorithm, which can be programmed in most data loggers. Environment Canada's reference station uses a legacy Campbell® Scientific CR23X data logger that is powerful enough to handle the compiled FC.

The core of most modern data loggers is a microcontroller with enough energy to support relatively complex algorithms, such as the appropriate estimation of the battery's state of charge (dependent on voltage, internal temperature, and discharge rate). Whenever a modern microcontroller is available, the implementation of properly designed advanced energy management techniques is recommended.

6.10 Conclusion

This chapter showed that CI techniques can be successfully applied to harvesting aware energy management problems. Only two studies that apply CI (hill climbing and bargaining game) approaches to harvesting energy management were found during a literature survey performed in 2007. A recent survey (2011) showed a growing trend of CI applications in this area and two energy management strategies based on reinforcement learning were discussed. CI is a vast field and its application to HAEM can be successfully achieved. Techniques that create low computational and energy overheads are of particular interest.

A multisource simulator was described and used in the design and testing of energy management algorithms for energy harvesting systems in cold climates. Climatological databases that span several decades were used to assess the performance of the energy management algorithms. Worst-case scenarios were considered from real datasets and from the simulation of random system failures. The simulator was also used to size the main components of the power sources (energy harvesters and storage devices). Optimal sizing of these components was realized with the aid of genetic algorithms—i.e., determination of the optimal solar panel size, battery capacity, etc.

The simulator was designed using a minimalist approach and could be easily modified to represent a wide range of low power renewable energy systems in cold climates. Engineering climatological databases that span several

decades were parsed and used as inputs for the simulator. For simulation purposes, four automatic weather monitoring stations were considered to be at three different places in Canada and at one location in the United States. This choice was supported by the availability and quality of climatological datasets for these locations.

Typically, AWSs gather data all year long with a fixed sampling rate. But naturally occurring energy resources such as sunlight and wind are weather dependent and vary stochastically. There are two approaches to solve this problem: an oversized power source or the use of a properly sized power source coupled to sophisticated energy management strategies. The oversized power source approach cannot guarantee a constant energy supply under all possible scenarios, and has the disadvantages of higher cost, weight, and volume.

A fuzzy logic approach that allowed the use of a relatively small power source was presented. The main goal of this strategy was to avoid system shutdowns due to energy shortages. The cost of using the strategy came from the enforcement of a reduced duty cycle when the energy availability was expected to be low. The use of a reduced duty cycle allowed sampling, logging, and transmission of valuable data with lower sampling rates. This was preferred to no sampling, logging, transmission at all (complete system shutdown). A typical climatological year was used for power source sizing and the initial setup of the FC. Worst-case scenarios were derived from the complete database, e.g., years with atypically low wind or low insolation. Other worst case scenarios were computer-generated, e.g., wind generator or solar panel failures.

The compiled FC can be implemented in most legacy or modern data loggers. The minimum requirements are one available analog input port to measure the battery's voltage, enough memory space to store the precompiled tables, and sufficient processing energy to handle look-up table readings and simple

decision making routines. A careful implementation of the algorithm would keep operations done by the data logger at a minimum by “embedding” them in the look-up tables. For example, scaling the state of charge of the battery so that 100% corresponds to 255 allows a straightforward implementation under an 8 bits platform.

Chapter 7 - Conclusions

Automatic weather monitoring stations in arctic regions are faced with harsh operational conditions, including extreme weather and remote locations. These systems are usually subject to Nature's will, as human access for upgrading or maintenance is usually restricted to once a year. The power source is a key element of the AWS and failure to guarantee continuous power to an AWS results in irretrievable information (data) loss.

Typically, the AWS power source consists of a solar panel, a rechargeable battery, and a power converter. Unfortunately, such a power source fails to provide current when the battery is discharged and solar energy is not available. The use of an oversized battery and solar panel can help diminish shutdown occurrence, but this solution is costly and impractical.

This thesis explored an advantageous energy management approach that merged the power source and the AWS (load) into a single energy harvesting device. A synergy was created between subsystems: that is, the power source "knew" the characteristics of the load it was feeding, while the load "acted" according to the status of the power source. This synergy was achieved by careful planning of the energy management strategy, supported by the use of computational intelligence techniques for control and optimization.

The developed energy management approach is especially relevant for energy harvesting systems operating under extreme conditions. Nevertheless, the same principles can be applied to other energy harvesting environments.

Harvesting aware energy management is a recent field of research. Most of the research efforts in this area focus on wireless networks and embedded applications. Energy management strategies for extraterrestrial rovers are a good example of operation under extreme conditions. The publications accessed for this project emphasized power management, but for most low power systems the term "energy management" is more appropriate. In a few words, energy management aims to guarantee the long term operation of the system, while power management focuses on the problem of feeding unusually high loads for short periods of time. Since electrochemical batteries have much higher power than energy capacities and arctic applications present a yearly energy cycle, AWSs will rarely face power management challenges. Instead, a long term, efficient energy usage strategy is required. Hence, "energy management" was featured in the experiments described here.

To date, there are very few publications that address *intelligent* HAEM issues, and no examples related to the application of these techniques to standalone equipment deployed in arctic environments or cold climates were located. The intelligent energy management techniques developed here from the perspective of automatic weather stations used in the arctic can be extended and adapted to a broad range of energy harvesting systems, including midpower and high power applications. Furthermore, systems energized by fueled generators can benefit from similar energy management approaches.

Wind flutter generators are novel energy harvesting devices. They fill a gap where wind turbines do not perform well: low power generation. These devices are cheap and mechanically simple. Commercial prototypes are already being sold, but there is a lack of technical and scientific information regarding this technology. In chapter 4, a 50 cm wind flutter generator was tested and a simple mathematical model was derived from this work. The data generated here for the wind flutter generator can be used to produce

advanced models and to analyze the mechanical and electrical properties of the device. No similar studies were found in the literature.

An energy harvesting power source consisting of a solar panel, a wind flutter generator, and a battery was studied by the means of simulations. It was found that utilization of solar and wind energy increased the robustness of the power supply, and that these energy sources complemented each other—i.e., there was a chance of wind during the absence of sunlight and vice-versa. The addition of a wind generator reduced the need for oversized solar panels and batteries, as the generator was active at night and during the winter. An intelligent energy management algorithm was developed to allow efficient utilization of the energetic resources, maximize the amount of electrical energy extracted from both harvesting devices, avoid energy losses, and guarantee adequate operation of the monitoring station.

This thesis provides a reference to feasible power generation alternatives for equipment operating in cold and remote regions, and provides some tools that can be useful to study and test candidate energy sources. The framework for the development of energy management strategies tailored to these areas is also covered. Energy requirements of arctic monitoring stations are presented and the characteristics of distinct energy sources and power generators are discussed in order to compare diverse energy sources and distinguish which is appropriate for a given application.

Finally, the work initiated in this thesis opens the way to several research opportunities. A logical suite to this project would be the implementation and testing of the intelligent energy management strategy in a real automatic monitoring station.

7.1 Contributions

This thesis defines the framework of energy management as a complement to power management. Both techniques rely on similar strategies to achieve their goals but are different in nature. Power management focuses on

immediate energy availability (generation) and consumption, while energy management deals with energy flows over long periods of time. An energy-aware harvesting system with energy management is introduced (analogous to power management for power-aware systems). The distinctive setting of AWSs in the arctic justifies this paradigm shift.

This is a study of renewable energy generation in arctic regions, with a focus on low power systems. The study covers electrical energy generation issues (such as solar panel function during the polar night), energy requirements of AWSs, energy management strategies, the use of specialized climatological databases, a study of state-of-the-art power sources for isolated arctic locations, energy harvesting systems (source, storage, and load) and energy balance models, and leading energy (energy) management techniques.

A novel wind energy generator for low power applications, the wind flutter generator, was identified as an alternative to low power wind turbines. A lack of characteristic behaviour curves and models for this new device led to a detailed experimental study. Key parameters for the study were selected, a test bed was designed and an experimentation protocol was developed. Two sets of experiments were performed with the aid of a wind tunnel and relevant data were recorded. The first set of experiments used a “regular” wind flutter generator, while the second aimed to test an “enhanced” version. The enhanced version was obtained as part of the research effort herein presented and performed considerably better than the regular generator. Interpretation of the data revealed that the generator presents nonlinear characteristics. A simple wind flutter generator mathematical model was derived and presented. This model was used for simulation purposes and the data obtained during the experimentation can be used to further study and characterize the device. Simulation results showed that the device could be tuned for maximum performance at the intended location of deployment.

A modular, flexible, and simple multisource simulator for energy harvesting systems was developed. The simplicity of the code permited reasonable simulation times in computers with modest hardware. Although the simulator was intended to represent AWSs in arctic regions, its core was flexible enough to accommodate a variety of energy systems and scenarios where (high) energy issues and high frequency dynamics can be neglected. The modular nature of the simulator provided an easy way to modify existing models and to add extensions, such as additional energy harvesters and loads. The implementation of different energy management strategies was straightforward. Additionally, the simulator used real or synthetic meteorological data, emulated generator failures, and was able to handle different modes of operation. The Matlab®/Simulink® code can be easily translated to other programming languages for increased simulation speed.

Efficient, yet simple, harvesting aware energy management techniques for AWSs in arctic regions were developed. The energy management algorithms can be handled by simple processors and implementation into embedded systems or (legacy) data loggers is feasible. Note that data loggers are not designed for system control and are very limited in terms of their instruction sets and computing capabilities. The energy management algorithms that were developed do not require advanced features such as DVS and can be applied with very little overhead. Algorithms are easily configurable and can be adapted to systems with energy sources of different natures and loads with specific requirements. Loads can be duty cycled in groups or independently. The energy and computational overhead created by the algorithms is low, thus effectively increasing the efficiency of the system.

An energy management algorithm based on a GA optimized FC that drastically reduced system shutdowns was developed. The algorithm had only two control inputs (real time SOC and precomputed average energy production). Other algorithms require forecasting, which adds complexity. A

fuzzy controller was compiled that could be implemented in low end microprocessors.

A comprehensive set of tools that can be used to develop and test energy management strategies for AWSs in arctic locations was developed with a focus on simplicity, flexibility, and ease of use. Solar panel and battery models take into account the effects of very low temperatures, while still allowing straightforward implementation. Existing commercial renewable energy simulators often lack features that are relevant to the study of low power AWSs in cold, isolated regions. PVToolbox (CanmetENERGIE) was designed to cope with these issues, but it is not available for public use. The free code included in the appendixes includes a full set of modules that are the core of the simulator for energy harvesting systems in arctic environments.

The simulation study of AWSs in arctic regions with a focus on energy issues included the use of distinct energy sources (solar and wind) and a wind flutter generator. Three approaches were used to improve energy efficiency: (1) multiparametric sizing of the power source, (2) proficient energy management algorithms, and (3) system optimization for the intended location of use. Each step increased energy efficiency while decreasing the size of the power source.

7.2 Future Work

This thesis provides a reference for energy management of automated arctic monitoring stations and leaves the doors open to several research opportunities. AWSs are standalone systems and the reliability of the power source (energy transducer, power conversion, and energy storage) is crucial. Each component plays an important role, but energy harvesting and electrical energy storage in cold environments need further development. Research on new energy transducers aims to improve efficiency and reduce costs, but it rarely stresses the development of devices that perform efficiently in very cold environments. Traditional battery technologies are

not good at storing large amounts of energy and underperform at very low temperatures. New generation secondary batteries, such as zinc-air or sodium aqueous electrolyte, present high energy densities and are very good candidates for low power and high energy applications. They can be studied and incorporated for use in arctic applications.

The development of mathematical models for state-of-the-art energy transducers and storage devices operating at low temperatures is a necessary step before these devices can be studied by the means of simulation and used in real settings. This includes new battery chemistries and architectures, solar panels, wind generators (turbine, magnus, and flutter) and thermoelectric transducers. This process requires extensive experimentation and a deep knowledge of the physics that underlies the operation of these systems.

Similarly, wind flutter generators can be studied with respect to aerodynamic and aeroelastic principles. Mathematical (theoretical) models can assist in the design of such devices and can help to validate experimental results. Furthermore, the wind flutter generator needs to be "winterized" and field tested. Arrays of various flutter generators should be designed and validated.

A critical part of the wind flutter generator is the airfoil (ribbon). In chapter 4 it was shown that tension plays a very important role and the following problems need to be solved before the generator can be effectively used in very cold environments. To be developed:

- A ribbon material with thermal expansion nearing zero;
- A ribbon material that maintains aeroelastic properties within a large range of temperatures;
- An adaptive tensioning system that responds to wind speed changes (for optimal operation at various wind speeds);
- An adaptive wind tracking mechanism;

- A frame design that boosts fluttering and protects the ribbon from weather.

The energy systems simulator introduced in chapter 5 can be redesigned to include a set of drag and drop libraries and to provide a better user interface. The libraries should include diverse climatological datasets, energy transducers, storage devices, energy converters, loads, and energy management algorithms. Adding new modules and changing parameters such as simulation time, intervals, and location should be straightforward.

The energy management algorithms need to be incorporated into a test bed formed by a solar panel, a wind generator, a lead-acid battery, energy converters, and traditional AWS hardware. The first step is to embed the code into the data logger and to perform outdoor tests. Finally, the energy management strategy can be implemented and tested in a real arctic setting.

The work presented in this thesis can be extended to multisource energy harvesting systems (with more than two energy sources or transducers). Increasing the number of energy transducers and energy sources can help to smooth the flow of incoming energy and increase the stability of the system. It is certainly more challenging to deal with multiple energy sources, but the approaches presented in chapter 6 can be used to size the power source components and to optimize the energy management strategy.

Bibliography

[1] M. Ross and J. Royer, *Photovoltaics in Cold Climates*. London, UK: James and James, Ltd., 1999.

[2] A. M. Knight, "Proposal," submitted to NSERC, 12 pages, 2009.

[3] Environment Canada, "Weatheroffice Frequently Asqued Questions - Environment Canada," 2010. [Online]. Available: http://www.weatheroffice.gc.ca/mainmenu/faq_e.html. [Accessed: September 3, 2010].

[4] Personal Communication, "Solar Radiation Database in the Arctic," Climate Services, Environment Canada, November 19, 2009.

[5] Personal Communication, A. Knight, "Arctic Monitoring Research," Environment Canada, April 1, 2009.

[6] Natural Resources Canada, "The Atlas of Canada - Weather Stations and Forecast Regions," 2003. [Online]. Available: http://atlas.nrcan.gc.ca/site/english/maps/archives/3rdedition/environment/climate/032. [Accessed: October 1, 2010].

[7] Personal Communication, "Arctic Monitoring Stations," Arctic and Alpine Research Group, University of Alberta, October 4, 2010.

[8] Personal Communication, "Arctic and Alpine Research Group Devon Island Ice Cap Weather Stations," Arctic and Alpine Research Group, University of Alberta, March 2, 2009.

[9] Cooperative Institute for Research in Environmental Sciences, "Greenland Climate Network," 2009. [Online]. Available: http://cires.colorado.edu/science/groups/steffen/gcnet/. [Accessed: October 20, 2010].

[10] Environment Canada, "Canadian Wind Energy Atlas," 2008. [Online]. Available: http://www.windatlas.ca/en/index.php. [Accessed: October 20, 2010].

[11] Natural Resources Canada, "Photovoltaic potential and solar resource maps of Canada," 2009. [Online]. Available: https://glfc.cfsnet.nfis.org/mapserver/pv/index_e.php. [Accessed: October 20, 2010].

[12] "Canadian Weather Energy and Engineering Data Sets and Canadian Weather for Energy Calculations Updated User's Manual," Environment Canada - Atmospheric Environment Service
National Research Council of Canada, pages, 2008.

[13] Environment Canada, "National Climate Data and Information Archive," 2010. [Online]. Available: http://www.climate.weatheroffice.gc.ca/prods_servs/index_e.html. [Accessed: May 5, 2010].
[14] National Renewable Energy Laboratory, "National Solar Radiation Data Base," 2007. [Online]. Available: http://rredc.nrel.gov/solar/old_data/nsrdb/. [Accessed: May 5, 2010].
[15] P. C. Symons and P. C. Butler, "Advanced Batteries for Electric Vehicles and Emerging Applications- Introduction," in *Handbook of Batteries*, 3rd ed: McGraw-Hill, 2002, pp. 37.1-37.25.
[16] B. Scrosati, "Challenge of portable power," *Nature,* vol. 373, pp. 557-558, 1995.
[17] J. A. Paradiso and T. Starner, "Energy scavenging for mobile and wireless electronics," *Pervasive Computing, IEEE,* vol. 4, pp. 18-27, 2005.
[18] B. Scrosati, "Nanomaterials: Paper powers battery breakthrough," *Nature Nanotechnology,* vol. 2, pp. 598-599, 2007.
[19] J. Alper, "The Battery: Not Yet a Terminal Case," *Science,* vol. 296, p. 1224, 05/17/ 2002.
[20] L. Mateu and F. Moll, "Review of energy harvesting techniques and applications for microelectronics," in *Proceedings of SPIE - The International Society for Optical Engineering*, 2005, pp. 359-373.
[21] "Assault on batteries," *Nature,* vol. 441, pp. 1046-1047, 2006.
[22] R. F. Service, "Shrinking fuel cells promise power in your pocket," *Science,* vol. 296, pp. 1222-1224, 2002.
[23] Ballard Power Systems, Inc., "Hydrogen Fuel Cell Technology, Hydrogen Power in Buses," 2009. [Online]. Available: http://www.ballard.com/. [Accessed: Oct. 30, 2009].
[24] S. F. J. Flipsen, "Power sources compared: The ultimate truth?," *Journal of Power Sources,* vol. 162, pp. 927-934, 2006.
[25] S. Roundy, D. Steingart, L. Frechette, P. Wright, and J. Rabaey, "Power sources for wireless sensor networks," in *Lecture Notes in Computer Science (including subseries Lecture Notes in Artificial Intelligence and Lecture Notes in Bioinformatics)*. vol. 2920, 2004, pp. 1-17.
[26] C. D. Cress, B. J. Landi, and R. P. Raffaelle, "Modeling Laterally-Contacted nipi-Diode Radioisotope Batteries," *Nuclear Science, IEEE Transactions on,* vol. 55, pp. 1736-1743, 2008.
[27] A. Lal, R. Duggirala, and H. Li, "Pervasive power: a radioisotope-powered piezoelectric generator," *Pervasive Computing, IEEE,* vol. 4, pp. 53-61, 2005.
[28] A. Lal, R. Duggirala, and S. Tin, "Radioisotope Powered Electrostatic Microactuators and Electronics," in *Solid-State Sensors, Actuators and Microsystems Conference, 2007. TRANSDUCERS 2007. International*, 2007, pp. 269-273.

[29] BetaBatt, Inc., "BetaBatt, Inc. Direct Energy Conversion Technology," 2004. [Online]. Available: http://www.betabatt.com/index.html. [Accessed: Oct. 13, 2009].

[30] V. Raghunathan, A. Kansal, J. Hsu, J. Friedman, and M. Srivastava, "Design considerations for solar energy harvesting wireless embedded systems," in *2005 4th International Symposium on Information Processing in Sensor Networks, IPSN 2005*, 2005, pp. 457-462.

[31] D. F. Mennicucci, "Photovoltaic Array Simulation Models," *Solar Cells,* vol. 18, pp. 383-392, 1986.

[32] R. Perez, P. Ineichen, R. Seals, J. Michalsky, and R. Stewart, "Modeling daylight availability and irradiance components from direct and global irradiance," *Solar Energy,* vol. 44, pp. 271-289, 1990.

[33] R. Perez, R. Seals, P. Ineichen, R. Stewart, and D. Menicucci, "A new simplified version of the perez diffuse irradiance model for tilted surfaces," *Solar Energy,* vol. 39, pp. 221-231, 1987.

[34] H. Shao, C. Y. Tsui, and W. H. Ki, "A micro power management system and maximum output power control for solar energy harvesting applications," in *Proceedings of the International Symposium on Low Power Design*, 2007, pp. 298-303.

[35] J. Yi, F. Su, Y. H. Lam, W. H. Ki, and C. Y. Tsui, "An energy-adaptive MPPT power management unit for micro-power vibration energy harvesting," in *Proceedings - IEEE International Symposium on Circuits and Systems*, 2008, pp. 2570-2573.

[36] M. A. Qidwai, J. P. Thomas, J. C. Kellogg, and J. Baucom, "Energy harvesting concepts for small electric unmanned systems," in *Proceedings of SPIE - The International Society for Optical Engineering*, 2004, pp. 84-85.

[37] ABS Alaskan, Inc., "Small Turbines (50-600W)," 2000-2010. [Online]. Available: http://www.absak.com/catalog/index.php/cPath/32_93_94. [Accessed: February 6, 2010].

[38] Humdinger Wind Energy, LLC, "Humdinger Wind Energy," 2009. [Online]. Available: http://www.humdingerwind.com/. [Accessed: February 9, 2010].

[39] "Power Chips PLC," 2009. [Online]. Available: http://www.powerchips.gi/index.shtml. [Accessed: Aug. 7, 2009].

[40] Thermonamic Electronics Corp., Ltd., "Power Module," 2007. [Online]. Available: http://www.thermonamic.com/Pspec.html. [Accessed: Nov. 28, 2008].

[41] Hi-Z Technology, Inc., "Thermoelectric Modules," 2009. [Online]. Available: http://www.hi-z.com/products.php. [Accessed: Jan. 23, 2009].

[42] P. Lailler, J.-F. Sarrau, and C. Sarrazin, "Comparative study for `36 V' vehicle applications: Advantages of lead-acid batteries," *Journal of Power Sources,* vol. 95, pp. 58-67, 2001.

[43] A. Kansal, J. Hsu, S. Zahedi, and M. Srivastava, "Power management in energy harvesting sensor networks," *Trans. on Embedded Computing Sys.,* vol. 6, p. 32, 2007.

[44] J. Hsu, S. Zahedi, A. Kansal, M. Srivastava, and V. Raghunathan, "Adaptive duty cycling for energy harvesting systems," in *Proceedings of the International Symposium on Low Power Electronics and Design*, 2006, pp. 180-185.

[45] P. Kiss and I. M. Jánosi, "Limitations of wind power availability over Europe: A conceptual study," *Nonlinear Processes in Geophysics,* vol. 15, pp. 803-813, 2008.

[46] Varmaraf, "Thermators," 2007. [Online]. Available: http://www.varmaraf.is/engl/prod.htm. [Accessed: Nov. 28, 2008].

[47] V. Raghunathan and P. H. Chou, "Design and power management of energy harvesting embedded systems," in *Proceedings of the International Symposium on Low Power Electronics and Design*, 2006, pp. 369-374.

[48] A. D. Joseph, "Energy harvesting projects," *Pervasive Computing, IEEE,* vol. 4, pp. 69-71, 2005.

[49] S. W. Arms, C. P. Townsend, D. L. Churchill, J. H. Galbreath, and S. W. Mundell, "Power management for energy harvesting wireless sensors," 2005, pp. 267-275.

[50] A. Kansal, J. Hsu, M. Srivastava, and V. Raghunathan, "Harvesting aware power management for sensor networks," in *Proceedings - Design Automation Conference*, 2006, pp. 651-656.

[51] S. Chalasani and J. M. Conrad, "A survey of energy harvesting sources for embedded systems," in *Southeastcon, 2008. IEEE*, 2008, pp. 442-447.

[52] R. B. MacCurdy, T. Reissman, and E. Garcia, "Energy management of multi-component power harvesting systems," in *Proceedings of SPIE - The International Society for Optical Engineering*, 2008.

[53] C. Moser, L. Thiele, D. Brunelli, and L. Benini, "Adaptive power management in energy harvesting systems," in *Proceedings -Design, Automation and Test in Europe, DATE*, 2007, pp. 773-778.

[54] A. Janek, C. Steger, J. Preishuber-Pfluegl, and M. Pistauer, "Power management strategies for battery-driven higher Class UHF RFID tags supported by energy harvesting devices," in *2007 IEEE Workshop on Automatic Identification Advanced Technologies - Proceedings*, 2007, pp. 122-127.

[55] A. Kansal, D. Potter, and M. B. Srivastava, "Performance aware tasking for environmentally powered sensor networks," in *Performance Evaluation Review*, 2004, pp. 223-234.

[56] C. M. Vigorito, D. Ganesan, and A. G. Barto, "Adaptive control of duty cycling in energy-harvesting wireless sensor networks," in *2007 4th Annual IEEE Communications Society Conference on Sensor, Mesh and Ad Hoc Communications and Networks, SECON*, 2007, pp. 21-30.

[57] A. Kansal and M. B. Srivastava, "Energy Harvesting Aware Power Management " in *Wireless Sensor Networks: A Systems Perspective*. vol. Paper 131: Center for Embedded Network Sensing, 2005.

[58] D. Niyato, M. M. Rashid, and V. K. Bhargava, "Wireless sensor networks with energy harvesting technologies: A game-theoretic approach to optimal energy management," *IEEE Wireless Communications,* vol. 14, pp. 90-96, 2007.

[59] V. Raghunathan, S. Ganeriwal, and M. Srivastava, "Emerging techniques for long lived wireless sensor networks," *Communications Magazine, IEEE,* vol. 44, pp. 108-114, 2006.

[60] L. R. Clare and S. G. Burrow, "Power conditioning for energy harvesting," in *Proceedings of SPIE - The International Society for Optical Engineering*, 2008.

[61] Darnell Research Group, "Energy Harvesting, Micro Batteries and Power Management ICs " 2007. [Online]. Available: http://www.electronics.ca/reports/power_components/dr1_energy_harvesting.html. [Accessed: October 14, 2008].

[62] A. R. Chandrakasan, N. Verma, and D. C. Daly, "Ultralow-power electronics for biomedical applications," 247-274 pages, 2008.

[63] C. Moser, L. Thiele, D. Brunelli, and L. Benini, "Robust and Low Complexity Rate Control for Solar Powered Sensors," in *Design, Automation and Test in Europe, 2008. DATE '08*, 2008, pp. 230-235.

[64] V. Sharma, U. Mukherji, V. Joseph, and S. Gupta, "Optimal Energy Management Policies for Energy Harvesting Sensor Nodes," *Submitted to the IEEE for possible publication,* 2008.

[65] Y. Zhu and L. M. Ni, "Probabilistic wakeup: Adaptive duty cycling for energy-efficient event detection," in *MSWiM'07: Proceedings of the Tenth ACM Symposium on Modeling, Analysis, and Simulation of Wireless and Mobile Systems*, 2007, pp. 360-367.

[66] A. S. Weddell, G. V. Merrett, N. R. Harris, and B. M. Al-Hashimi, "Energy harvesting and management for wireless autonomous sensors," *Measurement and Control,* vol. 41, pp. 104-108, 2008.

[67] X. Zhong and C. Z. Xu, "Energy-aware modeling and scheduling for dynamic voltage scaling with statistical real-time guarantee," *IEEE Transactions on Computers,* vol. 56, pp. 358-372, 2007.

[68] A. Lahiri, N. Bussa, and P. Saraswat, "A neural network approach to dynamic frequency scaling," in *Proceedings of the 15th International Conference on Advanced Computing and Communications, ADCOM 2007*, 2007, pp. 738-743.

[69] Q. Wu, P. Juang, M. Martonosi, L. S. Peh, and D. W. Clark, "Formal control techniques for power-performance management," *IEEE Micro,* vol. 25, pp. 52-62, 2005.

[70] P. H. Chou, J. Liu, D. Li, and N. Bagherzadeh, "IMPACCT: Methodology and tools for power-aware embedded systems," *Design Automation for Embedded Systems,* vol. 7, pp. 205-232, 2002.

[71] J. Glaser, D. Weber, S. A. Madani, and S. Mahlknecht, "Power aware simulation framework for wireless sensor networks and nodes," *Eurasip Journal of Embedded Systems,* vol. 2008, 2008.
[72] F. Sheriff, D. Turcotte, and M. Ross, "PV Toolbox: A Comprehensive Set OF PV System Components For The Matlab®/Simulink® Environment," in *SESCI 2003 Conference*, Kingston, Canada, 2003.
[73] Personal Communication, "PVToolbox," CanmetENERGY, May 20, 2009.
[74] J. Taneja, J. Jeong, and D. Culler, "Design, modeling and capacity planning for micro-solar power sensor networks," in *Proceedings - 2008 International Conference on Information Processing in Sensor Networks, IPSN 2008*, 2008, pp. 407-418.
[75] S. Dalola, M. Ferrari, V. Ferrari, M. Guizzetti, D. Marioli, and A. Taroni, "Characterization of Thermoelectric Modules for Powering Autonomous Sensors," *IEEE Transactions on Instrumentation and Measurement,* 2008.
[76] W. Qin, M. Hempstead, and Y. Woodward, "A realistic power consumption model for wireless sensor network devices," in *2006 3rd Annual IEEE Communications Society on Sensor and Adhoc Communications and Networks, Secon 2006*, 2007, pp. 286-295.
[77] D. Pimentel, P. Musilek, A. Knight, and J. Heckenbergerova, "Characterization of a Wind Flutter Generator," in *Ninth International Conference on Environment and Electrical Engineering*, Prague, 2010.
[78] ABS Alaskan, Inc., "Small Turbines (50-600W)," 2010. [Online]. Available: http://www.absak.com/catalog/index.php/cPath/32_93_94. [Accessed: February 6, 2010].
[79] Marlec Renewable Power, "Renewable Energy Systems," 2008. [Online]. Available: http://www.marlec.co.uk/. [Accessed: May 1, 2009].
[80] S. H. Kim, C. H. Ji, P. Galle, F. Herrault, X. Wu, J. H. Lee, C. A. Choi, and M. G. Allen, "An electromagnetic energy scavenger from direct airflow," *Journal of Micromechanics and Microengineering,* vol. 19, 2009.
[81] "Aerogen Wind Generators Datasheet," LVM, pages, 2010.
[82] J. Duffie and W. Beckman, *Solar Engineering of Thermal Processes*, 3rd ed. New Jersey: John Wiley & Sons, Inc., 2006.
[83] D. King, W. Boyson, and J. Kratochvil, "Photovoltaic Array Performance Model," Sandia National Laboratories, Albuquerque 2004.
[84] M. Ross, "Estimating Wintertime Battery Temperature in Stand-Alone Photovoltaic Systems with Insulated Battery Enclosures," in *Renewable Energy Technologies in Cold Climates*, Montreal, 1998, pp. 344-350.
[85] S. Shenoi, K. Ashenayi, and M. Timmerman, "Implementation of a learning fuzzy controller," *IEEE Control Systems Magazine,* vol. 15, pp. 73-80, 1995.

[86] D. Pimentel, P. Musilek, and A. Knight, "Energy Harvesting Simulation for Automatic Arctic Monitoring Stations," in *IEEE Electrical Power and Energy Conference*, Halifax, 2010.

[87] D. P. Miller, T. S. Hunt, and M. J. Roman, "Experiments & Analysis of the Role of Solar Power in Limiting Mars Rover Range," in *IEEE International Conference on Intelligent Robots and Systems*, 2003, pp. 317-322.

[88] ScienceDaily, "Mars Rovers Survive Severe Dust Storms, Ready For Next Objectives," 2007. [Online]. Available: http://www.sciencedaily.com/releases/2007/09/070907165711.htm. [Accessed: September 26, 2011].

[89] "Power Aware Computing and Communication - Power Management in Past and Present JPL/NASA Missions," NASA Center for Integrated Space Microsystems, 20 pages, 2000.

[90] M. Toshinori, *Fundamentals of the New Artificial Intelligence: Neural, Evolutionary, Fuzzy and More*: Springer, 2008.

[91] K. Karabulut, A. Alkan, and A. S. Yilmaz, "Long term energy consumption forecasting using genetic programming," *Mathematical and Computational Applications,* vol. 13, pp. 71-80, 2008.

[92] R. Chaoming Hsu, C. T. Liu, and W. M. Lee, "Reinforcement learning-based dynamic power management for energy harvesting wireless sensor network," 399-408 pages, 2009.

[93] S. Behrens, J. Ward, and J. Davidson, "Adaptive vibration energy harvesting," in *Proceedings of SPIE - The International Society for Optical Engineering*, 2007.

[94] "Deka Solar Photovoltaic Batteries Datasheet," East Penn Manufacturing Co., Inc., pages, 2010.

[95] Personal Communication, "Arctic Monitoring Research," Environment Canada, April 1, 2009.

Appendix 1 – Python™ Parsing Scripts

For the latest set of scripts e-mail pimentel@ualberta.ca and/or petr.musilek@ualberta.ca.

A1.1 CWEC Dataset to Comma Separated Values (cvs) File

```
#Author: D. Pimentel
#Date: 11/26/2009
#Purpose: Parse CWEC file (fixed width) and save as CSV

import csv

#Open files
pathread  = 'D:/PhD/Datasets/Original datasets/W22258W(Inuvik).CW2'
pathwrite = 'D:/PhD/Datasets/Inuvik TMY.csv'

#pathread  = 'D:/PhD/Datasets/Original datasets/W17901W(Resolute).CW2'
#pathwrite = 'D:/PhD/Datasets/Resolute TMY.csv'

#pathread  = 'D:/PhD/Datasets/Original datasets/W26316W(Whitehorse).CW2'
#pathwrite = 'D:/PhD/Datasets/Whitehorse TMY.csv'

loaddata = open(pathread, 'r')

writedata = open(pathwrite, 'w')
csvwrite = csv.writer(writedata)

for i in range(8760):
    row = loaddata.readline()
    csvwrite.writerow([ str(i),
                        #round(float(row[14:18])/3.6),      #Extraterrestrial
irradiance Wh/m2
                        #round(float(row[18:22])/3.6),      #Global horizontal
irradiance Wh/m2
                        round(float(row[24:28])/3.6),       #Direct normal
irradiance Wh/m2
                        round(float(row[30:34])/3.6),       #Diffuse horizontal
irradiance Wh/m2
                        round(float(row[89:93])/10,1),      #Dry bulb temperature
°C
                        #round(float(row[99:102])),         #Wind direction
degrees, 0° = north
                        round(float(row[103:107])/10,1)])   #Wind speed m/s
loaddata.close()
writedata.close()

print ("Done!")
```

A1.2 CWEEDS Dataset to Comma Separated Values (cvs) File

```
#Author: D. Pimentel
#Date: 11/26/2009
#Purpose: Parse CWEDS file (fixed width) and save as CSV

import csv

#Open files
pathread =  'D:/PhD/Datasets/Original datasets/22258(Inuvik 1958-2005).WY2'
pathwrite = 'D:/PhD/Datasets/Inuvik 1958-2005.csv'
```

```
#pathread  = 'D:/PhD/Datasets/Original datasets/17901(Resolute 1963-2005).WY2'
#pathwrite = 'D:/PhD/Datasets/Resolute 1963-2005.csv'

#pathread  = 'D:/PhD/Datasets/Original datasets/26316(Whitehorse 1953-2005).WY2'
#pathwrite = 'D:/PhD/Datasets/Whitehorse 1953-2005.csv'

loaddata = open(pathread, 'r')

writedata = open(pathwrite, 'w')
csvwrite = csv.writer(writedata)

for i in range(464592):
    row = loaddata.readline()
    csvwrite.writerow([ str(i),
                        str(row[6:16]),                     #Time stamp
                        #round(float(row[16:20])/3.6),     #Extraterrestrial
irradiance Wh/m2
                        #round(float(row[20:24])/3.6),     #Global horizontal
irradiance Wh/m2
                        round(float(row[26:30])/3.6),      #Direct normal
irradiance Wh/m2
                        round(float(row[32:36])/3.6),      #Diffuse horizontal
irradiance Wh/m2
                        round(float(row[91:95])/10,1),     #Dry bulb temperature
°C
                        #round(float(row[101:104])),       #Wind direction
degrees, 0° = north
                        round(float(row[105:109])/10,1)])  #Wind speed m/s
loaddata.close()
writedata.close()

print ("Done!")
```

A1.3 TMY3 Dataset to Comma Separated Values (cvs) File

```
#Author: D. Pimentel
#Date: 11/26/2009
#Purpose: Parse TMY3 file (CSV) and save as CSV

import csv

#Open files
pathread  = 'D:/Datasets/Original datasets/Desktop/700260TY.csv'
pathwrite = 'D:/Datasets/Original datasets/Desktop/Barrow TMY.csv'

loaddata = open(pathread, 'r')
writedata = open(pathwrite, 'w')

loaddata.readline()
loaddata.readline()

csvread = csv.reader(loaddata)
csvwrite = csv.writer(writedata)

for row in csvread:
    csvwrite.writerow([ csvread.line_num-1,
                        #row[2],     #Extraterrestrial irradiance Wh/m2
                        #row[4],     #Global horizontal irradiance Wh/m2
                        row[7],     #Direct normal irradiance Wh/m2
                        row[10],    #Diffuse horizontal irradiance Wh/m2
                        row[31],    #Dry bulb temperature °C
                        #row[43],    #Wind direction degrees, 360° = north
                        row[46]])   #Wind speed m/s

loaddata.close()
writedata.close()

print ("Done!")
```

Appendix 2 – Matlab® Simulator's Functions

For the latest set of functions e-mail pimentel@ualberta.ca and/or petr.musilek@ualberta.ca.

A2.1 Flutter Generator

```
function wind_energy = FG(modules, wind_speed, random_failure)

if random_failure == 1
    % Generator not working
    wind_energy = 0;
else
    % Generator working
    % Wind speed must be >= 2.3 m/s
    if wind_speed >= 2.3
        wind_energy = 25*wind_speed-56; % 110ohms,7.5N
    else
        wind_energy = 0;
    end

    %Limit energy to 319mW
    if wind_energy >= 319
        wind_energy = 319;
    end

    wind_energy = modules * wind_energy / 1000; %Watts
end
```

A2.2 Solar Panel

```
function sun_energy =
SP(time,latitude,longitude,local_standard_time_meridian,albedo,panel_area,inclinat
ion,azimuth,direct_normal_radiation,diffuse_horizontal_radiation,wind_speed,air_te
mperature,leap_year,random_failure)

if (diffuse_horizontal_radiation == 0) || (random_failure == 1)
    % No radiation or generator not working
    sun_energy = 0;

else

    % 1. DIFFUSE RADIATION ON INCLINED SURFACE
    days_in_year = 365 + leap_year;

    % The day of the year goes from 1 to 365 (366) (Duffie page 11), use 'time +
4344'  if year starts in July (TMY datasets)
    day_year = rem( floor((time+4344)/24) , days_in_year ) + 1;

    %1.6.1a
    declination = 23.442 * sind( 360/days_in_year*(284+day_year) );

    %1.4.2
    B = (day_year - 1) * 360/days_in_year;

    %1.5.3
    equation_of_time = 229.2 * ( 0.000075 + 0.001868*cosd(B) - 0.032077*sind(B) -
0.014615*cosd(2*B) - 0.04089 * sind(2*B) ) / 60;

    % Local standard time in hours (integer)
    local_standard_time = rem(time,24);
```

```
    %1.5.2
    local_solar_time = local_standard_time + 4/60*(longitude -
local_standard_time_meridian) + equation_of_time;

    % -15 degrees per hour before noon (Example 1.6.1)
    hour_angle = (local_solar_time-12)*15;

    sunrise_hour_angle = tand(latitude) * tand(declination);

    % Midpoint hour
    % At Sunrise
    if sunrise_hour_angle > hour_angle - 15,
        hour_angle = (hour_angle + sunrise_hour_angle) / 2;
    % At Sunset
    elseif -sunrise_hour_angle < hour_angle,
        hour_angle = ( hour_angle - 15 - sunrise_hour_angle ) / 2;
    % Between Sunrise and Sunset substract 7.5 degrees for midpoint hour
    else
        hour_angle = hour_angle - 7.5;
    end

    % 1.6.5
    solar_altitude = max( 0, cosd(latitude)*cosd(declination)*cosd(hour_angle) +
sind(latitude)*sind(declination) );

    solar_altitude = max(solar_altitude,0);

    solar_altitude_angle = asind(solar_altitude);

    %1.6.2 + 1.6.5
    incidence = cosd(inclination)*solar_altitude + sind(inclination)*(
cosd(declination)*( sind(latitude)*cosd(azimuth)*cosd(hour_angle) +
sind(azimuth)*sind(hour_angle) ) - sind(declination)*cosd(latitude)*cosd(azimuth)
);

    % Duffie p. 13 (by definition)
    solar_zenith_angle = (90 - solar_altitude_angle);

    % Table 2.16.1
    clearness_range = [1 1.065 1.23 1.5 1.95 2.8 4.5 6.2];
    f11 = [-0.008 0.130 0.330 0.568 0.873 1.132 1.060 0.678];
    f12 = [0.588 0.683 0.487 0.187 -0.392 -1.237 -1.6 -0.327];
    f13 = [-0.062 -0.151 -0.221 -0.295 -0.362 -0.412 -0.359 0.25];
    f21 = [-0.06 -0.019 0.055 0.109 0.226 0.288 0.264 0.156];
    f22 = [0.072 0.066 -0.064 -0.152 -0.462 -0.823 -1.127 -1.377];
    f23 = [-0.022 -0.029 -0.026 0.014 0.001 0.056 0.131 0.251];

    % Clearness category
    clearness_category = 8; % Clear sky
    if diffuse_horizontal_radiation > 0,

        %2.16.10
        clearness = 1 + direct_normal_radiation / (
diffuse_horizontal_radiation*(1 + 5.535e-6 * solar_zenith_angle^3) );

        while clearness_range(clearness_category) > clearness,
            clearness_category = clearness_category - 1;
        end

    end

    % Duffie p. 10, effect of altitude (above sea level) is neglected
        air_mass = 1 / ( solar_altitude + 0.5057*(96.08 - solar_zenith_angle)^(-
1.634) );

    % 1.4.1a Duffie
    extraterrestrial_normal_incidence_radiation = 1367 * ( 1 + 0.033*cosd(
360*day_year/days_in_year ) );

    % 2.16.11 Duffie
    brightness = air_mass * diffuse_horizontal_radiation /
extraterrestrial_normal_incidence_radiation;

    % Brightness coefficients
    % 2.16.12
    F1 = max( 0, f11(clearness_category) + f12(clearness_category)*brightness +
f13(clearness_category)*solar_zenith_angle*0.0175 );
    % 2.16.13
    F2 = f21(clearness_category) + f22(clearness_category)*brightness +
f23(clearness_category)*solar_zenith_angle*0.0175;
```

```
    % 2.16.9 (a/b)
    a_b = max(0,incidence) / max(0.0872,solar_altitude);

    isotropic_sky_diffuse_radiation = max( 0, diffuse_horizontal_radiation * (1-
F1) * (1+cosd(inclination)) /2 );

    circumsolar_diffuse_radiation = max( 0, diffuse_horizontal_radiation * F1 *
a_b );

    horizon_diffuse_radiation = max( 0, diffuse_horizontal_radiation * F2 *
sind(inclination) );


    % 2. GROUND REFLECTED RADIATION AND DIRECT RADIATION ON INCLINED SURFACE
    % Duffie p. 96
    direct_horizontal_radiation = direct_normal_radiation * solar_altitude;

    % 2.16.14
    ground_reflected_radiation = albedo * (diffuse_horizontal_radiation +
direct_horizontal_radiation) * (1-cosd(inclination)) / 2 ;

    % 1.8.1
    ratio_beam_radiation = a_b;

    % 2.16.14
    direct_radiation = direct_horizontal_radiation * ratio_beam_radiation;


    % 3. TOTAL RADIATION ON INCLINED SURFACE AND SUN ENERGY (Wh/m2)
    total_radiation_tilted = direct_radiation + isotropic_sky_diffuse_radiation +
circumsolar_diffuse_radiation + horizon_diffuse_radiation +
ground_reflected_radiation;

    % Photovoltaic Array Performance Model (King), (11), (12), open rack,
glass/cell/polymer sheet
    cell_temperature = total_radiation_tilted * (exp(-3.56-.075*wind_speed) +
0.003 )+ air_temperature;

    % Ross p. 39, -0.4% / degree Celsius, efficiency @ STC (25C) = 0.14
    efficiency = 0.155 - 0.0006*cell_temperature;

    % Ross p. 40, efficiency decreases at low light levels
    efficiency = efficiency * interp1( [0 27 93 200 400 625 1000 3000], [0 0.5
0.75 0.89 0.97 1 0.97 0.97], total_radiation_tilted );

    % (W)
    sun_energy = total_radiation_tilted * panel_area * efficiency;

end
```

A2.3 Energy Converter

```
function [incoming_current, net_energy] = P(wind_energy, sun_energy)

% 90% efficiency
net_energy = (sun_energy + wind_energy) * 0.9;

% 12V system
incoming_current = net_energy / 12;
```

A2.5 Energy Management

```
function [duty_cycle, satellite, battery_current] = PM(p_duty_cycle,
p_outgoing_current, incoming_current, time, fuzzy, fuzzy_lookup_table,
minimum_SOC, future_energy_avg, p_SOC)

% Fuzzy energy management
if fuzzy == 1,
    if p_SOC >=minimum_SOC,
        % Updates at midnight only! - to avoid oscillations
        if rem(time,24) == 0,
            duty_cycle = fuzzy_lookup_table(future_energy_avg+1,round((p_SOC-
minimum_SOC)/(100-minimum_SOC))*100+1);
```

```
        else
            duty_cycle = p_duty_cycle;
        end
        % Satellite transmission control
        % Consumption: data logger 0.039A, sensors 0.036A, satellite 0.054A*(hour
data points)
        satellite = 1;
    %     if p_SOC >= minimum_SOC,
    %         satellite = max( 0, floor( (incoming_current-0.039-0.036)/0.054 ) );
    %     else
    %         satellite = 0;
    %     end
    else
        duty_cycle = 0;
        satellite = 0;
    end

% Simple energy management
else
    if p_SOC >= minimum_SOC,
        % Duty cycle for logger and sensors
        duty_cycle = 100;
        % Transmit data every hour
        satellite = 1;
    else
        duty_cycle = 0;
        satellite = 0;
    end

end

battery_current = incoming_current - p_outgoing_current;
```

A2.6 Battery

```
function [SOC, excess_energy_avg, stored_energy] = B( battery_current,
battery_capacity, air_temperature, p_excess_energy_avg, p_stored_energy )

% Hourly self-discharge
stored_energy = p_stored_energy * 0.99997;

% Add incoming current
if battery_current >= 0,
    % Charging efficiency is 90%
    stored_energy = stored_energy + battery_current*0.9;
else
    % Discharging efficiency is 95%
    stored_energy = stored_energy + battery_current/0.95;
end

% Temperature effect
if air_temperature >= 25,
    max_capacity = battery_capacity;
elseif air_temperature < 0,
    max_capacity = battery_capacity*0.85;
else
    max_capacity = battery_capacity*(3/5 * air_temperature + 85)/100;
end

if stored_energy > max_capacity,
    excess_energy_avg = p_excess_energy_avg + stored_energy - max_capacity;
else
    excess_energy_avg = p_excess_energy_avg;
end

% Stored energy saturation
stored_energy = max( 0, min(max_capacity,stored_energy) );

% SOC (%)
SOC = stored_energy / battery_capacity * 100;
```

A2.7 Load

```
function [outgoing_current,data_buffer] = L(duty_cycle,satellite,p_data_buffer)

satellite = min(satellite,p_data_buffer*38.55);

% Consumption: data logger 0.039A, sensors 0.036A, satellite 0.054A*(hour data
points)
outgoing_current = duty_cycle/100*(0.039+0.036) + satellite*0.054;

% Data buffer capacity is 1Mbyte or 3855 hours of recordings (Environment Canada
Reference Station)
data_buffer = p_data_buffer + (1-satellite)/38.55;
```

A2.8 Performance

```
function performance = P(duty_cycle)

performance = zeros(1,5);

if duty_cycle == 0,
    performance(1,1) = 100;
elseif duty_cycle == 25,
    performance(1,2) = 100;
elseif duty_cycle == 50,
    performance(1,3) = 100;
elseif duty_cycle == 75,
    performance(1,4) = 100;
else
    performance(1,5) = 100;
end
```

Appendix 3 – Matlab® Simulation Scripts

For the latest set of scripts e-mail pimentel@ualberta.ca and/or petr.musilek@ualberta.ca.

A3.1 Initialization

A3.1.1 TMY Dataset

```
clear
clc

% Initialize global variables (used by GA optimization tool - energy source
sizing)
global battery_capacity panel_area azimuth inclination
global battery_capacity_selection panel_area_selection
global azimuth_selection inclination_selection
global minimum_SOC

% Initialize global variables (used by GA optimization tool - fuzzy parameters
optimization)
global fuzzy_lookup_table panel_random_failure flutter_random_failure

% Initialize climatological datasets
climatological_data = load('D:\PhD\Datasets\Whitehorse TMY (starts July).csv');
leap_year = climatological_data(:,1);
direct_normal_radiation = climatological_data(:,2);
diffuse_horizontal_radiation = climatological_data(:,3);
air_temperature = climatological_data(:,4);
wind_speed = climatological_data(:,5);
future_energy_avg = climatological_data(:,6); % Scaled to the range 0-100
clear climatological_data

% Initialize simulation parameters
stop_time = length(leap_year);
fuzzy = 0;
fuzzy_lookup_table = 0;
panel_random_failure = zeros(1,stop_time);
flutter_random_failure = zeros(1,stop_time);

% Initialize location and system parameters
latitude = 60.72;
longitude = -135.07;
local_standard_time_meridian = -120;
albedo = 0.7;
modules = 10;
minimum_SOC = 20;

% Initialize GA optimized parameters % 148.7Wh energy waste
battery_capacity = 300;
panel_area = 0.07;
inclination = 90;
azimuth = 10;

% Initialize vectors for GA optimization - each vector contains a set of
% possible parameters
battery_capacity_selection = 200:20:320; % Real values can be obtained from
manufacturer's datasheets
panel_area_selection = 0.05:0.01:0.3; % 0 to 0.3 m2 panel area, 10 cm2 increments
azimuth_selection = -20:5:20; % -15 to 15, 5 degrees increments
inclination_selection = 45:5:90; % 45 to 90, 5 degrees increments
```

```
% Initialize fuzzy controller variables
% Battery State of Charge
SOC_a = 22.4;
SOC_b = 38.4;
SOC_c = 41.6;
SOC_d = 57.6;
% Future incoming energy average (3 months)
% System consumption average is 1.6W
incoming_energy_a = 30;
incoming_energy_b = 35;
incoming_energy_c = 40;
incoming_energy_d = 45;
% System Duty Cycle
duty_cycle_a = 28.75;
duty_cycle_b = 50.5;
duty_cycle_c = 52;
duty_cycle_d = 74.5;
```

A3.1.2 Full Dataset

```
% Initialize climatological datasets
climatological_data = load('D:\PhD\Datasets\Whitehorse 1995-2005 (starts
July).csv');
leap_year = climatological_data(:,1);
direct_normal_radiation = climatological_data(:,2);
diffuse_horizontal_radiation = climatological_data(:,3);
air_temperature = climatological_data(:,4);
wind_speed = climatological_data(:,5);
clear climatological_data

% Initialize simulation parameters
stop_time = length(leap_year);
panel_random_failure = zeros(1,stop_time);
flutter_random_failure = zeros(1,stop_time);
```

A3.1.3 Fuzzy Controller

```
% FUZZY LC
% Creates a control surface (table)
% duty_cycle = fuzzy_lookup_table(incoming_energy,SOC);

% Simulator in fuzzy control mode
fuzzy = 1;

% Membership functions
% Battery State of Charge
SOC_ud = linspace(minimum_SOC,100,101);
SOC_l = trapmf(SOC_ud,[minimum_SOC minimum_SOC SOC_a SOC_b]);
SOC_m = trapmf(SOC_ud,[SOC_a SOC_b SOC_c SOC_d]);
SOC_h = trapmf(SOC_ud,[SOC_c SOC_d 100 100]);
% Future incoming energy average (3 months)
% System consumption average is 1.6W
incoming_energy_ud = linspace(0,100,101);
incoming_energy_l = trapmf(incoming_energy_ud,[0 0 incoming_energy_a
incoming_energy_b]);
incoming_energy_m = trapmf(incoming_energy_ud,[incoming_energy_a incoming_energy_b
incoming_energy_c incoming_energy_d]);
incoming_energy_h = trapmf(incoming_energy_ud,[incoming_energy_c incoming_energy_d
100 100]);
% System Duty Cycle
duty_cycle_ud = linspace(25,100,101);
duty_cycle_l = trapmf(duty_cycle_ud,[25 25 duty_cycle_a duty_cycle_b]);
duty_cycle_m = trapmf(duty_cycle_ud,[duty_cycle_a duty_cycle_b duty_cycle_c
duty_cycle_d]);
duty_cycle_h = trapmf(duty_cycle_ud,[duty_cycle_c duty_cycle_d 100 100]);

% Compute table values
fuzzy_lookup_table = zeros( length(incoming_energy_ud), length(SOC_ud) );
for i = 1:length(SOC_ud)
    for j = 1:length(incoming_energy_ud)

        %Degrees of Fulfillment
        lambda1 = SOC_l(i)*incoming_energy_l(j);
        lambda2 = SOC_l(i)*incoming_energy_m(j);
        lambda3 = SOC_l(i)*incoming_energy_h(j);
```

```
        lambda4 = SOC_m(i)*incoming_energy_l(j);
        lambda5 = SOC_m(i)*incoming_energy_m(j);
        lambda6 = SOC_m(i)*incoming_energy_h(j);
        lambda7 = SOC_h(i)*incoming_energy_l(j);
        lambda8 = SOC_h(i)*incoming_energy_m(j);
        lambda9 = SOC_h(i)*incoming_energy_h(j);

        %Apply Fuzzy Relation
        duty_cycle1 = duty_cycle_l*lambda1;
        duty_cycle2 = duty_cycle_m*lambda2;
        duty_cycle3 = duty_cycle_m*lambda3;
        duty_cycle4 = duty_cycle_m*lambda4;
        duty_cycle5 = duty_cycle_m*lambda5;
        duty_cycle6 = duty_cycle_h*lambda6;
        duty_cycle7 = duty_cycle_h*lambda7;
        duty_cycle8 = duty_cycle_h*lambda8;
        duty_cycle9 = duty_cycle_h*lambda9;

        %Aggregate Consequent
        duty_cycle_max =
max([duty_cycle1;duty_cycle2;duty_cycle3;duty_cycle4;duty_cycle5;duty_cycle6;duty_
cycle7;duty_cycle8;duty_cycle9]);

        %Defuzzification
        fuzzy_lookup_table(i,j) = defuzz(duty_cycle_ud,duty_cycle_max,'bisector');
    end
end

% Normalize table (min = 0, max is 1)
fuzzy_lookup_table = fuzzy_lookup_table - min(min(fuzzy_lookup_table));
fuzzy_lookup_table = fuzzy_lookup_table / max(max(fuzzy_lookup_table));

% duty cycle takes values of 25, 50, 75 and 100%
% multiply by (number of values - 1)
fuzzy_lookup_table = 75 * round(fuzzy_lookup_table * 3) / 3 + 25;
```

A3.2 Tools

A3.2.1 Future Average Energy Estimation

```
% Compute future average energy estimation (90 days)

fuzzy = 0;
future_energy_avg = zeros(8760,1);
stop_time = stop_time+2159;
sim('Simulator_full')
for i = 1:8760
future_energy_avg(i) = mean(net_energy(i:i+2159));
end
stop_time = stop_time-2159;

% Scaling from 0 to 100
future_energy_avg = future_energy_avg - min(future_energy_avg);
future_energy_avg = round(future_energy_avg / max(future_energy_avg) * 100);
```

A3.2.2 Random Failure Generator

```
% Generation of random wind and sun generators failures
x = stop_time;
panel_random_failure = zeros(x,1);
flutter_random_failure = zeros(x,1);

for i = 1:randi(round(x/8760)+1)-1
    random_1 = randi(x);
    random_2 = min(x,random_1+randi(360)-1); % from one hour to 15 days
    panel_random_failure(random_1:random_2,1) = 1;
end

for i = 1:randi(round(x/8760)+1)-1
    random_1 = randi(x);
    random_2 = min(x,random_1+randi(360)-1); % from one hour to 15 days
    flutter_random_failure(random_1:random_2,1) = 1;
end
```

A3.2.3 Fuzzy Controller Plots

```
% Plots fuzzy parameters, run fuzzy_initialization first

% Battery State of Charge
subplot(2,2,1)
plot(SOC_ud,SOC_l,'LineWidth',2);
hold on
plot(SOC_ud,SOC_m,'--r','LineWidth',2);
plot(SOC_ud,SOC_h,'-.k','LineWidth',2);
hold off
xlabel('State of Charge (%)')
legend('low','medium','high')


% Future incoming energy average (3 months)
% System consumption average is 1.6W
subplot(2,2,2)
plot(incoming_energy_ud,incoming_energy_l,'LineWidth',2);
hold on
plot(incoming_energy_ud,incoming_energy_m,'--r','LineWidth',2);
plot(incoming_energy_ud,incoming_energy_h,'-.k','LineWidth',2);
hold off
xlabel('90 Days Future Average Energy (W)')
legend('low','medium','high')


% System Duty Cycle
subplot(2,2,3)
plot(duty_cycle_ud,duty_cycle_l,'LineWidth',2);
hold on
plot(duty_cycle_ud,duty_cycle_m,'--r','LineWidth',2);
plot(duty_cycle_ud,duty_cycle_h,'-.k','LineWidth',2);
hold off
xlabel('Duty Cycle')
legend('low','medium','high')


% Control surface
[x,y]=meshgrid(incoming_energy_ud,SOC_ud);
subplot(2,2,4)
mesh(x,y,fuzzy_lookup_table);
ylabel('State of Charge (%)')
xlabel('90 Days Future Average Energy (W)')
zlabel('Duty Cycle')
```

A3.3 Energy Source Optimization

A3.3.1 Optimization tool

```
% Simulator in simple control mode
fuzzy = 0;

% lower bound, upper bound and number of variables
lb = [1 1 1 1];
ub =
[length(battery_capacity_selection),length(panel_area_selection),length(inclinatio
n_selection),length(azimuth_selection)];
nvars = 4;

% Start with the default options
options = gaoptimset;
% Modify options setting
options = gaoptimset(options,'PopulationType', 'doubleVector');
options = gaoptimset(options,'PopulationSize', 40);
options = gaoptimset(options,'Generations', 20);
options = gaoptimset(options,'StallGenLimit', 10);
options = gaoptimset(options,'CreationFcn', @int_pop);
options = gaoptimset(options,'CrossoverFcn', @int_crossoverscattered);
options = gaoptimset(options,'MutationFcn', @int_mutation);
options = gaoptimset(options,'Display', 'off');
options = gaoptimset(options,'PlotFcns', { @gaplotbestf });
[results,fval,exitflag,output,population,score] =
ga(@fitness,nvars,[],[],[],[],lb,ub,[],options);
```

```
fval
results
```

A3.3.2 Initial Population

```
function Population = energy_source_population(GenomeLength,FitnessFcn,options)

totalpopulation = sum(options.PopulationSize);
range = options.PopInitRange;
lower= range(1,:);
span = range(2,:) - lower;
% The use of ROUND function will make sure that individuals are integers.
Population = repmat(lower,totalpopulation,1) +  ...
    round(repmat(span,totalpopulation,1) .* rand(totalpopulation,GenomeLength));
% End of creation function
```

A3.3.3 Mutation

```
%-----------------------------------------------------
% Mutation function to generate childrens satisfying the range and integer
% constraints on decision variables.
function mutationChildren = energy_source_mutation(parents,options,GenomeLength,
...
    FitnessFcn,state,thisScore,thisPopulation)
shrink = .01;
scale = 1;
scale = scale - shrink * scale * state.Generation/options.Generations;
range = options.PopInitRange;
lower = range(1,:);
upper = range(2,:);
scale = scale * (upper - lower);
mutationPop =  length(parents);
% The use of ROUND function will make sure that childrens are integers.
mutationChildren =  repmat(lower,mutationPop,1) +  ...
    round(repmat(scale,mutationPop,1) .* rand(mutationPop,GenomeLength));
% End of mutation function
%-----------------------------------------------------
```

A3.3.5 Fitness

```
function fitn = energy_source_fitness(variables)

global battery_capacity panel_area azimuth inclination
global battery_capacity_selection panel_area_selection
global azimuth_selection inclination_selection minimum_SOC

battery_capacity = battery_capacity_selection(variables(1));
panel_area = panel_area_selection(variables(2));
inclination = inclination_selection(variables(3));
azimuth = azimuth_selection(variables(4));

sim('Simulator_full')

% multiple parameters
fitn = [ (performance(1)+1)*excess_energy_avg*sqrt(min(SOC)/minimum_SOC) -
SOC(length(SOC)) ];
```

A3.3.6 Optimization Results

```
function component_sizes(batt_sel, panel_sel, inc_sel, azi_sel)

global battery_capacity panel_area azimuth inclination
global battery_capacity_selection panel_area_selection
global azimuth_selection inclination_selection


battery_capacity = battery_capacity_selection(batt_sel);
panel_area = panel_area_selection(panel_sel);
```

```
inclination = inclination_selection(inc_sel);
azimuth = azimuth_selection(azi_sel);
```

A3.4 Fuzzy Controller Optimization

A3.4.1 Optimization tool

```
% Simulator in simple control mode
fuzzy = 0;

% lower bound, upper bound and number of variables
lb = [1 1 1 1];
ub =
[length(battery_capacity_selection),length(panel_area_selection),length(inclinatio
n_selection),length(azimuth_selection)];
nvars = 4;

% Start with the default options
options = gaoptimset;
% Modify options setting
options = gaoptimset(options,'PopulationType', 'doubleVector');
options = gaoptimset(options,'PopulationSize', 40);
options = gaoptimset(options,'Generations', 20);
options = gaoptimset(options,'StallGenLimit', 10);
options = gaoptimset(options,'CreationFcn', @int_pop);
options = gaoptimset(options,'CrossoverFcn', @int_crossoverscattered);
options = gaoptimset(options,'MutationFcn', @int_mutation);
options = gaoptimset(options,'Display', 'off');
options = gaoptimset(options,'PlotFcns', { @gaplotbestf });
[results,fval,exitflag,output,population,score] =
ga(@fitness,nvars,[],[],[],[],lb,ub,[],options);

fval
results
```

A3.4.2 Initial Population

```
function population = fuzzy_population(number_variables,fitness_function,options)

population_size = sum(options.PopulationSize);

population = cell(population_size,number_variables);
for i = 1:population_size
    for j = 1:number_variables
    population{i,j} = sort(randi([0 100],1,4)); % Each fuzzy set is represented by
4 parameters
    end
end
end
```

A3.4.3 Mutation

```
function mutation_children = fuzzy_mutation(parents ,options, number_variables,
fitness_function, state, this_score, this_population)

mutation_children = cell(length(parents),number_variables);

for i=1:length(parents)
    mutation_children(i,:) = this_population(parents(i),:);
    p = randi(number_variables);
    q = randi(4,1);
    mutation_children{i,p}(1,q) = randi([0 100],1);
    mutation_children{i,p} = sort(mutation_children{i,p});
    %mutation_children{i,p} = sort(randi([0 100],1,4)); % Each fuzzy set is
represented by 4 parameters, this line entirely mutates one fuzzy set
end
```

A3.4.4 Single Crossover

```
function crossover_children  =
fuzzy_crossover_single(parents,options,number_variables,fitness_function,this_scor
e,this_population)

number_children = length(parents)/2;
crossover_children = cell(number_children,number_variables);

for i=1:number_children
    crossover_children(i,:) = this_population(parents(i),:);
    p = randi(number_variables);
    crossover_children{i,p} = this_population{parents(i+number_children),p};
end
```

A3.4.5 Fitness

```
function fitn = fuzzy_fitness(variables)

%global SOC_a SOC_b SOC_c SOC_d
%global incoming_energy_a incoming_energy_b incoming_energy_c incoming_energy_d
%global duty_cycle_a duty_cycle_b duty_cycle_c duty_cycle_d
global fuzzy_lookup_table minimum_SOC

SOC_a = variables{1}(1) * (100-minimum_SOC)/100 + minimum_SOC; % minimum_SOC to
100%
SOC_b = variables{1}(2) * (100-minimum_SOC)/100 + minimum_SOC;
SOC_c = variables{1}(3) * (100-minimum_SOC)/100 + minimum_SOC;
SOC_d = variables{1}(4) * (100-minimum_SOC)/100 + minimum_SOC;
incoming_energy_a = variables{2}(1); % incoming energy from 0 to 100, no scaling
incoming_energy_b = variables{2}(2);
incoming_energy_c = variables{2}(3);
incoming_energy_d = variables{2}(4);
duty_cycle_a = variables{3}(1) * 0.75 + 25; % 25 to 100%
duty_cycle_b = variables{3}(2) * 0.75 + 25;
duty_cycle_c = variables{3}(3) * 0.75 + 25;
duty_cycle_d = variables{3}(4) * 0.75 + 25;

fuzzy_initialization

%fuzzy_plots

sim('Simulator_full')

fitn = sum( performance.*[16 8 4 1 -1] ); %single parameter
```

A3.4.6 Optimization Results

```
SOC_a = optimresults.x{1}(1) * (100-minimum_SOC)/100 + minimum_SOC; % minimum_SOC
to 100%
SOC_b = optimresults.x{1}(2) * (100-minimum_SOC)/100 + minimum_SOC;
SOC_c = optimresults.x{1}(3) * (100-minimum_SOC)/100 + minimum_SOC;
SOC_d = optimresults.x{1}(4) * (100-minimum_SOC)/100 + minimum_SOC;
incoming_energy_a = optimresults.x{2}(1); % Scaling to maximum future average
energy
incoming_energy_b = optimresults.x{2}(2);
incoming_energy_c = optimresults.x{2}(3);
incoming_energy_d = optimresults.x{2}(4);
duty_cycle_a = optimresults.x{3}(1) * 0.75 + 25; % 25 to 100%
duty_cycle_b = optimresults.x{3}(2) * 0.75 + 25;
duty_cycle_c = optimresults.x{3}(3) * 0.75 + 25;
duty_cycle_d = optimresults.x{3}(4) * 0.75 + 25;

fuzzy_initialization

figure(1)

fuzzy_plots
```